Investigation to observe spin entanglement from elastic scattering of electrons

Dissertation
zur Erlangung des Doktorgrades
der Naturwissenschaften

vorgelegt beim Fachbereich Physik
der Johann Wolfgang Goethe - Universität
in Frankfurt am Main

von
Rustam Berezov
aus Kharkov, Ukraine

Frankfurt am Main 2009
D 30

vom Fachbereich Physik der Johann Wolfgang Goethe - Universität als Dissertation angenommen.

Dekan:	Prof. Dr. Dirk Rischke
1. Gutachter:	Prof. Dr. Joachim Jacoby
2. Gutachter:	Priv. Doz. Dr. Kurt Aulenbacher

Datum der Disputation:

Abstract

Quantum entanglement plays a basic role in quantum information science. The creation of entanglement between qubits is of fundamental importance for further computation processing like quantum computation, quantum cryptography, quantum teleportation, quantum computers…

We present here a symmetric electron-electron scattering experiment to determine the experimental parameters which are necessary to produce a source of entangled electrons. In this Moeller scattering experiment the electrons differ from each other only by their spin direction. At these conditions a spin entanglement of the scattered electrons is expected. To demonstrate the spin entanglement, a single particle resolved spin measurement of the electrons has to be performed. A high ratio of measured coincidences compare to random could be demonstrated. It is shown, that this ratio is related to an experiment depended nearly constant efficiency for the coincidence detection.

In order to proof the spin entanglement, the goal is to measure the final polarization state of the electrons at different scattering directions to observe a spin anti correlation between these spin states of the Moeller electrons. The usual method to determine the electron polarization is based on an asymmetric scattering experiment with a high Z target. This scattering may yield an asymmetry due to a different spin-orbit coupling of the electrons.

The main problem of polarized electron studies at keV-particle energy is the low efficiency of usual spin polarimeters. This low efficiency impedes or prevents electron spin resolved coincidence measurements because of necessarily induced random coincidences. To enhance the efficiency of the spin detection, a new compact mini-Mott spin analyzer has been developed. Due to a compact small size of this analyzer, a higher efficiency is obtained now, which is a prerequisite to the electron spin resolved coincidence measurements. Till date, the asymmetry measurement have been performed where one Mott analyzer rotated by an angle around the axis. The reducing asymmetry is in agreement with a prediction of quantum mechanic; however, the large systematic errors of the measurement have been estimated.

As a next step for investigation of spin entanglement it is planned to increase the overall efficiency of the experiment by having higher initial energy and minimize error of the measurement by applying new kind of detectors.

Contents

Zusammenfassung

Elastische Streuungen von Elektronen an Teilchen sind grundlegende Prozesse, die in der Plasmaphysik stattfinden. Ausgehend von der Theorie von Zweikörperstoßprozessen lassen sich Vielkörperprozesse wie z.B. die Bestimmung des Energieverlustes von Ionen in Plasmen oder das Verhalten von stark gekoppelten Plasmen modellieren. Zur Beschreibung von elastischen symmetrischen Streuprozessen wie zum Beispiel von Elektronen an Elektronen (Möllerstreuung), Protonen an Protonen oder Helium an Helium müssen quantenmechanische Betrachtungen herangezogen werden. Für diesen Fall können die Teilchen nach der Streuung als voneinander abhängige Teilchen beschrieben werden, besser bekannt in der Literatur als Verschränkung von Teilchen. Zwei oder mehr Teilchen bezeichnet man als verschränkt, wenn sie innerhalb eines quantenmechanischen Systems nicht unabhängig voneinander beschrieben werden können. Vor der Trennung der beiden Teilchen innerhalb des quantenmechanischen Systems steht jedoch noch nicht fest, in welchem Zustand sich die Teilchen bei der Messung befinden werden. Die Verschränkung ist eine besondere quantenmechanische Eigenschaft.

Die Verschränkung des Spins zweier Teilchen ist ein Beispiel für diese quantenmechanische Eigenschaft. Ist der Spin eines verschränkten Teilchens bekannt, so ergibt sich automatisch der Spin des zweiten verschränkten Teilchens. Dabei hängt die Eigenschaft des einen Teilchens von der Messung des anderen Teilchens ab. Für jedes einzelne der verschränkten Quantenteilchen ist also der Ausgang einer Messung unbestimmt, während die Korrelation von Beginn an feststeht. Durch die Verschränkung von Zuständen können verschränkte Teilchen die räumlich sehr weit von einander getrennt sind simultan wechselwirken. Dabei spielt die Entfernung zwischen den korrelierten Teilchen keine Rolle. Sie bleiben im verschränkten Zustand für den Zeitraum für den sie voneinander isoliert sind bis zu einer Messung des Zustandes. Es ist jedoch nicht möglich Informationen schneller als mit

Lichtgeschwindigkeit zwischen zwei beliebigen Orten zu übermitteln, da ein Eingriff durch eine Messung bzw. eine Abfrage des quantenmechanischen Zustandes zu einer Störung des Systems führen würde und somit über den anderen Zustand keine Vorhersagen gemacht werden können.

Nach der Theorie der Quantenmechanik besitzt das Teilchen, solange es nicht gemessen wird, überhaupt keine konkrete Spinrichtung. Es befindet sich anfangs, je nach Präparation, in einer Superposition aus vielen möglichen Spinorientierungen. Erst im Augenblick seiner Messung nimmt der Spin des Teilchens einen festen Wert an, nämlich entweder nach oben oder nach unten zeigend. Die im Falle der Messung angenommene Spinorientierung ist nur durch die aus der Wellenfunktion des Partikels resultierende Wahrscheinlichkeit vorherzusagen. Vor der Messung liegt zum Beispiel für Elektronen die Wahrscheinlichkeit für eine Spinmessung zu 50% für Spin-up und ebenso 50% für Spin-down vor. Falls bei einer Messung die Spinkomponente up gemessen würde, sollte im Falle verschränkter Elektronen für das andere Teilchen im zweiten Detektor die Spinkomponente „down“ gemessen werden. Der Spin der beiden Teilchen ist nach Aussagen der Quantenmechanik miteinander korreliert. Verschränkung kann nur bewiesen werden wenn diese Korrelation zwischen den Spinzuständen unabhängig von der horizontalen- oder vertikalen Einstellung vermessen werden kann.

Verschränkte Zustände führen zu besonderen Eigenschaften von quantenmechanischen Systemen die kein Analogon in der klassischen Physik besitzen. Die Widersprüche zwischen quantenmechanischen Vorhersagen und klassischer Intuition wurden nach den Namen der Autoren einer vielzitierten Veröffentlichung als „Einstein-Podolsky-Rosen-Paradoxon“ (EPR) Effekt bezeichnet. Die EPR-Theorie behauptet, dass die Quantenmechanik eine unvollständige Theorie sei, die gegen den lokalen Realismus verstößt. Mit der Einführung von verborgenen Variablen würde eine realistische Möglichkeit geschaffen die Quantenmechanik zu vervollständigen.

Die Ergebnisse der bislang durchgeführten Experimente stehen in guter Übereinstimmung mit den quantenmechanischen Vorhersagen, die jedoch auch immer eine Verletzung der Bellschen Ungleichung zeigen. Ein ähnliches Experiment zur Verschränkung von Protonen wurde bereits im Jahre 1976 von

Lamehi-Rachti und W. Mittig durchgeführt. Die Ergebnisse dazu stehen in guter Übereinstimmung mit den quantenmechanischen Vorhersagen.

Die Motivation dieser Arbeit ist es nun die notwendigen Parameter zu bestimmen um eine Quelle für verschränkte Elektronen zu erzeugen. Hierzu wurde ein experimenteller Aufbau konzipiert um die Verschränkung von symmetrisch quasielastisch gestreuten Elektronen nachzuweisen.

Für das Moellerstreuexperiment wurde ein Elektronenstrahl aus nicht polarisierten Elektronen an einem Kohlenstoff-Target elastisch gestreut. Für identische Fermionen ist die Streuung unter 90 Grad verboten, während für Bosonen der Streuquerschnitt unter dem gleichen Winkel zweimal so groß ist als für unterscheidbare Teilchen. Dadurch ist eine Streuung von Elektronen unter 90 Grad erlaubt, wenn die Elektronen unterscheidbar sind. Die Spineinstellung beider Teilchen muss daher antikorreliert zueinander sein.

Zur Überprüfung der Spinverschränkung von unterscheidbaren Teilchen ist die Messung der nach der Streuung resultierenden Polarisation der Elektronen in den verschiedenen Streurichtungen notwendig, um eine Antispinkorrelation für die verschiedenen Streurichtungen der Möllerelektronen nachzuweisen. Die herkömmliche Methode zum Messen der Elektronenpolarisation basiert auf einer asymmetrische Streuung an einem Target mit hoher Ladungszahl. Dieser Streuprozess kann zu einer Winkel-Asymmetrie durch die Spin-Bahn-Kopplung der Elektronen führen.

Ein wichtiges Hauptproblem, das bei den Untersuchungen von Elektronen mit keV-Energien auftritt ist die niedrige Effizienz der gebräuchlichen Spinpolarimeter. Durch die niedrige Effizienz der Polarimeter wird die Messung der eigentlichen Koinzidenzen gegenüber den zufälligen Koinzidenzen erschwert oder sogar völlig verhindert. In dieser Arbeit wird daher ein neuer kompakter Minimottspinanalysator vorgestellt und im Experiment untersucht. Durch die kompakte Bauweise der zylindrischen Elektroden konnte damit eine hohe Nachweiswahrscheinlichkeit für die Messung von polarisierten Elektronen erreicht werden. Dies eröffnet die Perspektive neuartige Experimente zu grundlegenden quantenmechanischen Eigenschaften von freien geladenen Teilchen, die über große Distanzen getrennt sind, durchführen zu können.

Für das Moeller Streuexperiment wurden Elektronen mit Energien von einigen 10 keV durch eine handelsübliche Elektronenkanone erzeugt. Der

Strahlstrom konnte zwischen 1 und 100μA variiert werden. Ein freistehendes Kohlenstofftarget mit einigen μg/cm^2 wurde als Targetmaterial für die Streuung verwendet. Nach der Streuung am Kohelstoffarget unter einem Winkel von $\Theta_{lab} = 45°(\Theta_{c.m.} = 90°)$ erreichen die beiden Elektronen die Mottdetektoren. In den Mottdetektoren streuen die Elektronen erneut an einer Goldfolie die eine Flächendichte von 70 μg/cm^2 (Dicke-36nm) besitzt.

Zur Minimierung des Messfehlers ist darauf zu achten einen hohen Anteil an echten Koinzidenzen gegenüber den Zufälligen zu erlangen. Zur Abschätzung dieses Verhältnisses der verschiedenen Koinzidenzen muss die Effizienz des Experiments abgeschätzt werden. Eine gute Effizienz war nur mit dünnen Kohlenstofftargets mit einer Flächendichte von 4 μg/cm^2 zu erreichen, wobei die Energie des Elektronenstrahls gleichzeitig auf 35 keV erhöht wurde. Zur Trennung zwischen den gestreuten Möller- und Mottelektronen wurden zusätzliche Strahlfokussierungselemente und elektrostatische Ablenker in die Streukammer integriert. Die Energieauflösung ist hierbei ein wichtiger Aspekt zur Reduzierung der Untergrundelektronen, die durch hochenergetische Mottstreuung entstehen. Mit Hilfe der kompakten elektrostatischen Ablenker konnte weiterhin die Distanz zwischen der Streukammer und den Detektoren vermindert werden, wodurch sich keine starke Verminderung der Intensität der ankommenden Teilchen im Mottanalysator ergab.

Sechs verschiedene Arten an Detektoren wurden für dieses Experiment untersucht. Der wichtigste Parameter zur Vermeidung von zufälligen Koinzidenzen ist die zeitliche Auflösung der Detektoren, die für dieses Experiment so hoch wie möglich sein sollte. Zusätzlich sollte die zeitliche Auflösung des Detektors aber lang genug sein um geringe zeitliche Schwankungen der Messsignale noch zu erfassen. Wäre dies nicht der Fall würden Verluste von echten Koinzidenzen auftreten. Mit einer maximalen zeitlichen Auflösung in der Größenordnung von 2-4 ns erwiesen sich ein Magnumanalyser und ein Plastik–Szintillator für dieses Experiment gegenüber anderen Detektoren als am besten geeignet.

Die folgende Abbildung 1-1 zeigt die experimentellen Ergebnisse zu der erreichten Zählrate und zur Effizienz des Detektors in Abhängigkeit des Quotienten aus den gemessenen zu den zufälligen Koinzidenzen. Das Verhältnis von gemessenen zu zufälligen Koinzidenzen nimmt durch den Anstieg der zufälligen Koinzidenzen bei zunehmender Intensität ab. Für

niedrige Strahlintensitäten bei einer Zählrate im Bereich von kHz ist die Rate für echte Koinzidenzen um den Faktor tausend höher als die Rate der zufälligen Koinzidenzen. Es konnte somit gezeigt werden, dass für verschiedene Zählraten die experimentelle Effizienz für die Messung der Koinzidenzen nahezu konstant blieb. Eine hohe Effizienz des Detektors und ein hohes Verhältnis zwischen gemessenen und zufälligen Koinzidenzen sind die wichtigsten Anforderungen zum Nachweis einer quantenmechanischer Verschränkung für dieses Experiment.

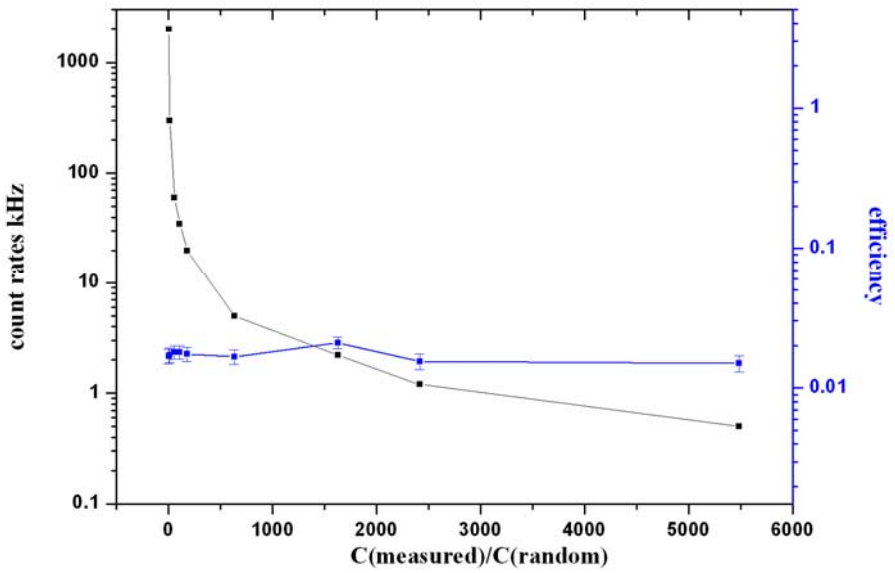

Abbildung 1-1: Experimentell ermitteltes Verhältnis von gemessenen- zu zufälligen Koinzidenzen in Abhängigkeit der Intensität des Elektronenstrahls (schwarz) verglichen mit der Effizienz zum Nachweis einer echten Koinzidenz im Detektor (blau).

Die maximale während der Experimente erreichbare Effizienz zum Nachweis der echten Koinzidenzen der Elektronenpaare (ohne Nachweis der Elektronen in den Mott-Analysatoren) lag bei einem Wert von etwa $\varepsilon=2\cdot10^{-2}$.

Für das Gesamt-Experiment konnte eine Effizienz von $\varepsilon\approx10^{-5}$ erreicht werden, wobei sich bei einer Frequenz von 1-2 kHz an den Magnum-Detektoren insgesamt eine vierfach höhere gemessene Koinzidenzrate im Vergleich zu den statistischen Koinzidenzen ergab.

Für die Auswertung der Messdaten wurden zwei verschiedene LabVIEW-Oberflächen verwendet. Während ein Modul am Oszilloskop zur

Datenerfassung installiert wurde befand sich das Zweite zum Auslesen der Daten extern auf einem Computer, der mit dem Oszilloskop über LAN verbunden war. Mit dem Oszilloskop wurden dabei die Signale aus den Detektoren erfasst und gespeichert. Die Totzeit des Oszilloskop wurde mit einem „fast frame“ Aufnahmemodus klein gehalten, weil es damit möglich war bis zu einigen tausend Ereignisse (Signale) direkt zu speichern und auf den Datenspeicher des Computers zu übertragen. Mit dem zweiten externen Programmmodul, das Auswertemodul, wurde für jedes gemessene Ereignis die Flankenanstiegszeit aller Kanäle bestimmt.

Ein entscheidender Test zum Nachweis der Verschränkung der Elektronen wird durch eine Drehung eines der Mottanalysatoren um einen Winkel Θ erreicht. Dabei muss die erwartete Anti-Koinzidenz in der Spinausrichtung der Elektronen verschwinden, wenn zueinander orthogonale Spinkomponenten gemessen werden. Die hier nachgewiesene Verminderung der Asymmetrie bei einer Drehung um 90° ist in guter Übereinstimmung mit den quantenmechanisch getroffenen Vorhersagen.

Die Abbildung 1-2 zeigt die Ergebnisse der Messungen zur Asymmetrie der Verschränkung in Abhängigkeit vom Winkel Θ eines Mottdetektors radial um die Symmetrieachse.

Der rote Messpunkt ist die durch den experimentellen Aufbau, bei vertauschen eines Gold- durch ein Aluminiumtarget erhaltene apparative Asymmetrie. Aus den Messergebnissen ist zu erkennen, dass die durch den apparativen Aufbau erzeugte Asymmetrie geringer ist als die real auftretende Asymmetrie der verschränkten Elektronen. Zur Bestätigung dieser Annahme sind weitere, präzisere Messungen der aparativ erzeugten Asymmetrien notwendig. Die blauen Messpunkte in der Grafik zeigen eine Reduzierung der Asymmetrie bei Erhöhung des Drehwinkels des Mottdetektors. Dieses Ergebnis ist innerhalb der vorliegenden Fehler Übereinstimmung mit der Quantentheorie, die eine Reduzierung der Asymmetrie auf Null vorhersagt.

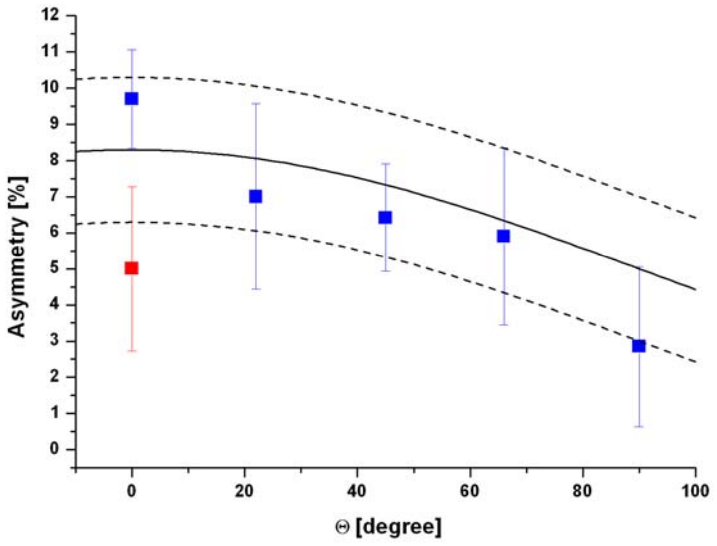

Abbildung 1-2: Experimentelle Ergebnisse der Asymmetrie in Abhängigkeit des Winkels eines Mottdetektors zur Rotationsachse (blaue) und die Ergebnisse der apparative Asymmetrie (rot). Des Weiteren zeigt die schwarze Kurve den theoretischen Verlauf der zu erwarteten Koinzidenzen, während die gestrichelte schwarze Linie den Fehler des Offsets von ±2% berücksichtigt.

Die schwarze Linie der Abbildung 1-2 zeigt den abgeschätzten theoretischen Verlauf der Koinzidenzen für Zweifachstreuung und den Fehler der apparative asymmetrie. Die Kalibrierung der Geräte wurde an der Universität Mainz durchgeführt und dabei Asymmetrieabweichung von etwa 3.3% festgestellt. Der Offset der durch diese apparative Asymmetrie bestimmt wurde betrug 5% mit einem relativen Fehler von ± 2%. Aus der gemessenen apparativen Asymmetrie und unter Berücksichtigung quantenmechanischer Vorhersagen ergab sich ein theoretisch erwarteter Verlauf für die zu bestimmenden Koinzidenzen bei Zweifachstreuung mit der folgenden Abschätzung:

$$Y = Amp \cdot \cos(x) + Offset$$

Mit Amp als die Asymmetrie des bekannten polarisierten Elektronenstrahls,

$Offset$ – Wert der apparative Asymmetrie des Zweifachstreuexperiments,

x – Winkel des Mottanalysators um die Achse.

Allerdings ergaben die Abschätzungen für die Ungenauigkeit der durchgeführten Messungen einen sehr hohen statistischen Fehler. Es kann somit in diesem Experiment bisher nicht sicher zwischen den

quantenmechanischen Vorhersagen und den Vorhersagen durch die Bellsche Ungleichung unterschieden werden. Um den statistischen Fehler auf einige Prozent einzuschränken sind wegen der geringen totalen Effizienz des Gesamtexperimentes Messdauern von etwa 100 Stunden pro Messwert nötig, was zu einer Gesamtmessdauer von etwa zwei bis drei Monaten führen würde. Es erscheint sinnvoller im nächsten Schritt die Effizienz und die Zeitauflösung des Experiments weiter zu erhöhen. Zu diesem Zweck sollten verbesserte Detektoren (Microchannel plates) verwendet werden. Es wird erwartet, dass dadurch die zeitliche Auflösung bis zu einem Faktor 10 auf etwa 0,2 ns gesteigert werden kann, wodurch das Verhältnis zwischen den gemessenen und den zufälligen Koinzidenzen entsprechend gesteigert werden könnte. Eine Möglichkeit die Effizienz des Experimentes zu steigern besteht in der Erhöhung der Anfangsenergie der Elektronen. Zum Beispiel wird bei einer Erhöhung der Energie von 32 auf 48 keV eine Steigerung der Effizienz um einen Faktor zwei erwartet.

Zusammenfassend ergeben sich durch den hier begonnenen Aufbau einer Quelle von verschränkten Elektronen neue Möglichkeiten zur Untersuchung fundamentaler quantenmechanische Eigenschaften wie z.B. die Untersuchung der Dekohärenz von verschränkten Systemen. Bei dekohärenten Teilchen verliert das quantenmechanische Superpositionsprinzip hervorgehend aus den Kohärenzeigenschaften von Teilchen seine Gültigkeit. Mit den quantenmechanischen Eigenschaften von verschränkten Zuständen lassen sich neue technologische Anwendungen in der Quanteninformationstechnologie verwirklichen, wie das zum Beispiel für Quantenkryptographie gezeigt werden konnte. Weitere moderne Anwendungen verschränkten Systemen lassen sich auch in der Quanten-Teleportation, und für die Telekommunikation in Quantennetzwerken finden.

1. Introduction

1.1. Motivation of the work

Elastic scattering is a basic interaction process in plasma physics. Starting from binary collisions a many body process like stopping power or the behaviour of strongly coupled plasmas can be modelled. Fundamental quantum properties have to be considered, if symmetric elastic scattering, e.g. electrons with electrons (Moeller scattering), of protons with protons or of helium with helium is considered. In these cases spin entanglement appears if two particles scattered to a CM (center of mass)-angle of 90° are indistinguishable. Similar to the Pauli-principle for bound electrons, the scattering of indistinguishable fermions to 90° is forbidden, whereas for identical bosons the scattering cross-section at that angle is twice as big as the one for distinguishable particles [Fey-65].

Particles, such as photons, electrons, or helium ions produced in non linear crystals or during scattering can be correlated in pairs, known as entanglement. Knowing the spin state of one entangled particle allows knowing the spin of its mate. The direction of the spin for the individual particle is however unknown before measurement, and even the basis of the measurement, e.g. whether a vertical or horizontal spin measurement is performed, can be chosen freely for entangled particles.

As example, the processes of cascade decay of atomic excitations [Cla-78] and spontaneous parametric down-conversion of light in nonlinear crystals are the traditional sources of entangled states. Using these processes, one can create photon pairs with entangled polarization states.

Quantum entanglement is rooted in the superposition principle of quantum states. It is a specific feature of composite quantum system and reflects the non-localized characteristic of quantum mechanics.

Quantum entanglement plays a basic role in quantum information science [Deu-98]. The creation of entanglement between qubits is of fundamental importance for further computation processing: quantum computation, quantum algorithm, quantum cryptography, quantum teleportation, quantum computers. The entangled states have also applications in plasma physics, for example, the investigation of quantum effects on the entanglement fidelity in low-energy elastic electron-ion scattering in strongly coupled semiclassical plasmas [You-08].

Entanglement presents also a particular case of spin-squeezed states [Kit-93]. This application can be very useful in ultrahigh-resolution spectroscopy. Other metrological applications of entangled states include special methods for the calibration of photodetectors like absolute brightness and high-precision of polarization dispersion in briefringent media [Klu-87].

The main motivation of our work is devoted to determine the experimental parameters necessary to produce a source of entangled electrons. For this purpose we set up an experiment to test this entanglement for a symmetric scattering of electrons with electrons [Jac-01, Ber-09a]. In order to give proof of the spin entanglement, the goal is to measure the final polarization state of the electrons at different scattering directions to observe a spin anti correlation between these spin states of the Moeller electrons. The usual method to determine the electron polarization is based on an asymmetric scattering experiment with a high Z target [Kes-85]. This scattering may yield an asymmetry due to a different spin-orbit coupling of the electrons.

The main problem of polarized electron studies at keV-particle energy is the low efficiency of usual spin polarimeters. This low efficiency impedes or prevents electron spin-resolved coincidence measurements because of necessarily induced random coincidences. We present here also the design and performance of a compact mini-Mott spin analyzer and the efficiencies obtained in the experiment. Due to the compact size the cylindrical-electrode Mott polarimeter achieves high detection sensitivity. In turn, the increasing

sensitivity improves the figure of merit [Kes-85] and opens a path for a new class of experiments, where fundamental quantum properties of free charged particles at large distances can be measured.

1.2. Contents of the thesis

For the investigation of spin entanglement a symmetric electron-electron scattering experiment has been set up [Jac-01] where the electrons differ from each other only by their spin direction.

The main goal for the presented experiment was to investigate the experimental parameters necessary to observe spin entanglement from elastic scattering of electrons. To achieve this goal the following aims have to be performed:

1 to observe higher ratio of measured coincidence compared to random after the scattering in carbon target,

2 to characterize the performance of the Mott analyzer (calibration with known polarized beam),

3 to measure the efficiency of the experimental setup,

4 to observe higher ratio of measured coincidence compared to the background after double scattering in detectors of the Mott analyzer.

This thesis is dedicated to the first investigation of spin entanglement produced from elastic scattering of unpolarized electrons. In Chapter 2 some theoretical aspects of quantum mechanical behaviour are discussed like the connection of which-path information with coherence of elastic scattering. The famous Einstein-Podolsky-Rosen paradox is shortly described together with Bell's inequalities and the general overview of entanglement. Some overview of spin correlation experiments is also given. The threshold for a particles energy is estimated for a scattering experiment, where only above this threshold interference effects can be observed.

The Mott analyzers that are used for measuring the electron spin polarization are described in Chapter 3. The important difficulties (multiple, plural scattering, instrumental asymmetry) and the main parameters for Mott

scattering (Sherman function and figure of merit) are discussed. Two designs of Mott analyzers that have been used for the anti coincidence scattering experiment are presented together with the experimental facility at MAMI IKP Mainz where the calibration of these analyzers has been performed. Some estimation of Mott analyzer efficiency and experimental results are also given.

Chapter 4 is dedicated to investigation of the spin asymmetry of backscattered electrons from magnetized targets as additional option for spin detection with high efficiency. Some simulation and also experimental results from the efficiency and asymmetry of polarized backscattering electrons are also represented in this chapter.

The whole experimental setup with the procedure of the measurements together with the results is presented in Chapter 5. The scheme of the acquisition setup and data analysis tool which is programmed in Labview and the detectors that has been developed for the experiment is shown here. The higher ratio from the measured coincidences compared to the random is demonstrated here. It is shown that this ratio is related to an experiment-depending nearly constant efficiency of coincidence detection. The experimental result of asymmetry with dependence from the angle where one Mott analyzer rotated around the axis is also presented in this chapter.

Finally, Chapter 6 contains the conclusions of the presented work, future suggestions and plans for further research.

2. Theoretical background

This chapter describes the theoretical aspects of the presented work. Some of the quantum mechanical properties like wave particle duality in a double-slit experiment and their connection with coherence in an elastic scattering experiment are described. The definition of entanglement and some examples are presented here. The contradiction between quantum mechanical predictions and classical intuitions is shown by the Einstein-Podolsky-Rosen (EPR) paradox.

Bells inequalities, which allow to decide which of the hypothesises is correct shortly described in this chapter. Some of the earlier experiments to test these inequalities are also mentioned here. A calculation of a threshold energy above which interference effects can be observed is also described in this chapter.

2.1. Double-slit experiment

Complementarity expresses the fact that every quantum system has at least two properties, which cannot be observed simultaneously. “The observation of an interference pattern and the acquisition of which-way information are mutually exclusive [Eng-96]”. As example, the two-slit experiment of electron interference [Fey-65] is shown diagrammatically in Figure 2-1 This experiment has never been done in just this way. It is only a “thought experiment” imagined for better understanding of quantum behaviour of electrons that sometimes has properties of both waves and particles (*wave particle duality*).

In this thought experiment a thermal electron gun emits electrons. In front of the gun is a wall with two slits in it. Only electrons that move through the slits can arrive at the plate and generates sparks. Beyond the wall is another plate which will serve as a “backstop”. In front of the backstop we place a movable detector (Geiger counter or electron multiplier).

If only slit 1 is opened then the results of measurement are given by the curve marked P_1. That is, $P_1 = |\psi_1|^2$, where ψ is the probability amplitude. On the other hand, if slit 2 is opened and slit 1 is closed; the distribution of electrons which have arrived to the plate is labelled with curve P_2. That is $P_2 = |\psi_2|^2$. The results are showed in Figure 2-1 a. If two slits are opened than according to classical mechanics the joint distribution should be the sum of curve 1 and curve 2: $P_{12} = P_1 + P_2 = |\psi_1|^2 + |\psi_2|^2$. But the result P_{12} (Figure 2-1 b) obtained with both holes open is clearly not the sum of P_1 and P_2, the probabilities for each hole alone. It is interference: $P_{12} = |\psi_1 + \psi_2|^2$.

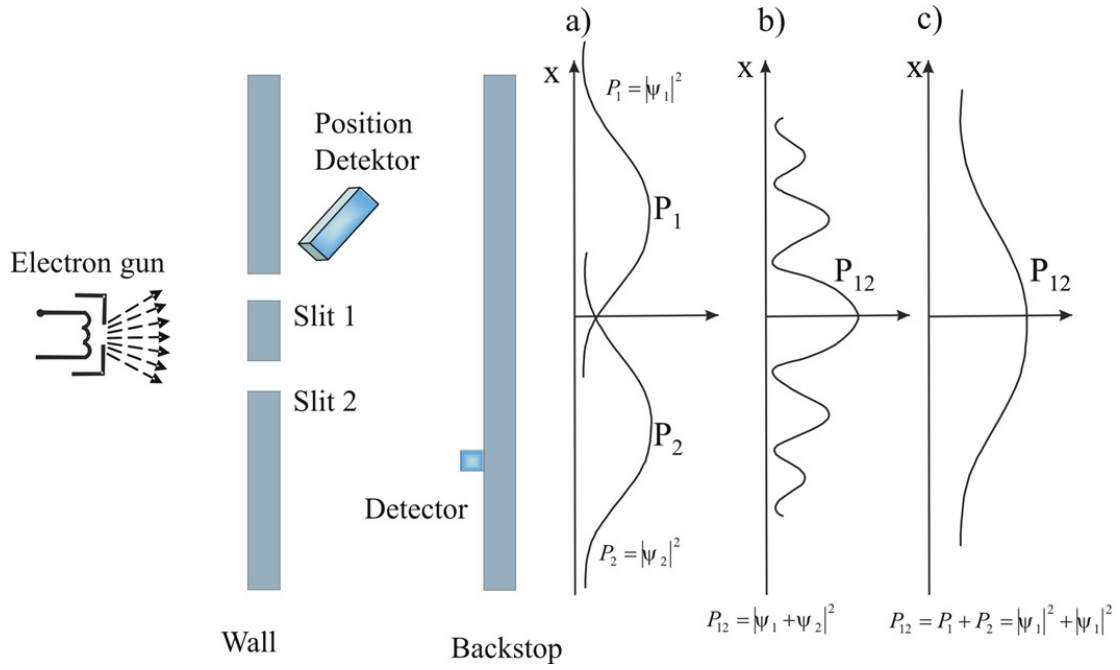

Figure 2-1: Two-slit experiment of electron interference.

In terms of the intensities, we could write:

$$I_{12} = I_1 + I_2 + 2\sqrt{I_1 I_2}\cos\delta \qquad (2.1)$$

where δ - is the phase difference between the amplitudes.

The last term is the "interference term". The distribution of the interference is quite similar to that of light or water waves going through two

slits. The distribution remains the same even if the electron gun is throttled down so that it will emit only one electron at a time, and also when the interval between two emissions is prolonged in such a way that there can never be two electrons flying at the same time. It seems, that the electrons interfere with themselves. Indeed, according to quantum mechanics, a particle interferes only with itself.

But, according to classical physics an electron can go either through slit 1 or slit 2 but not through both slits. To check this conclusion, one can introduce a position detector near slit 1 (Figure 2-1) so that whenever an electron comes through slit 1, a spark is generated. In order for the electron to be able to continue its journey to the plate, the position detector has to employ some sort of non-destructive measurement technique, such as shining a light on the electron. In this way one knows whether the electron goes through slit 1 or slit 2. But in this case, the interference disappears and the curve predicted by classical mechanics is observed (Figure 2-1c): $P_{12} = P_1 + P_2 = |\psi_1|^2 + |\psi_2|^2$. Classical mechanics becomes suddenly correct again.

In summary, it is impossible to design an apparatus to determine which slit the electron passes through and at the same time not disturb the electrons enough to destroy the interference pattern. This exclusion of interference and which-path information is a fundamental concept of quantum mechanics.

2.2. Cross section for distinguishable and indistinguishable particles

The connection between which-path information and coherence observed from elastic scattering is described here. The scattering of two particles at each other yields as result of pure quantum mechanic effects two different cross sections, depending whether the two particles are distinguishable or not.

In order to obtain indistinguishable particles, we consider the elastic scattering of beam particles with target particles only of the same species (e.g. electrons with electrons). Then, similar as for the Pauli principle in atomic physics beyond the possible quantum threshold only the spin of a particle allows to distinguish two scattered particles at elastic scattering or not. If we consider non polarized particles for beam and target, we have to take into account the statistical weight to obtain distinguishable or indistinguishable scattering [Jac-01].

For spin ½ particles like electrons or protons, we obtain four possible spin directions of beam versus target, from which two are distinguishable and two are indistinguishable. Thus, at a given energy the average cross section at $\Theta = \frac{\pi}{2}$ yields only half the value of an experiment which would be always distinguishable e.g. the scattering of protons with deuterons, even without taking any measure to determine spin or mass of the final particles in a detector.

For a scattering experiment the cross section at a given scattering angle Θ is the result of the superposition of two possible branches which originate either from beam or from the target (Figure 2-2). If the two branches are indistinguishable, the different possible paths of the scattered particles have to be added coherently, otherwise incoherently.

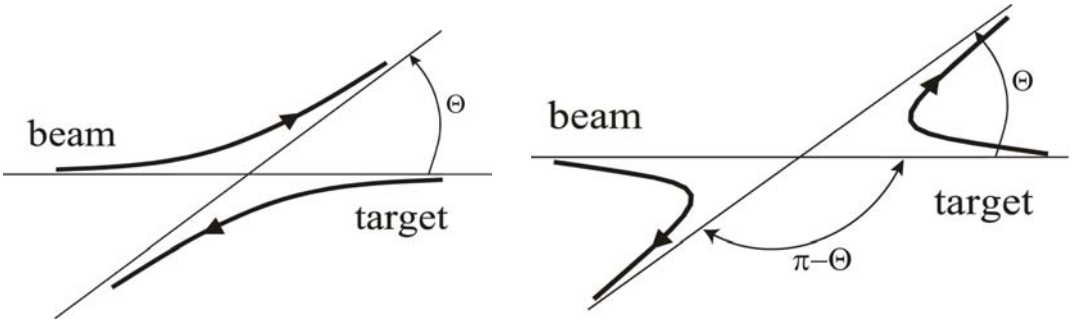

Figure 2-2: For a scattering experiment the cross section at a given scattering angle Θ is the result of the superposition of two possible branches. The interference occurs between different possible paths of the scattered particles, if the two branches are indistinguishable.

Similar, as superposition for the double-slit experiment or for two beams of light of the same wavelength can be carried out in two ways: *coherently,* so that there is a definite and constant phase relation between two beams, or *incoherently*, so that there is not [Par-64]. The characteristic interference phenomena of light are found only when superposition is coherent. This might be achieved by deriving both beams from a common source. Otherwise, the addition of two beams produces an intensity which is the sum of the separate intensities. And interference washes out if the phase relation between two beams is not constant.

If we have a target particle in the position Θ, there must be a beam particle on the opposite side at the angle $(\pi - \Theta)$. So if $f(\Theta)$ is the amplitude for target scattering through the angle Θ, then $f(\pi - \Theta)$ is the amplitude for beam scattering through the angle $\pi - \Theta$, or opposite.

Thus, in a non relativistic treatment the cross section σ_{di} for the elastic scattering of two distinguishable particles to the scattering angle Θ has to be added incoherently for bosons and fermions in the centre of mass system [May-79]:

$$\sigma_{di} = |f(\Theta)|^2 + |f(\pi - \Theta)|^2 \tag{2.2}$$

For two indistinguishable particles the elastic scattering cross section σ_{in} is a function of the scattering amplitude $f(\Theta)$ for the scattering angle θ:

$$\sigma_{in} = |f(\Theta) \pm f(\pi - \Theta)|^2 \tag{2.3}$$

Due to symmetry considerations of the quantum mechanical wave function for the scattering of two bosons the plus sign has to be applied, and for the scattering of two fermions the minus sign. The total wave function which represents the identical fermions during scattering is known to be anti-symmetric, and the wave function for the scattering of two identical bosons is symmetric [Daw-92].

The variation of the scattering cross section is symmetric to the scattering angle $\Theta = \pi/2$. For this special scattering angle at $\Theta = \pi/2$ the equation for bosons is given by

$$\sigma_{in}^{b}(\pi/2) = |f(\pi/2) + f(\pi/2)|^2 = 4 \cdot |f(\pi/2)|^2 \tag{2.4}$$

and for fermions to

$$\sigma_{in}^{f}(\pi/2) = 0 \tag{2.5}$$

In this case at the fixed scattering angle of $\Theta = \pi/2$ for distinguishable particles (bosons and fermions) if they did not interfere, the result of Eq.(2.2) gives only:

$$\sigma_{di}(\pi/2) = 2 \cdot |f(\pi/2)|^2 \qquad (2.6)$$

The reason for the factor two in this last equation is entirely classical physics. We have two distinguishable possibilities here: to detect a particle that originates either from the beam or from the target. Although both particles are in-principle distinguishable, they are in usual experiments collected for practical reasons at a single unified cross section. As a result of these equations for bosons and fermions, at a given scattering angle for distinguishable and for indistinguishable particles a well defined, but different cross section is obtained.

In summary, for identical fermions a scattering to $\Theta = \pi/2$ is not allowed, where for identical bosons a scattering to this angle is magnified by a factor two in comparison to distinguishable bosons [Jac-01]. This difference for the cross section of elastic scattering is a purely quantum mechanical effect, similar to the Pauli principle or to the difference between Fermi- or Bose-statistics in quantum mechanics.

2.3. Entanglement

Particles, such as photons, electrons, or helium produced in non linear crystals or during scattering can be correlated in pairs, known as entanglement. Knowing the spin state of one entangled particle - whether the direction of the spin is up or down - enables one to know that the spin of its mate is in the opposite direction. The direction of the spin for the individual particle is however unknown before the measurement, and even the basis of the measurement, whether e.g. a vertical or horizontal spin measurement is performed, can be chosen freely for entangled particles.

Quantum entanglement allows particles that are separated by incredible distances to interact with each other immediately. No matter how large the distance between the correlated particles, they will remain entangled as long as they are isolated. But, of course here no information could be transmitted between any two points with faster than light velocity; because the values of the measurements at these points in a single measurement are accidental and can not be predicted.

As example for electrons, each vertical spin measurement has an equal 50% probability for the spin pointing up or down after the measurement. If at

one of this measurements one vertical spin component (up) is detected, then the measurement at the second detector has to result in the opposite spin direction (down). The spin measurement of these two electrons is correlated. Entanglement is demonstrated only if this correlation can be shown independent of the horizontal or vertical basis of the measurement.

Quantum correlation of the entangled states may arise in a system that consists of two or more interacting subsystems. There is no entanglement when the system occurs in the state of the form $|\Psi\rangle = |\psi\rangle|\varphi\rangle$, where $|\psi\rangle$ and $|\varphi\rangle$ are the states of respective subsystems. Such a state is referred to as factorized. However, even if in the beginning the state is factorized, it may become entangled after the subsystems interact with one another.

As definition, a pure state combined of two quantum systems $Q = A + B$ is called entangled, if its wave function cannot be written into a tensor product of the wave functions of its constituent parts:

$$\psi \neq \psi_A(x_A) \otimes \psi_B(x_B) \tag{2.7}$$

where $\psi_{A,B}$ are the wave functions of the individual system A and B depending on parameters $x_{A,B}$. In another hand, the wave functions that can be written to form (2.7) contain no correlations because any operator is then averaged independently over each constituent part.

As example: we have two spins A and B in the external magnetic field and they have the same direction. We will make a preposition that they have never interacted at earlier times and now also. In this case the measurement of one spin has no influence on the state of the other spin. With the measurement one of the spins we known automatically that the direction of the other spin has also direction of the external magnetic field. Than the total state of the system could be described for two particles as a product of states of the individual subsystems:

$$|\psi\rangle = |00\rangle = |\uparrow\uparrow\rangle = |\uparrow\rangle_A \otimes |\uparrow\rangle_B$$

Here, spins always have the direction “up” with a probability 1. Here works classical physics and every particle is a local object with its individual characteristics. This is the case if the particles have no interaction with each other, but if they have interacted earlier then entanglement may occur. In this

case appears a state which is called sometimes EPR state [Ein-35] and given by:

$$|\psi_{EPR}\rangle = \frac{1}{\sqrt{2}}\left(|\uparrow\rangle_1 \otimes |\downarrow\rangle_2 - |\downarrow\rangle_1 \otimes |\uparrow\rangle_2\right) \qquad (2.8)$$

where $|\uparrow\rangle_i$ and $|\downarrow\rangle_i$ ($i = 1,2$) are the wave functions of the i^{th} spin aligned "up" and "down", respectively. The state (2.8) is an entangled state of two particles. The direction of the spin of each particle is not determined, but there is a quantum correlation between the directions of the spins of the two particles [Bar-01]. Since the total spin of the system in the EPR state is zero, the spins of individual particles are always antiparallel, i.e. anticorrelated.

The properties of entangled states are interesting for potential applications of quantum mechanics like quantum information technology [Deu-98, Kil-99]. The most promising application is quantum cryptography [Eke-92]. More futuristic applications include dense coupling [Ben-92], quantum teleportation [Bou-97], and more generally, quantum networks and other quantum information processing.

2.4. Einstein's incompleteness argument

The entangled states lead to certain features of quantum systems that have no analogs in classical physics and therefore seems very strange compared to the analysis of classical systems. This contradiction between quantum mechanical predictions and classical intuitions became known as the Einstein-Podolsky-Rosen (EPR) paradox and was analyzed in 1935 by the work of Albert Einstein, Boris Podolsky and Nathan Rosen. In this paper they are developed a so called "*Gedanken*experiment" [Ein-35] to argue that quantum mechanics is not a "complete" physical theory.

The argument of EPR-paradox begins with the assumption that there are two particles **A** and **B** after interaction (e.g. which was produced in the result of decay from particle **C**). In this case, according to the conservation of momentum, their total momentum is: $\vec{p}_a + \vec{p}_b = \vec{p}_c$. If, for example, one measures the momentum value of system **A** than by conservation of momentum one can infer the momentum of the system **B:** $\vec{p}_b = \vec{p}_c - \vec{p}_a$ without any disturbance of the motion of this particle.

Therefore, by the measuring coordinate of the second particle, we will manage to receive for this particle the value of two immeasurable simultaneously parameters, that according to laws of quantum mechanics is impossible. In turn, it shows that laws of quantum mechanics must be incomplete.

In summary, EPR argued by means of a gedankenexperiment that quantum mechanics is not a “complete” theory. This incomplete description could presumably be avoided by postulating the presence of some hidden variables that would permit deterministic predictions for microscopic events. So, by knowing this hidden variables of elementary particles one can built a theory, that would be unambiguously predict experimental results and the measurement of characteristics of one particle would not have any influence of the characteristics of another particle that is far away.

2.5. Bell’s inequalities

The EPR-paradox asserted that quantum mechanics is incomplete in terms of a local realism. Bell rendered this argument quantitative and amenable to experimental verification. He showed that any local hidden variable theory will results in an inequality, which can contradict quantum mechanical predictions. In 1964 he calculated the differential cumulative probabilities for correlated photons [Bell-64], assuming the *truth* of Einstein's condition of locality.

The main principle in the objective local theory can be written as:

1. Each particle is characterized by a number of variables (f.g. wave function), which are possibly correlated for two particles;
2. The results of measurements on one particle do not depend on whether the other particle is measured or not, and if it is, they do not depend on the result of such a measurement;
3. The characteristics of statistical ensembles (and therefore the statistics of measurement) depend only on the conditions that existed at earlier time.

Bell’s theorem showed that the objective local theory and quantum mechanics give different predictions as to the statistics of the results of measurements. According to quantum mechanics, the value of a certain

combination of correlations for experiments of two distant systems can be higher than the highest value allowed by any local-realistic theory proposed by Einstein, Podolsky and Rosen [Ein-35], in which local properties of a system determine the result of any experiment on that system.

The original inequality that Bell derived was:

$$\left|P(a,b)-P(a,c)\right| \le 1+P(b,c) \qquad (2.9)$$

where P - is a correlation function of the particle pairs

a,b,c -unit vectors.

If the results violate the inequality, than it is in principle not possible to build a theory with a hidden variables and the results would support the non-locality of quantum mechanics. Non-locality means that even though particles are separated from each other, they are still considered as one unit and acting on one part you affect the other part instantaneously. As example, if one photon is polarized in, for example, the vertical direction, the other will be always polarized in the horizontal direction, no matter how far away it is.

Bell's original formulation of the inequalities was idealized and not readily suited to realistic experimental conditions. After the appearance of the first Bell inequalities, many similar relations have been derived [Cla-78] that are more experimentally amenable. The more known examples are the Bell-Clauser Horne (BCH) inequality [Cla-74] and Clauser-Horne-Shimony-Holt (CHSH) inequality [Cla-69] which is described in terms of correlation functions by considering the correlations between measurements performed on two entangled spin-1/2 particles. The CHSH inequality is:

$$S\left(\Theta_1,\Theta_2,\Theta_1',\Theta_2'\right)=\left|E\left(\Theta_1,\Theta_2\right)-E\left(\Theta_1',\Theta_2\right)\right|+E\left(\Theta_1,\Theta_2'\right)+E\left(\Theta_1',\Theta_2'\right)\le 2 \qquad (2.10)$$

Θ_1,Θ_1' - are two values of angles for the first spin analyzer.

Θ_2,Θ_2' - are two values of angles for the second spin analyzer.

In Eq. (2.10) the quantities $E\left(\Theta_1,\Theta_2\right)$ are expectation values:

$$E\left(\Theta_1,\Theta_2\right)=\frac{N_{\uparrow\uparrow}\left(\Theta_1,\Theta_2\right)-N_{\uparrow\downarrow}\left(\Theta_1,\Theta_2\right)-N_{\downarrow\uparrow}\left(\Theta_1,\Theta_2\right)+N_{\downarrow\downarrow}\left(\Theta_1,\Theta_2\right)}{N_{total}} \qquad (2.11)$$

$N_{\uparrow\downarrow}(\Theta_1,\Theta_2)$ - is the number of pairs of particles for which analyzer 1 (oriented in direction Θ_1) would give spin up for particle 1 and analyzer 2 (oriented in direction Θ_2) would give spin down for particle 2. Definitions for the other N's are analogous.

N_{total} - is the total number of pairs of particle.

This inequality is experimentally testable if the detectors have 100% efficiency otherwise some extra assumptions should be made.

The inequality will never be violated by a local hidden variables theory. It will be maximally violated by a factor $\sqrt{2}$ by quantum predictions of a maximally entangled state. So, Bell and others showed that it was possible to distinguish between quantum mechanics and these hidden-variable theories in a certain type of an experiment to measure a parameter known as S. Put simply, the local theories predict that S will always be less than two, whereas the quantum prediction is $S = 2\sqrt{2}$. When S is more than two, Bell's inequality is said to be violated.

In contrast to CHSH, the BCH inequality is:

$$S(\Theta_1,\Theta_2,\Theta_1',\Theta_2') = \frac{R_{\uparrow\uparrow}(\Theta_1,\Theta_2) - R_{\uparrow\uparrow}(\Theta_1,\Theta_2') + R_{\uparrow\uparrow}(\Theta_1',\Theta_2) + R_{\uparrow\uparrow}(\Theta_1',\Theta_2')}{R_{1\uparrow}(\Theta_1') + R_{2\uparrow}(\Theta_2)} \le 1 \quad (2.12)$$

$R_{\uparrow\uparrow}(\Theta_1,\Theta_2)$ - the experimental coincidence count rates when both particles are detected with spin up in the directions Θ_1 and Θ_2 respectively.

$R_{1\uparrow}(\Theta_1')$, $R_{2\uparrow}(\Theta_2')$ - single count rates at detectors 1 and 2, respectively.

In the case of BCH inequality it is not necessary to simultaneously measure both projections. The BCH inequality is especially important because it provides a direct constraint on the experimentally observed detection count rates; it does not require any additional assumptions for experimental implementation [Edw-01]. However, it is depending on the detector efficiency, which is proportional to the ratio between coincidence rates and the single rates. Therefore, Eq.(2.12) can only be used for a definitive test if the detectors have a very high efficiencies.

Except the tests of Bell inequalities there exists another fundamental application of entangled states which consists in the studies of decoherence in

quantum systems. Decoherence is the process in which quantum superposition loose their coherence owing to the interaction with the environment [Joo-85, Men-00].

2.6. Experimental tests of Bell's inequalities

Many experiments have been performed to check Bell's inequality. Till date, the experiments have yielded results in agreement with quantum mechanics, but in disagreement with a local realistic theory. More details of some experiments concerning test of the Bell inequality are summarized in [Cla-78, Asp-99]. In this paragraph only a very short overview is presented.

The first experiment to verify the inequality of Bell was the measurement of the correlation of polarization of positronium annihilation γ rays by Kasday [Kas-71], [Kas-75]. Here the positrons were emitted by a ^{64}Cu source, stopped and annihilated in copper. Agreement with quantum mechanics was obtained. Later the correlation of polarizations of photons of an atomic cascade was studied by Freedman and Clauser [Fre-72] and again an agreement with QM was obtained.

The experiment with atomic photons has the advantage that in atomic physics it is possible to built polarization analyzers of nearly 100% transmission and analyzing power, which is not the case for the experiment with annihilation γ rays and especially for the electron spin resolved coincidence measurements [Ber-09a].

An experiment very similar to [Kas-71] (but with ^{22}Na as a source) was performed by Faraci et al [Far-74] with very different results. Their data disagree sharply with the quantum-mechanical predictions and are at the extreme limit permitted by Bell's inequalities. Their data also showed a variation in correlation strength which depends upon the source-to-scatterer distances. However, it was difficult to conjecture whether or not a systematic error is responsible for these results.

This experiment has been repeated by Wilson et al [Wil-76] with using ^{64}Cu as a source. In contrast with [Far-74] they found complete agreement with the QM predictions, and no significant variation of the correlation strength when the scatterer positions were changed.

The experiments by [Far-74] have been repeated by Bruno et al [Bru-77] also using ^{22}Na as a source, but used alternatively Cu and Plexiglas as the annihilator. To discriminate against multiple scattering events they imposed sum-energy restriction and also varied the scatter sizes. Again, for any of various source-scatter distances no violation of the quantum-mechanical prediction was observed.

To summarize, numerous experiments to measure polarization correlations between entangled photon pairs have been made in order to demonstrate that Bell's inequality is violated. Somewhat older examples are positronium decay, atomic cascades, (see also [Fry-76, Asp-81]), and parametric down conversion lasers [Shi-88, Kie-93, Kwi-95, Wei-98]. Recently, experiments using $^{9}Be^{+}$ ions [Row-01] and a hybrid system of an atom and a photon [Moe-04] have been performed.

All this experiments relied on entangled systems produced by electromagnetic (EM) interactions, with exception of Lamehi-Rachti and Mittig (described in some details below), and Polachic et al [Pol-04]. These experiments also show a good agreement with quantum mechanics. Recently, the results of test of the local hidden variable theories (Bell-CHSH) involving strongly interacting pairs of massive spin ½ hadrons from the decay of ^{2}He spin-singlet states have been performed by [Sak-06]. The spin correlation function is deduced to be $S_{\exp}(\pi/4) = 2.83 \pm 0.24_{stat.} \pm 0.07_{sys}$. This results is in agreement with non-local quantum mechanical predictions and it violates the Bell-CHSH inequality of $|S| \leq 2$ at a confidence level of 99,3%.

However, despite a substantial number of experimental tests of the Bell inequalities, no experiments to date have been entirely loopholes free [Cla-74, Zei-86, San-96] (f.g, spatial correlation loophole, the detection efficiency loophole, communication loophole and etc.). So, the quest for a final answer in the test of Bell inequalities and thus the answer to the question whether or not quantum mechanics is a complete theory creates new ideas for more and more refined experiments.

2.6.1. Proton-proton scattering experiment

An experiment with a measurement of the spin correlation in low-energy proton-proton scattering has been performed by M. Lamehi-Rachti and W. Mittig in 1976 [Lam-76]. It is described in some detail here, because it is

more related to our experiment. The schematic experimental setup for the measurement of the spin correlation in proton-proton scattering is shown in Figure 2-3 (left). A beam of protons from Saclay tandem accelerator with an energy of $E_p = 13.2$ MeV hits a target containing hydrogen. After scattering, the two protons enter in coincidence into the analyzer at $\Theta_{lab} = 45°(\Theta_{c.m.} = 90°)$. In the analyzers the protons are scattered by a carbon foil (surface mass density $18.6 mg/cm^2$) and the coincidences between the detectors of one analyzer with detectors of the other are counted. The detectors of one analyzer are in the reaction plane, and the detectors of the other rotated by an angle Θ around the axis defined by the protons entering in the analyzer.

Than the measured correlation function is:

$$P_{meas}(a,b) = \frac{N_{LL} + N_{RR} - N_{RL} - N_{LR}}{N_{LL} + N_{RR} + N_{RL} + N_{LR}} \qquad (2.13)$$

N_{LL} - are the coincidence between the left counters L_1 and L_2, and so on.

For comparison this correlation function with the inequality of Bell some additional assumptions are necessary, [Lam-76].

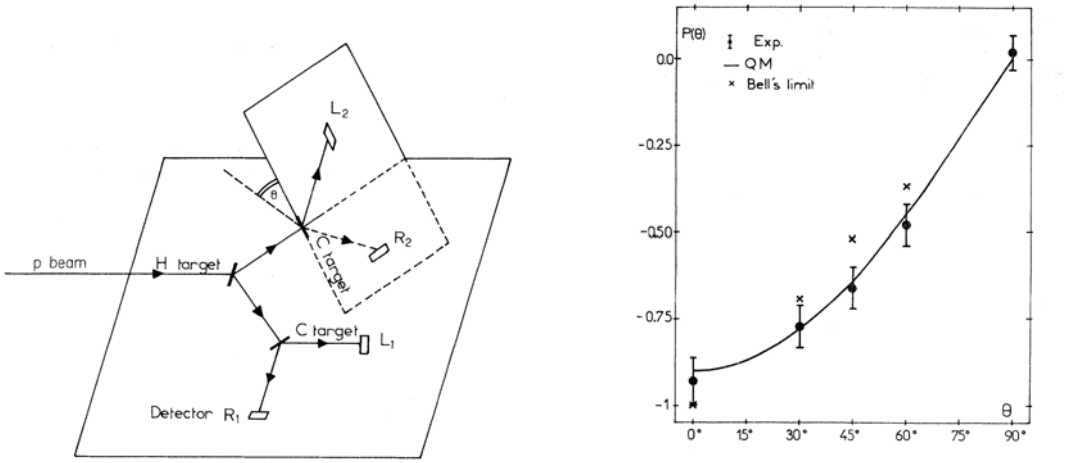

Figure 2-3: Schematic experimental setup for proton-proton scattering (left) and experimental result (right).

The experimental results for the correlation function $P_{\exp}(\Theta)$ compared to the limit of Bell and the predictions of quantum mechanics are presented in Figure 2-3 (right). As can be seen, they obtain a good agreement with the

quantum-mechanics predictions. If one accepts their assumptions, then Bell's inequalities are violated.

For an electron-electron scattering experiment similar results are expected with the requirement that the spin entanglement for electrons is not destroyed before measurement.

2.7. Electron-electron scattering

The scattering experiment with charged fermions (e.g. electrons or protons) is presented in the Figure 2-4. Suppose, a vertical (e.g. up) polarized electron beam is scattered at a reverse (down) polarized electron target with the scattering angle in the center of mass $\Theta = \pi/2$ [Jac-01].

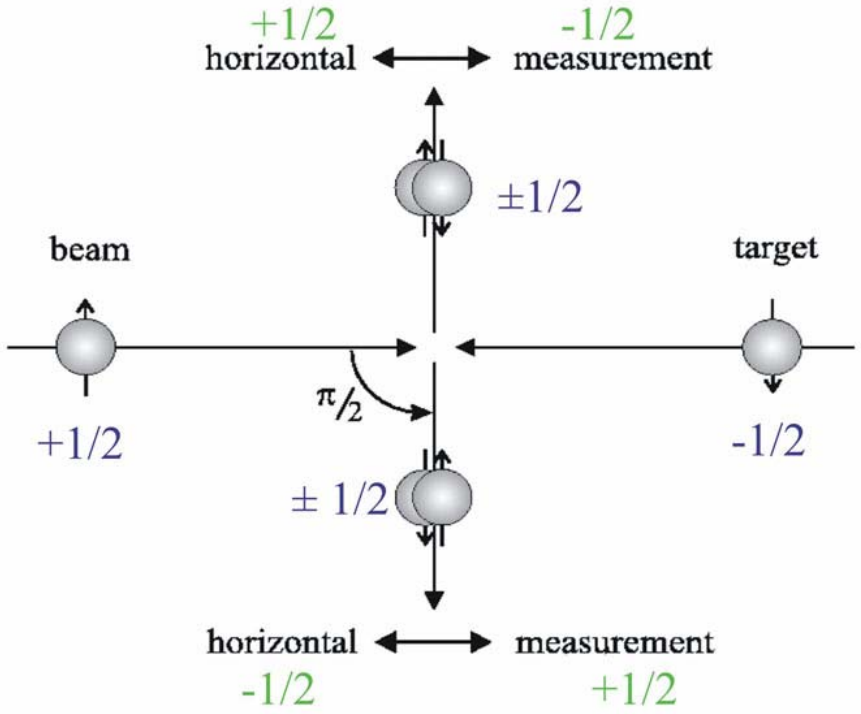

Figure 2-4: A spin up polarized beam is scattered at a spin down polarized target. The scattered particles at $+\pi/2$ and at $-\pi/2$ have an equal probability to originate from beam or from target. Thus, the average polarization at each branch is zero, but to each particle with spin up belongs a second particle with spin down from the other branch.

The measurement of a horizontal spin leads to a complementary quantum information compared to a vertical spin measurement. Each horizontal spin measurement has an equal 50% probability for a spin pointing left or right

after the measurement. Thus, two independent measurements have a 50% probability to obtain either identical indistinguishable or not identical distinguishable spin directions. Due to the Eq. (2.6) all scattered particles are initially distinguishable. This has not to change for measuring the horizontal spin components instead of the vertical spin components after scattering. Indistinguishable fermions pairs are not allowed to scatter at $\Theta = \pi/2$, because the cross section for such particles is zero according to Eq.(2.5).

If for one of these measurements a horizontal spin component (e.g. right) is detected, then the measurement at the second position has to result in the opposite spin direction (left). The spin measurement of the two electrons is not independent, but correlated. In turn, an observation of this spin correlation is considered as the experimental prove of coherence. Of course here, no information could be transmitted between any two points with fasterthan light velocity, because the value of the horizontal spin (left or right) measured at these points in a single measurement can not be predicted.

2.8. Threshold energy

For usual which-path experiments low particle energy is preferable in order to increase the de-Broglie wavelength in an interferometer. Whereas for a scattering experiment a lower threshold exists for a particle's energy where only above this threshold interference effects can be observed [Jac-01]. This is easily understood by calculating the kinetic energy necessary, to bring the particles within a distance given by their de-Broglie wavelength λ_B (Figure 2-5).

For observing interference in the experiment the distance of the particles should be comparable with the de Brogile wavelength λ_B (in the centre of mass system). This in turn causes a restriction to the particle velocity:

$$\lambda_B^{CM} = \frac{h}{m \cdot v} = \frac{h}{\sqrt{2m \cdot E_k}} \qquad (2.14)$$

h - is Planck's constant, m - is the mass, v - the velocity

$2E_k$ - is the total kinetic energy of the particles.

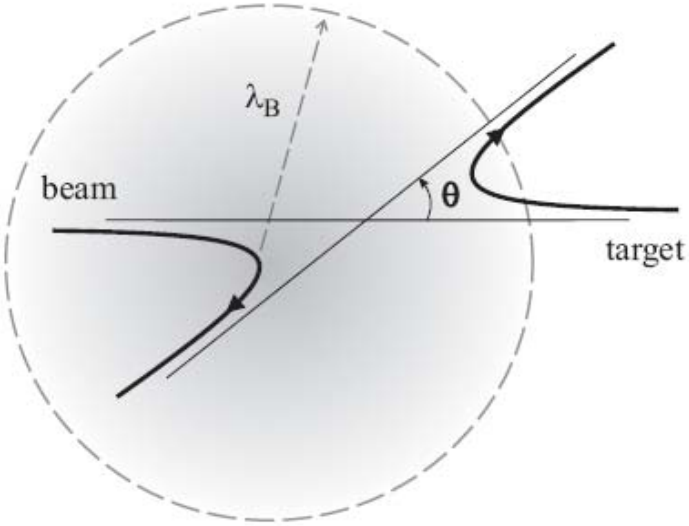

Figure 2-5: The minimal distance between two particles during scattering should be much shorter than the de-Broglie wavelength λ_B of the particles. Within a radius defined by λ_B different possible paths of particles became indistinguishable. Only in this case the quantum mechanical coherent superposition for the cross section should be obtained for elastic scattering.

For a central collision of two identical particles both with kinetic energy E_k, the minimal distance r (in the CM-system) between both particles can be obtained, with the assumption that the whole kinetic energy of the particles is transformed to potential Coulomb energy:

$$r^{CM} = \frac{z^2 e^2}{4\pi\varepsilon_0} \cdot \frac{1}{2E_k} \tag{2.15}$$

e - charge of the particles, z – atomic number of particles.

For maximal distance $r < 2\lambda_B$ the threshold energy of two particles hitting each other inside a distance given by the de-Broglie wavelength:

$$E_k = \frac{m}{8}\left(\frac{z^2 e^2}{4\pi\varepsilon_0 h}\right)^2 \tag{2.16}$$

For the minimal distance $r < \lambda_B$ the threshold energy E_k yields to:

$$E_k \geq \frac{m}{2}\left(\frac{z^2 e^2}{4\pi\varepsilon_0 h}\right)^2 \tag{2.17}$$

According to the relation (2.17) the threshold energy to observe quantum effects for two scattered electrons is $E_k \leq 0.37eV$. The minimal distance r decreases linear with the kinetic energy E_k, but the de-Broglie wavelength λ_B decreases with the root of E_k. Because of this higher kinetic energies bring the particles even closer inside the required distance. This is consistent with the observation that a reduced interference of elastic scattering is observed even at relativistic electron energies [Kes-85].

At lower kinetic energies the two different paths of target and beam ion remain in principle distinguishable and consequently no interference effects are expected for electron-electron scattering below this threshold energy [Jac-01]. However, there is no experimental verification have been performed. At least it is not known to the author.

As example, the experimental verification of the quantum threshold effect could be done by investigation of the threshold energy for the beam particles with target particles of the same species (e.g. electrons with electrons, protons with protons, deuterons with deuterons etc.) between minimal ($r < \lambda_B$) and maximal distance ($r < 2\lambda_B$) [Jac-07].

The effect of quantum threshold is well known for many experiments, where usually the particle velocity or the temperature has to be minimized. E.g. in a Bose-Einstein condensate or in superconducting materials the temperature has to be decreased to observe the desired quantum effect. Similar results are observed in interference experiments with particles.

As example, for bosons we have especially the choice of using spin 0 particles like ^{12}C or ^{4}He which would allow obtaining the full quantum cross section for all events.

Of course, many experiments have been performed to determine the cross section for elastic scattering and indeed the reduction of the cross section for a scattering angle $\Theta = \frac{\pi}{2}$ has been observed. For protons even two experiments are known, which observe a spin anti-correlation for elastic scattering. The observation of a quantum threshold for elastic scattering is however not known to the author.

According to the relation (2.16 and 2.17) the threshold energy where the observation of quantum effect for two scattered particles (protons P, helium He and carbon C) are expected shown in the Table 2.1.

Table 2.1: The threshold energy for observing quantum effects.

	P (keV)	^{4}He (keV)	^{12}C(MeV)
$r<\lambda$	1.263	80.836	19.64
$r<2\lambda$	0.315	20.209	4.9

The investigation of the threshold energy between minimal distance $r < \lambda_B$ and maximal distance $r < 2\lambda_B$ should gives observation of the quantum threshold effect. This experimental verification of the quantum threshold effect is not described further and has been presented here shortly as a next possible experiment [Jac-07].

3. Mott scattering electron polarimetry

This chapter describes mainly the Mott analyzer that is used to measure electron spin polarization. Firstly, some introduction in the physics of polarized electrons and concept of the Mott polarimiters are given. The principle of Mott scattering together with the main difficulties that are caused by multiple and plural scattering and instrumental asymmetries is shortly described. Further important parameters of the Mott analyzer as analyzing power (Sherman function) and efficiency (figure of merit) are also discussed here.

In the second part of this chapter some of the experimental setups and results are presented. The experimental facility at U Mainz where the calibration of the Mott analyzer with a known polarized beam was performed is described. In addition, a new design of a compact mini-Mott spin analyzer with a better performance is presented.

3.1. The concept of polarized electrons

Electrons are polarized if the spins are oriented in some preferred direction [Kes-85]. The analogy to polarized electrons is a polarized light in which it is the field vectors that have a preferred orientation. If all spins have the same direction then the electrons are totally polarized. If only a majority of the spins have the same direction, the ensemble of electrons is called partially polarized.

The idea that electrons have an intrinsic spin angular moment and associated spin magnetic moment was introduced in 1925 by Goudsmith and Uhlenbeck [Uhl-25] to explain the fine structure of certain atomic spectral features. In 1929 Mott has raised the question how the physical effects caused due to electron spin could be observed directly [Mot-29]. As example, the Stern and Gerlach magnet has been used to detect the polarization of atoms by

sending an atomic beam through an inhomogeneous magnetic field. When an alkali atomic beam passes through this magnet, it splits into two beams with opposite spin direction of the valence electrons. For the production of polarized beam one can eliminate one of these beams hence causing an intensity loss of a factor 2. This is similar to the production of polarized light by sending unpolarized light through an optical polarizer. But conventional spin filters, like Stern-Gerlach magnets; do not work with free electrons. This is because the Lorentz force which does not appear with neutral atoms arises in the Stern-Gerlach magnet [Kes-85]. This, together with the uncertainty principle, prevents spin-up and spin-down electrons from being separated by a macroscopic field of the Stern-Gerlach setup.

So, Mott proposed that spin magnetic moment could be detected in a double scattering experiment in which a beam of unpolarized electrons is initially scattered at high energies from high-Z nuclei in a target beam or foil. In 1942 Shull, Chase and Myers [Shu-43] demonstrated the existence of a scattering asymmetry that was in agreement with Mott's calculated value.

The main problem in polarized electron studies at keV-particle energy is rather the low efficiency of usual electron polarimiters. As example, scattering of unpolarized electrons by heavy atoms yields highly polarized electrons. However, one does lose of several orders intensity and not only a factor 2, as with conventional polarization filter. For polarization experiments one also needs a sensitive analyzer as well as efficient polarizer for the polarization. The two factors together easily make an intensity reduction for the measurement of a factor of 10^6 or more.

In summary, there are many reasons for the interest in polarized electrons. One of the essential reasons is that for physical investigations it is important to define initial and/or final states of the system being considered. For many measurements it is important to have electrons available in well-defined spin states and to be able to select electrons of uniform energy for the investigation of the large number of spin dependent process (e.g. from bombarding a target or observing the excitation of particular energy states of atoms). Additional information concerning many physical processes can be obtained through spin-dependent measurement: like the investigation of parity violation in high energy nuclear scattering [Pre-78], spin dependent

effects in atomic collisions [Kes-85], the analysis of surface magnetization of solids [Koi-86, Rob-88] or even spin resolved coincidence experiment to determine the entanglement of electrons [Jac-01, Ber-09a].

3.2. Spin-orbit interaction

Electron beams can be polarized by scattering, in analogy to the case of light beams. The angular distribution of scattered electrons depends on the state of the polarization of the incident beam. These effects can be treated by the Dirac equation, which is the basic equation for describing the electron, including spin and spin-orbit coupling.

Dirac discovered this equation in 1928 when he tried to find a relativistic generalization of the Schrödinger equation. In some detail it is described in [Kes-85], here only some of the main principles are presented.

The Dirac equation describes:

1. Relativistic electrons
2. Spin ½ of electrons
3. The magnetic moment $\varepsilon\hbar/2mc$ of electrons (in CGS-system)
4. Spin-orbit coupling

If we consider electrons in external fields, then the Dirac equation is:

$$\left[H - \varepsilon\phi - c\vec{\alpha} \cdot \left(\vec{p} - \frac{\varepsilon}{c}\vec{A} \right) - \beta mc^2 \right] \psi = 0 \qquad (3.1)$$

with H - the Hamiltonian function, ϕ and $\vec{A}$ - is the electric and magnetic potentials, ε - the electron charge$=-e$, $\vec{p}$ -momentum, m -rest mass.

To compare it with the Schrödinger equation it should be reduced to the normalized form and by multiplying out and making the approximation that the kinetic and potential energies are small compared with the rest energy mc^2 so that two components of the spin function can be neglected. Than we obtain the following equation:

$$\left[\frac{1}{2m}\left(\vec{p}-\frac{\varepsilon}{c}\vec{A}\right)^2+\varepsilon\phi-\frac{\varepsilon\hbar}{2mc}\vec{\sigma}\cdot\vec{B}+i\frac{\varepsilon\hbar}{4m^2c^2}E\cdot\vec{p}-\frac{\varepsilon\hbar}{4m^2c^2}\vec{\sigma}\cdot\left(\vec{E}\times\vec{p}\right)\right]\psi=W\psi \qquad (3.2)$$

where $W+mc^2$ - is the total energy.

The first two terms on the left are identical to the Hamiltonian operator of the Schrödinger equation for external fields. The third term corresponds to the interaction energy $-\vec{\mu}\cdot\vec{B}$ between an external magnetic field and a dipole moment of:

$$\vec{\mu}=\left(\varepsilon\hbar/2mc\right)\vec{\sigma}$$

The fourth term is a relativistic correction of the energy and has no classical analogue. The last term describes the spin-orbital coupling. The spin-orbit interaction can be illustrated in the following way:

The polarization effects in scattering are caused by spin-orbit coupling, or in other words, by the magnetic field which the electrons experience in their rest frame. The charged scattering center moves in the rest frame of the electrons; the current that is represented by this moving charge produces a magnetic field by:

$$\vec{B}=-\frac{1}{c}\vec{v}\times\vec{E}=-\frac{1}{mc}\left(\vec{E}\times\vec{p}\right) \qquad (3.3)$$

So, in its rest frame, an electron moving relative to the electric field of an atomic nucleus experiences this magnetic field which affects its spin. The energy of the electron, due to its magnetic momentum $\vec{\mu}$, in this field is:

$$-\vec{\mu}\cdot\vec{B}=-\frac{\varepsilon}{mc}\vec{s}\cdot\vec{B}=-\frac{\varepsilon}{m^2c^2}\vec{s}\cdot\left(\vec{E}\times\vec{p}\right)$$

If we substitute the spin operator $\left(\hbar/2\right)\vec{\sigma}$ for $\vec{s}$, we obtain the fifth term in the Hamiltonian operator (3.2). The additional factor of 1/2 should be included to take into account Thomas precession (in changing the frame of reference, the time transformation changes the precession frequency of the electron spin in the magnetic field) [Tho-26].

The term:

$$-\frac{\varepsilon\hbar}{4m^2c^2}\vec{\sigma}\cdot\left(\vec{E}\times\vec{p}\right) \qquad (3.4)$$

is called the spin-orbit energy, as it arises from the interaction of the spin with the magnetic field produced by the orbital motion of the electron.

3.3. Mott polarimetry

The polarimiters based on Mott scattering are extensively used in atomic and molecular, solid state, nuclear, and high-energy physics. For higher energies the electron spin polarization is frequently measured using the Mott analyzer, which takes advantage of the left-right asymmetry observed in scattering of transversally polarized beams from thin gold targets. The majority of Mott analyzers involve scattering from gold targets. Gold is selected because of it's high $Z = 79$ which leads to large value of the Sherman function S. Gold is nonreactive and does not form a thick oxide layer and thin gold films, which reduce multiple and plural scattering are easy to fabricate. Thorium and uranium, having a higher Z, provide a higher sensitivity, but they are not as accessible as gold and are not as easily fabricated into foils.

Mott scattering serves as a research standard for measuring electron spin polarization since the late 1950^{th} [Fra-57]. For earlier studies a design nowadays called 'conventional' Mott polarimeter [Jos-66, Lan-85, Wai-78] has been used, where transverse polarized electrons are first accelerated to approximately 100 keV in a conventional accelerating column and subsequently forced to strike thin gold foil targets.

Conventional Mott scattering devices are rather cumbersome because of their bulky high voltage accelerating column is and in part because their electron detectors and target must be maintained at high voltage. In addition discrimination against inelastically scattered electrons is poor.

A better discrimination against inelastically scattered electrons is achieved by retarding-potential Mott polarimeters [Hod-79, Cam-85, Uhr-89, Ran-90]. In these polarimeters the incident electrons are accelerated by an electric field established between an inner and outer electrode. The outer electrode is operated near ground potential, the inner electrode at a large positive potential. So the electrons scattered from a target exit the inner electrode and are decelerated as they pass again to the outer electrode. Scattered electrons with sufficient energy to overcome the retarding field are detected by two symmetrically positioned detectors.

One significant advantage of high-voltage cylindrical polarimeters is, that if a very thin target foil is used, the majority of the incident electrons will pass through the target foil without significant scattering and can transit the entire instrument with little degradation of the beam quality or energy distribution. Another advantage is that at high energies the value of analyzing power is relative large, while the effects of plural and multiple scattering in the target are minimized. It makes high precision polarization measurements easier. However, it also leads to low statistical efficiencies because the scattering cross section decreases with increasing energy.

Mott polarimeters have been also employed in the overwhelming majority of investigations involving polarized electrons at low energies like mercury-vapour [Dei-65, Jos-81] and low-energy diffuse [Ung-86, Sch-89, 90] scattering Mott polarimeters. These polarimeters combine a high efficiency with small size. The better efficiency is provided due to the specifically design that allows to increase the solid angle over which scattered electrons are detected. Low-energy electron scattering is, however, strongly influenced by multiple and plural scattering.

In summary, while the compact Mott devices greatly improve the ease with which electron polarization can be measured, they still suffer in some aspects of the same limitations of the conventional Mott polarimeter. The weak point in the efficiencies of all analyzers is the ratio I/I_0 (detected electron current I referred to the incident current I_0) rather than S_{eff} (effective asymmetry function of the analyzer). Each of this expression should be unity in an ideal case. Usually, S_{eff} is larger than 0,2, whereas even for thick gold foils the efficiency value I/I_o is typically only in the range of 10^{-3} or even much less, which in turn causes a figure of merit FOM of the order of 10^{-4} or smaller. For comparison, the corresponding value for an analyzer of polarized light is near 1. A Mott detector of this quality would have to scatter all the electrons of a totally polarized incident beam towards to one of the detector [Kes-85]. This difference between optical and electronic properties is the explanation for the big success of quantum optics in recent years. Typical quantum optics experiments looking for spin entanglement like teleportation, encryption, cloning etc. require a photon spin coincidence measurement with high efficiency.

3.3.1. Principle of a Mott scattering

If a beam of electrons is scattered in a Mott polarimeter from a high Z-target into two detectors at equal polar angles and opposite azimuthal angles [Kes-85] the electron polarization transverse to the scattering plane P is determined as

$$P = A/S \tag{3.5}$$

where S - is asymmetry function (well known as a Sherman function)

A - scattering asymmetry.

Equation (3.5) is the basis of Mott electron polarimetry. A more detailed presentation of the physical basis of Mott scattering by using a classical picture is given in [Gay-92].

The left-right asymmetry which is observed in the scattering of a polarized electron beam can be interpreted in Figure 3-1.

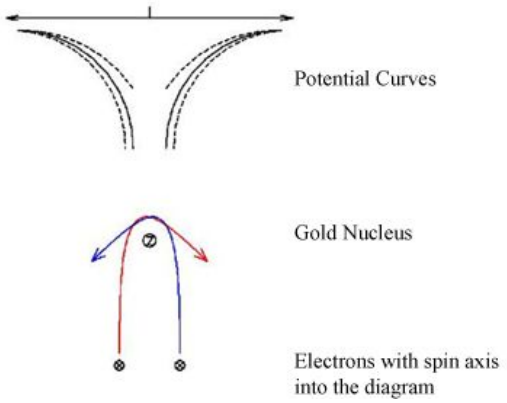

Figure 3-1: The principle of Mott scattering with the potential curve with (---) and without (——) spin-orbit coupling for electrons with spin up and down.

In the following we consider a single electron scattering from a high Z gold nucleus. In the resulting interaction of the spin of electrons with his orbital momentum the cross sections of the two beams with opposite polarization differ slightly from each other because the scattering potential essentially consists of the electrostatic V_0 and the spin-orbit potential V_{ls}:

$$V = V_0 + V_{ls}$$

Since V_{ls} contains the scalar product $l \cdot s$, it has different signs for electrons of the same orbit but different spin directions.

In this case the resulting scattering potential would be higher or lower for electrons with spin up than for electrons with spin down, depending on which side of the atom they pass. The electrons which pass the atom on the left, i.e., that are scattered to the right, experience a stronger potential than those scattered to the left. Different scattering potentials cause different scattering intensities and this leads to an asymmetry in the left/right scattering probabilities:

$$A = \frac{N_L - N_R}{N_L + N_R} \tag{3.6}$$

where N_L and N_R are the currents detected in the left and right channels of the polarimeter.

3.3.2. Multiple and plural scattering

One cannot simply use the theoretical value of the Sherman function S_{th} which was calculated for single scattering by one atom. Every target contains so many atoms that plural or multiple scattering processes also occur.

Multiple scattering describes the large number of small angle deflections which normally precede and follow a single 120° elastic scattering event in a thick foil. Plural scattering describes a sequence of two or three large-angle scattering events after which an electron emerges with a resultant deflection of 120°. If, for example, making a measurement at 120°, we would detect not only electrons that have been once scattered through 120°. But also electrons that have been scattered by more than two consecutive processes, as example, three times through the angle of 40°, or scattered once through the angle α and then through 120°-α. The probability of such plural processes increases as the number of atoms in the target increases.

The majority of Mott polarimiters make use of solid targets to increase the scattered electron signal. But a disadvantage of this, that the detected electrons may have suffered scattering from more than one atom in the target. Such plural scattering can significantly reduce S_{eff} because, for gold, the Sherman function in case of 120 keV for 40° scattering is only-0.014, whereas

for 120° scattering it is -0.4. Multiple scattering can also reduce S_{eff} but is generally not so important than plural scattering for total scattering angles more than 90° [Gay-92].

So, the thicker the target foil, the more important become these two processes. Electrons which arrive at the counters after several consecutive scattering processes usually reduce the asymmetry measurement. This is illustrated in the Figure 3-2 which shows, the asymmetry measurement for scattering 40-keV polarized electrons at gold targets of various thickness [Uhr-89]. Decreasing the inelastic energy loss window ΔE also leads to increased asymmetry.

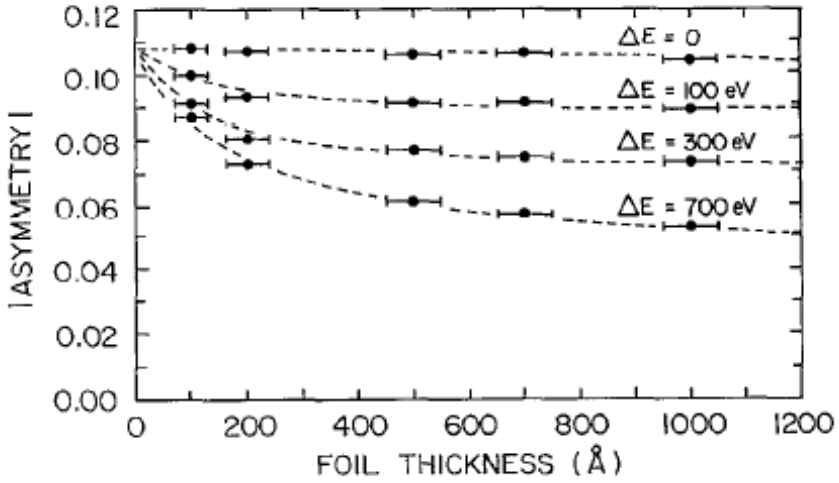

Figure 3-2: Observed asymmetry A for scattering of 40-keV polarized electrons at 120° as a function of (gold) target thickness for different inelastic energy loss windows ΔE (taken from Ref. [Uhr-89]).

Background electrons can arrive at the counters not only due to the plural scattering in the foil but also due to reflection at the walls of the scattering chamber. As example, some typical cases:

- unscattered electrons from the incident beam are reflected on the chamber wall and, after hitting the foil arrive to detectors,
- scattered electrons from the walls of chamber are scattered directly into a detector,
- electrons from the incident beam reach a detector after double reflection at the wall.

In order to suppress spurious electrons it is advantageous to make a coating of the chamber with a material having a small backscattering coefficient (small atomic number, such as carbon). Using apertures and good energy resolution of the counters can help to discriminate against the backscattered electrons since they loose a large fraction of their energy due to the reflection.

3.3.3. Sherman function

In order to determine the polarization P from the asymmetry $PS(\Theta)$ observed in a Mott analyzer it is necessary to know the accurate value of analyzing power of the apparatus S_{eff}, which is often called the "effective Sherman function".

The Sherman function could be measured using either by a double-scattering experiment, or by using a beam of electrons of known polarization by observing the scattering asymmetry. In a double scattering experiment an unpolarized beam is scattered through the angle Θ' (Figure 3-3).

The scattered beam which has a polarization then hits a second target of the same kind. The respective numbers of electrons N_l and N_r scattered through the same angle Θ' to the left and to the right are measured:

$$\frac{N_l - N_r}{N_l + N_r} = S^2(\Theta') \qquad (3.7)$$

So that one obtains the value of $|S|$ for the angle Θ'.

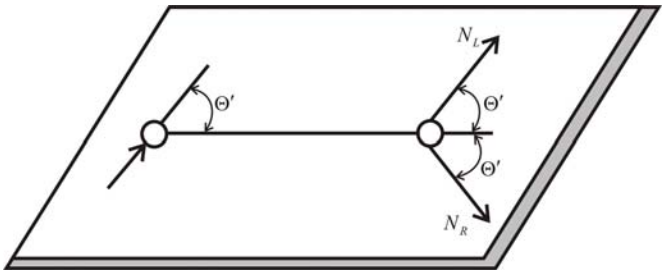

Figure 3-3: Scheme of the double scattering experiment.

The angular dependence $S(\Theta)$ can be found if one varies the first scattering angle and leaves the scattering angle at the second target unchanged. Then one measures:

$$\frac{N_l - N_r}{N_l + N_r} = S(\Theta)S(\Theta') \tag{3.8}$$

As $|S(\Theta')|$ is known from the first experiment, this measurement yields to $S(\Theta)$. But the sign of $S(\Theta)$ is not determined because only the magnitude of $S(\Theta')$ is known. By using a source that produces polarized electrons of known spin direction, one can, however, determine the sign of $S(\Theta')$ by measuring the sign of the left-right asymmetry which arises in the scattering of these electrons through Θ'.

The Sherman function describes two important features: the extent of the asymmetry in the scattering of a polarized beam and the amount of polarization produced by scattering an unpolarized beam [Kes-85].

The Sherman function in the energy range from 25 to 120 keV has a broad maximum at the angle close to $\Theta = 120°$ (Figure 3-4). This scattering angle is mainly used for Mott polarimetry. With decreasing energy the scattering cross section at $\Theta = 120°$ strongly increases.

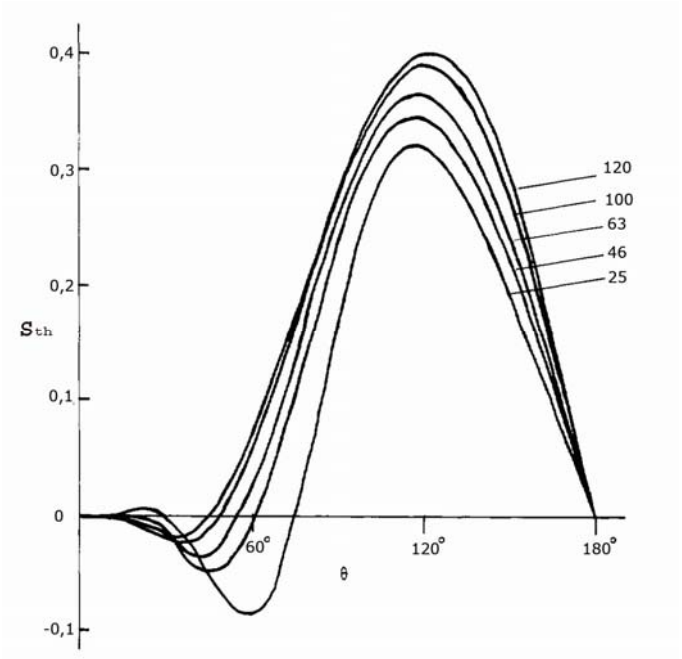

Figure 3-4: The angular dependence of the Sherman function S_{th} for a wide range of energies (in keV), as calculated by Holzwarth and Meister [Hol-64], (taken from Ref. [Cam-85]).

The S_{th} is reduced at lower energies. This effect is even made worse by the effects of plural and multiple scattering which further reduce S_{th} to S_{eff} at low energies. Since these effects cannot be modelled with high accuracy by theory, Mott polarimrters are commonly used at energies well above 50 keV. Only in cases where accuracy is of no concern the statistical advantage of the cross section justifies to usage of lower energies, as it is the case for this work (see section 3.5).Using an energy filter between target and detectors, - as for example, if the electrons are decelerated in a spherical or cylindrical electric field in retarding field poarimiters - gives a possibility to reduce inelastically scattered electrons to yield values of S_{eff} closer to the values S_{th}.

3.3.4. Figure of merit

An important parameter for the performance of the Mott polarimiters is the figure of merit (FOM), which defined as [Kes-85]:

$$FOM = \left(\frac{I}{I_0} \right) S_{eff}^{\ 2} \tag{3.9}$$

where I_0 - is the current entering the polarimiter,

I - is the total scattered current measured by the detectors,

S_{eff} - is again the analyzing power of the apparatus.

The quantity FOM, also known as the “figure of merit,” is proportional to the inverse square of the statistical error in an electron counting experiment to measure the polarization P of an incident beam. To obtain significant left-right asymmetries, large values of the effective Sherman function S_{eff} are desirable. However, at angles where the Sherman function is large, the cross sections, and thus scattering intensities, are small. Therefore one must find a compromise between high scattering intensity I and high asymmetry. So, $S_{eff}^2 I$ should be chose as large as possible, in order to make the statistical error as small as possible. As I also depends on the incident intensity I_0, it is reasonable to use the question (3.9) as a figure of merit when comparing different Mott detectors.

To increase the efficiency of a Mott polarimiter it is necessary to enhance I/I_0, the ratio of scattered to incident beam currents. This could be achieved by increasing the solid angle subtended by the detectors at the target surface. This is simply done by mounting the detectors close to the target, or by increasing the thickness of the target. But the latter can result in a decrease in S_{eff} due to plural and multiple scattering, and it is necessary to find a compromise between the increase of I/I_0 and the decrease of S_{eff}.

However, even if one chooses a foil thickness of about 250nm as typical example the values of I/I_0 still do not exceed 10^{-3} to 10^{-2}. This means that from a thousand polarized electrons, less than ten can be detected. For a Mott detector the efficiency (figure of merit) is in the range 10^{-4}[Rau-84]. In comparison with this an analyzer for polarized light is practically without loss. This is one of the reasons why experiments with polarized electrons are more difficult.

3.3.5. Instrumental asymmetries

Instrumental asymmetries in high-energy Mott polarimeters have been considered in [Gre-60, Kes-85, Gel-91] and only some examples are presented in this thesis. In the polarization analysis by measurement of the left-right scattering asymmetry several sources of errors occur that create uncertainties for the extracted poalrization. For example, even for an unpolarized incident electron beam the measured scattering asymmetry may be nonzero due to instrumental asymmetries. This is caused by different counter efficiencies on the right and left (including difference of the solid angle accepted by the detectors or difference of discriminator settings), by not strictly axial alignment of the incident polarized beam and inhomogeneity of the target or of the beam, etc.

The simplest way to measure such instrumental asymmetries is to replace the target with a low-Z, such as aluminium, for which $S_{eff} \approx 0$. However, low-Z target foils have higher transmission coefficients compare to high-Z, which can result in changes in the spurious background signals at the detectors. This means that the measured asymmetry may not exactly correspond to the one which is appropriate for the high-Z target. The instrumental asymmetries could be also checked by reducing the electron polarization to zero. However,

in this case polarized and unpolarized electron beams should have the same spatial characteristics which are in reality difficult to achieve. The spurious asymmetry could be also eliminated by reversing the polarization direction of the incident beam by rotating the primary beam through an azimuthal angle of 180°. This leads to reversal of the vector normal to scattering plane and thus to reversal of polarization. Such a flip of the polarization results in an inversion of the scattering asymmetry and the number of incident particles and the effective target thickness can be different [Kes-85]. This technique has been perfected in modern day in parity violation experiments where experimental asymmetries are reduced to values below 10^{-6} [Bau-09].

In order to check whether the changes of the beam polarization made to eliminate instrumental asymmetries affect by position and angle of the beam, or if the flipping has effect to the beam characteristic it is useful to monitor spurious asymmetries by two additional detectors which are mounted symmetrically at small angles. With proper positioning of these detectors, it is possible to eliminate the false asymmetries measured by the left and right detectors from a measurement of the real asymmetries. As example, if the angles are chosen in such a way that $S(\Theta) \approx 0$, any asymmetries observed are purely instrumental. This is especially necessary for experiments with magnetic materials where the reversal of the polarization must be carried out by reversal of a magnetic field; the influence of the field on the beam trajectory is otherwise hard to control [Kes-85].

3.4. Calibration of the Mott analyzer

The calibration of the Mott analyzer with a beam of known polarization has been performed in collaboration with the Johannes Gutenberg, Universität Mainz, Institut für Kernphysik.

3.4.1. The experimental setup

A schematically picture of the experimental facility, where a calibration of the Mott analyzer with known polarized beam was performed is shown in Figure 3-5. It consists of an electron gun, a beam transport system and radiofrequency deflector resonator followed by an electron spectrometer [Har-96]. The Mott analyzers that are described in detail below have been

placed after spectrometer with additional pairs of quadrupoles for the better focussing of the incoming electron beam on the gold target.

The electron gun is shown in the inset of the Figure 3-5. It has a triode configuration. Photoemission is excited by an incident laser beam coming from below. The electrons are extracted antiparallel to the laser beam by a 100 kV accelerating voltage. The laser spot at the cathode has a diameter of 0.6 mm. A strained layer Ga $As_{0.95}P_{0.05}$-cathode is used. The thickness of the electron emitting epilayer is 150nm. Details of the electron gun design may be found in Refs. [Rei-95, Aul-97].

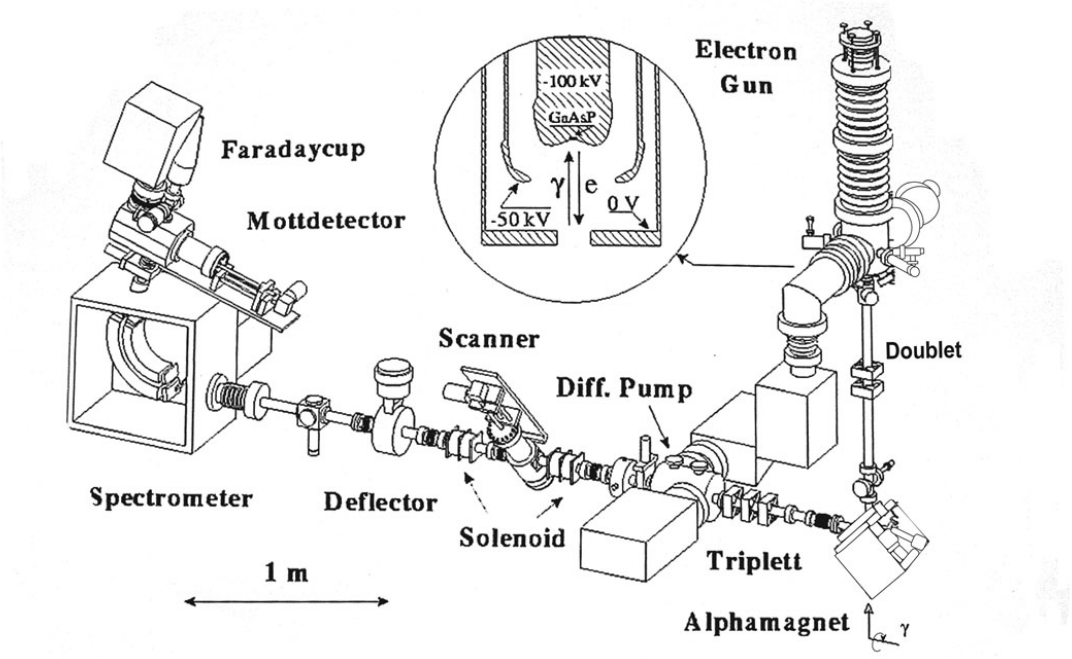

Figure 3-5: Sketch of the experimental setup (the tested Mott analyzer is described in the section 3.4.2 and not shown in this picture).

The laser beam intensity is adjusted with a liquid crystal phase shifter acting between fixed polarizers. Circular light polarization is obtained with the help of a Pockelscell in the beam. The voltage across the Pockelscell may be reversed to switch from positive to negative helicity.

The electron beam transport system consists of a set of five quadrupoles and two double solenoid lenses along the beam line in Figure 3-5. An achromatic, non-isochronic alphamagnet [Ste-93] separates it from the

incident laser beam. The last double solenoid focuses the beam on the entrance slit of an electron spectrometer.

The electrostatic electron spectrometer consists of two toroidal condensator plates. The ratio of two toroidal radii of curvature of 0.85 is chosen to form a stigmatic image of the incident beam spot. The main purpose of the toroidal spectrometer is to transform an incident longitudinal beam polarization into a transverse polarization that can be tested by Mott analyzer.

3.4.2. Mott analyzer

The cylindrical Mott analyzer which has been earlier designed and produced in GSI Darmstadt is presented in Figure 3-6. It has been calibrated with a known polarized beam in the experimental facility that has already been described.

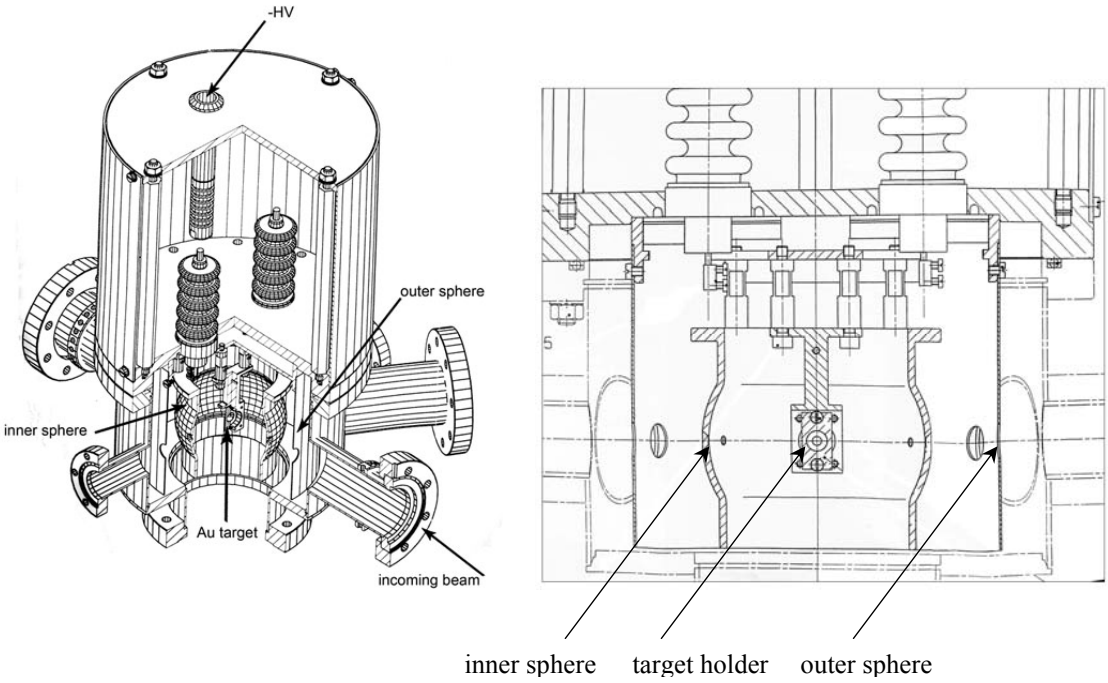

Figure 3-6: The schematically drawing of the Mott analyzer.

The polarized electron beam is coming to the gold target through the outer and inner cylinder with a small slit (of several mm) to prevent suppress background signals. The outer electrode is supposed to be at ground potential, whereas a positive potential may be applied to the inner cylinder, in order to accelerate low energy electrons. Applying the voltage also helps to further

reduce inelastically scattered electrons. The scattering Au-target of 70μg/cm^2 (thickness-36nm) is mounted inside the inner cylinder. The electrons are scattered at the gold target through ±120° (where the Sherman function has a broad maximum) to the direction of detectors. Those electrons that pass through the target foil are collected by a Faraday cup.

Two kinds of detectors have been tested in this Mott analyzer (described in details in paragraph (5.2.2)). The first detector consists of a YAP - Yttrium Aluminum Perovskite doped with Cerium single crystal scintillator disc which is covered with a 50 nm Al entrance window, a quartz view port and a photon counting system. For the second type of detectors the YAP crystal has been replaced by a P47 phosphor scintillator mounted at the same photon counting system.

By reducing a threshold level in a constant fraction discriminator the count rates increase mainly due to additional background signals e.g., by incident electrons that reach the detectors on an indirect path. The incident electrons might reach the detectors by, for example, scattering from the walls or faraday cup and subsequently to the detector. This effect together with a signal electrons with low level signal will result in a decreasing asymmetry as it is demonstrated in Figure 3-7.

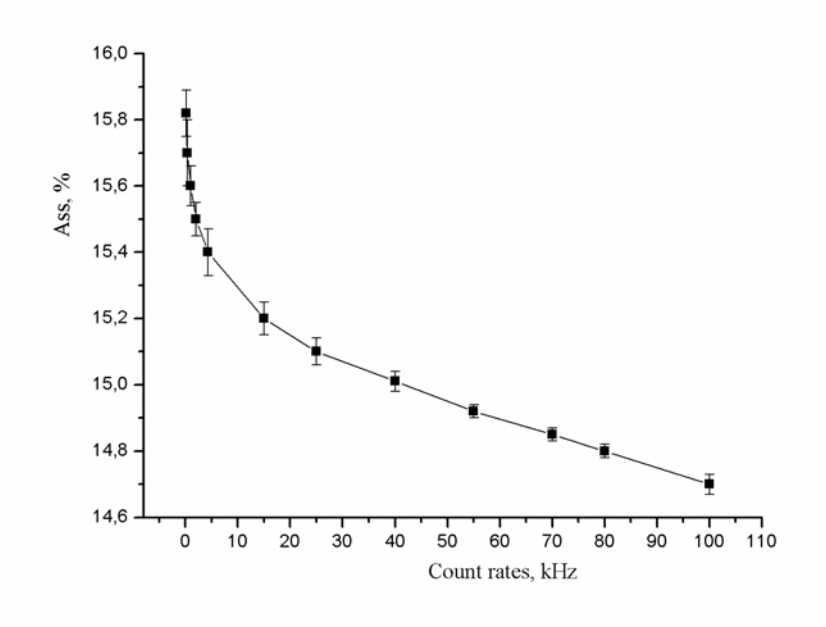

Figure 3-7: Asymmetry in dependence from the intensity coming to the detector by changing threshold level in a constant fraction discriminator.

This influence could be even stronger, but for this Mott analyzer we have reduced this background by tight collimation of the incident beam and by using detectors with a small slit in the entrance spheres (Figure 3-6).

The collimation of the incident beam for reducing background decreases the desired high efficiency which is mandatory for (anti-)coincidence measurements. A better way to reduce the background is to use detectors with a high energy resolution, because the electrons that reach the detectors by indirect paths typically suffer significant energy loss. One way to reduce lower energy background electrons of several keV is realized by covering the scintillators with an aluminium layer that has been performed by these detectors.

The efficiency (sensitivity) of the described Mott analyzer which is calculated by scattered current to the detectors divided by initial current for the initial energy 50 keV with target thickness 100 µg/cm² is $4{,}9 \cdot 10^{-5}$. The Sherman function was inferred from the known polarization of the beam by $S_{eff} = A_{\exp} / P$ and equal ≈ 0.2 where $A_{\exp}$ the observed asymmetry in Mott analyzer. Than according to formula (3.9) gives figure of merit:

$$FOM = \left(\frac{I}{I_0} \right) S_{eff}{}^2 = 4{,}9 \cdot 10^{-5} \cdot S_{eff}{}^2 = 9{,}2 \cdot 10^{-7} \qquad (3.10)$$

To improve the sensitivity which is a prerequisite for the electron spin resolved coincidence measurements a new design of a mini-Mott analyzer (described in paragraph 3.4.3) was developed and also tested with known polarized beam at U-Mainz.

3.4.3. High efficient spin-resolved electron detection with a mini-Mott analyzer

As already mentioned the electron spin-polarization is frequently measured using Mott-scattering from a thin gold target [Kes-85]. The disadvantage of this method is the low efficiency of common electron polarimeters. The previous version of a Mott analyzer has a smaller efficiency that virtually prevents electron spin resolved coincidence measurements, because of the necessarily induced random coincidences in low efficiency spin detectors.

We present here the design and performance of a compact mini-Mott spin analyzer [Ber-09a] (Figure 3-8), of which the efficiency (sensitivity), figure

of merit and the size were improved as compared with our previously designed analyzer. Due to the compact small size the cylindrical-electrode Mott polarimeter achieves high detection sensitivity and we can mount analyzer more narrow to the scattering chamber in order to prevent lost of intensity that have been observed by the previous design.

The polarimeter is mounted on a CF63 and consists of two cylindrical electrodes mounted on an insulator (PEEK). The outer electrode is supposed to be at ground potential, whereas a positive potential may be applied to the inner cylinder, in order to accelerate low energy electrons. The scattering target is mounted inside the inner cylinder. Scattered electrons can be detected at the outer cylinder at an angle of ±120°. The analyzer is symmetric with the possibility to measure in backscattering and in forward scattering direction.

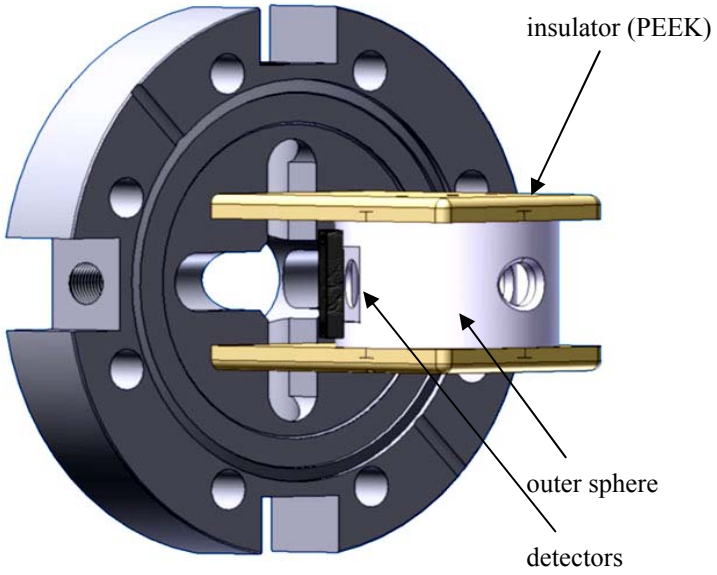

Figure 3-8: Picture of the mini-Mott analyzer.

The sensitivity of this Mott-analyzer has been determined to be in the order of $2 \cdot 10^{-3}$ for an initial energy 40 keV for a thin gold target of 100 µg/cm². That, in turn, by knowing measurement asymmetry with known polarized beam the figure of merit according to formula (3.9) is:

$$FOM = \left(\frac{I}{I_0}\right) S_{eff}{}^2 = 2 \cdot 10^{-3} \cdot S_{eff}{}^2 = 2 \cdot 10^{-5}$$

This value is approximately two orders higher compared to the previous design mainly due to higher value I/I_0, in spite of a smaller value of S_{eff} that have been reduced from 0.2 to 0.1. An asymmetry of 7% for initial energy 30keV was achieved whilst applying +10keV on the target and inner sphere, indicating a beam polarization of $A/S_{eff} = 0.7$. The experimental asymmetry with Magnum (electron multiplier) has been measured of 3-4%. This asymmetry was smaller probably due to not possible direct mounting in the Mott analyzer.

The presented Mott analyzer is used now for the electron spin resolved measurements. The more important parameter for our experiment is the sensitivity that could be more increased by using a thicker target; however, it would yield to reducing of the asymmetry. As example, some estimation of efficiency with compare to the energy and thickness of the target is described in some details in paragraph 3.5.

3.4.4. The detectors for mini-Mott analyzer

One of the tested detectors for the new design of mini-Mott polarimeter is an Absolute XUV Silicon Photodiodes (AXUV) with 100% internal carrier collection efficiency. Unlike common p-n junction diodes, these diodes do not have a doped dead-region and have zero surface recombination resulting in near theoretical quantum efficiencies for XUV photons and other low energy particles. The AXUV diodes are internal photoelectric devices and hence are less sensitive to vacuum system contamination than conventional XUV detectors based on the external photoelectric effect. This detector has been mainly tested to perform analogue measurement of asymmetry for comparison with electron multiplier.

The diode response time is determined by the resistance and capacitance of the detector and the measuring circuit and the charge carrier transit time. The capacitance C of the diode is given by the silicon permittivity ε, area A, and the p-epitaxial layer thickness D.

$$C = \frac{\varepsilon \cdot A}{D} \tag{3.11}$$

The AXUV20HS1 doide has a 25 μm thick silicon sensitive layer, the capacitance C is 700pF.

The diode resistance is determined by the distance electrons which have to travel in the front field free n region towards the n^+ electrode. The resistance of AXUV20HS1 is only 1Ohm. Using the 50 Ohm scope impedance, 1Ohm diode resistance and 700pF capacitance, the rise time given by 2,2RC is 1,7ns [AXUV].

These diodes are fabricated by an ULSI (Ultra Large Scale Integrated Circuit) compatible process and their construction is shown in the following (Figure 3-9 left).

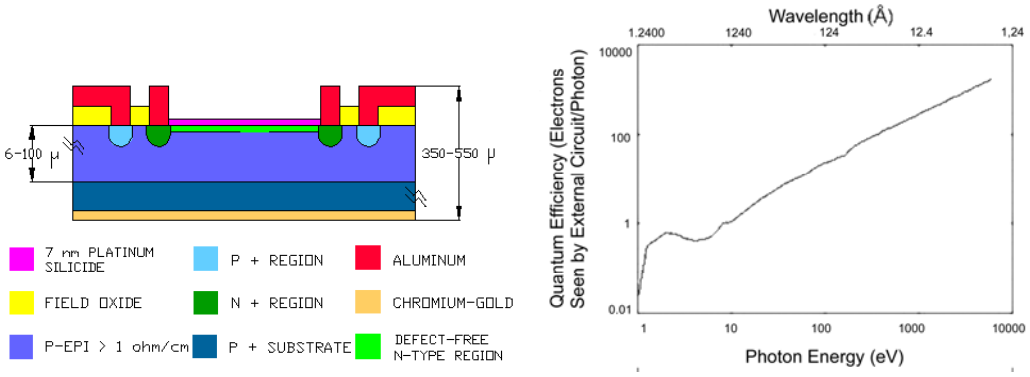

Figure 3-9: Left: The structure scheme of AXUV photodiodes. Right: The quantum efficiency curve.

The operating principles of silicon photodiodes is following: when these diodes are exposed to photons or electrons of energy higher than 1.12 eV (wavelength less than 1100 nm) electron-hole pairs (carriers) are created. These photogenerated charge carriers are separated by the p-n junction electric field and a current proportional to the number of electron-hole pairs created flows through an external circuit. For the majority of XUV photons, about 3.7 eV energy is required to generate one electron-hole pair. Thus more than one electron-hole pair is generally created by these photons. (Figure 3-9 right) shows the typical quantum efficiency plot of AXUV photodiodes.

The unique properties of the AXUV photodiodes provide stable quantum efficiencies for XUV photons which can be approximately predicted in most of the XUV region by the theoretical expression:

$$\varepsilon_{quant.}(electrons/photons) = \frac{E_{ph}}{3{,}7eV} \qquad (3.12)$$

where: E_{ph} - photon energy in electron-volts.

Mainly this is due to the absence of a surface dead region i.e. there is no recombination of photogenerated charge carriers in the doped n-region or at the silicon-silicon dioxide interface. As absorption depths for the majority of XUV photons are less than 1 micrometer in silicon, the absence of a dead region yields complete collection of the photogenerated carriers by an external circuit resulting in 100% carrier collection efficiency and which is near the theoretical calculated quantum efficiency.

The second unique property of the AXUV diodes is their extremely thin (3 to 7 nm), radiation-hard silicon dioxide junction passivating, and protective entrance window. The only quantum efficiency loss is due to the front (3 to 7 nm) silicon dioxide window at wavelengths for which (mainly for 7 to 100 eV photons) oxide absorption and reflection are not negligible.

As alternatively, second type of detectors is electron multipliers "Magnum" which are used in a wide variety of analytical instruments to detect weak signals from ions, electrons and UV photons [Magn].

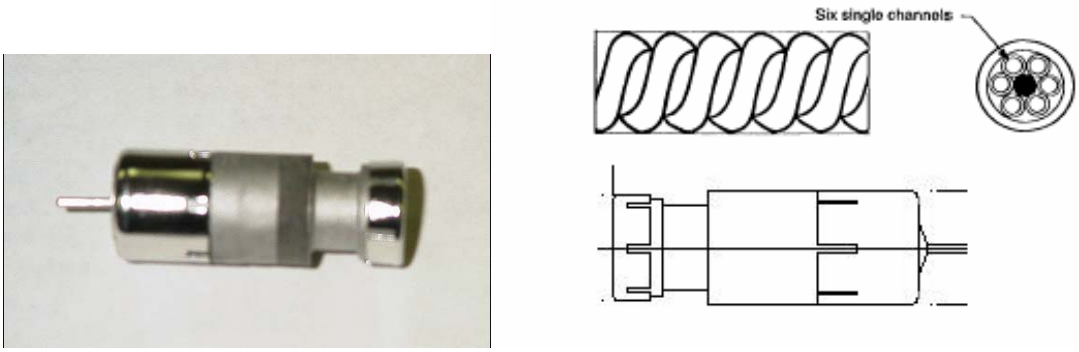

Figure 3-10: Magnum (electron multiplier).

The Magnum consists of six helical multiplier channels tightly wound around a central axis (Figure 3-10). This tight radius helps to prevent the onset of an ion feedback, enabling the multiplier to operate in poor vacuums (7×10^{-4}torr) at reduced noise levels. The ion feedback is produced due to a high electron density within the channel near the output end. Gases absorbed on the surface of the walls are desorbed and ionized, forming positive ions.

These ions travel back toward the input of the device. When they strike the walls near the input, they produce secondary electrons which are subsequently amplified and detected at the output end as a noise pulse (i.e. not due to an incident particle). The tight radius of the channel effectively minimizes this problem by preventing desorbed ions from travelling far enough to gain sufficient energy to produce further secondary electrons. This enables to construct devices which produce analog gains of 10^7 or more.

Unfortunately, electron multipliers have a limited life time. It is common for multiplier gain to decrease with usage, requiring periodic voltage adjustment to bring the gain back up to the instrument sensitivity requirement.

3.5. Estimation of efficiency of Mott analyzer

As mentioned above the efficiency (sensitivity) of Mott polarimeter can be defined as $\varepsilon = I / I_0$ (the ratio of scattered to incident beam currents). The probability that an electron passing through a gold foil will be scattered into a solid angle Ω is given by [Cam-85]:

$$p = \frac{10^3 N_A \rho}{A} \gamma \cdot t \cdot \overline{\frac{d\sigma}{d\Omega}} \cdot \Omega \qquad (3.13)$$

where: N_A-Avogadro's number, t-thickness of target

ρ and A- density and atomic weight of gold respectively

$\overline{d\sigma / d\Omega}$ - the differential scattering cross section averaged over the appropriate angular range.

If each detector subtends a solid angle Ω at the target, the efficiency will be

$$\varepsilon = 2p = 1.2 \times 10^{29} \gamma \cdot t \cdot (\overline{d\sigma / d\Omega})\Omega \qquad (3.14)$$

(with t in m and cross section in m^2, γ-detector efficiency).

For the estimation of scattering cross section the Rutherford formula has been used:

$$\frac{d\sigma}{d\Omega} = \left(\frac{z_1 z_2 e^2}{16\pi\varepsilon_0 E} \right)^2 \cdot \frac{1}{\sin^4\left(\frac{\Theta}{2}\right)}$$

where z - atomic number of particles ($z_1 = 1$ and $z_2 = 79$ (for gold target)), e-elementary charge of an electron, Θ-scattering angle=120°,

ε_0-electric constant and E - initial energy.

The Rutherford formula has a deviation in the order of 1.8 for high Z-targets at 120° [Mot-64] and presented here just as, example, for comparison efficiency ε with dependence from the initial energy and thickness of the target is presented in the Table 3.1(the factor γ is not included in the calculation).

Table 3.1 Dependence efficiency from the energy and thickness of target.

Initial energy (keV)	Thickness of target (nm)	$\varepsilon(I/I_0)$
40	36	$1.94 \cdot 10^{-3}$
40	100	$5.4 \cdot 10^{-3}$
25	36	$4.9 \cdot 10^{-3}$
25	100	$1.38 \cdot 10^{-2}$

With 12 keV initial energy for thicker target the maximum estimated efficiency is in the order of 10^{-2}. So, with consideration of the efficiency alone, it the operation of the polarimeter at the lowest practicable value of energy E and with thickness gold target would be recommended. However, the polarization figure of merit, measured by the analyzing power S_{eff}, decreases with decreasing energy and also decreases with a thicker target. This occurs mainly due to the increasing importance of multiple and plural scattering effects at lower energies. By increasing energy with applying voltage on the target and inner cylinder the analyzing power would increased, that in turn would reduce the efficiency because of reducing cross section. It is obviously necessary to find a compromise to optimize the statistical figure of merit $S_{eff}^{\ 2} \cdot I/I_0$ for a single scattering experiment.

The more important parameter for a spin resolved coincidence double scattering experiment is the experimental efficiency (described in detail in paragraph 5.5) rather than asymmetry and FOM as for the single scattering experiment. Because, for the double scattering experiment even a low spin

detection asymmetry is acceptable, making use of the fact that the statistical error of the measurement can be made smaller by measuring long enough.

4. Investigation of the spin asymmetry of backscattered electrons from magnetized targets as additional option for spin detection with high efficiency

This chapter is dedicated to a candidate of a new type of “spin filter” with a high efficiency for spin resolved measurements. One of the main important parameters in our experiment is efficiency. Due to a high efficiency of the backscattering process a spin filter polarimeter has the potential to achieve a figure of merit for keV electrons which is 2-3 orders of magnitude higher than the values for a Mott polarimeter. Of course, the asymmetry of the spin filter polarimeter has to be known for using it in our experiment.

In the first step of this chapter some of the theoretical background is discussed. The experimental setup where the magnetized Fe-target is used to produce polarized electrons is presented. The simulation of the efficiency of backscattered electrons is estimated and compared with the experimental results. The asymmetry from the backscattered polarized elctrons is measured by a Mott polarimeter that has been tested with known polarized beam. The main difficulty with measurement of asymmetry and analyzing power is also described.

4.1. Theoretical background

The main problem in polarized electron studies at keV-particle energy is now not longer the source intensity, but rather the low efficiency of usual electron polarimiters, like Mott scattering polarimeter. This low efficiency prevents electron spin resolved coincidence measurements because of the necessarily induced random coincidences in low efficiency spin detectors.

In terms of spin detector, a quantity of great interest is defined as the figure of merit (FOM) (paragraph 3.3.4). Conventional spin polarimeters have

a figure of merit below $2 \cdot 10^{-4}$. So far various groups have worked with using exchange scattering of low energy electron (several electron volts) by ferromagnetic surfaces as a promising route towards achieving significantly improved efficiency.

As already mentioned, the spin-orbit interaction can give rise to a spin polarization in electron scattering (the mechanism causing the polarization effects in Mott scattering). Another mechanism that can cause a polarization of the scattered electrons is the exchange interaction. For example, scattering from a target of alkali atoms whose valence electrons have all the same spin direction. If exchange processes occur between the valence electrons and the free electrons, one obtains polarized electrons in the scattered beam [Kes-85].

For example, detailed investigations of the Fe(110) surface have shown that figure of merit (FOM) of the order of $8 \cdot 10^{-3}$ can be achieved [Fas-92, Ham-92]. The different surfaces have been investigated to increase FOM, the lifetime and the reproducibility [Hil-02]. A different approach suggest even higher FOM $5 \cdot 10^{-2}$ using high quality ultarthin Co or Fe films on W(110) [Zdy-02]. Unfortunately, the microscopic size of this ultrathin film is problematical in spin polarimetry applications. However, even by larger film of lower quality FOM can be easily increased and reproduced at room temperature and values of $2 \cdot 10^{-2}$ have been observed [Gra-05].

Here, we propose investigation of a spin asymmetry of polarized backscattered electrons from the ferromagnetic target for spin detection with high efficiency. By achieving higher efficiency of keV-electrons backscattering from surfaces we consider a possibility to use it as a "spin detector" [Fil-98, Sie-81, Ham-92] for our coincidence experiment. Of course, the asymmetry of the spin filter polarimeter has to be known.

For our experiment the rate of real coincidence events has to be higher or comparable than the rate of random coincidences. In this case even a low spin detection asymmetry is acceptable, because the statistical error of the measurement can be made smaller by measuring long enough. Even if this asymmetry would be small the high efficiency of the backscattering spin filter enables a new type of a spin polarimeter which would be of high importance for spin resolved coincidence measurements.

4.2. Polarization from ferromagnetic materials

The investigations of polarized free electrons produced from secondary emission of spin-oriented electrons from magnetized materials provide information of the structure of magnetic solids.

The band model is used to describe the magnetism in these materials. As example, here, in the ferromagnets like Fe, Co and Ni the magnetism is caused by the 3*d* electrons. According to band model, the exchange interaction which is responsible for the ferromagnetism causes an energy shift of the $e\uparrow$ and $e\downarrow$ in the 3d band. The shift is determined by strength of the exchange interaction and has different direction for $e\uparrow$ and $e\downarrow$. Since both subbands are filled up to the Fermi energy, the $3d\uparrow$ band holds more electrons than the $3d\downarrow$band. For example for nickel there are 5 electrons per atom in the $3d\uparrow$ band and 4.46 electrons per atom in the $3d\downarrow$ band. It gives a resulting magnetic moment of about $0.54\,\mu_B$ per atom [Kes-85].

If the secondary electrons emitted from magnetized materials they have significant polarization. Polarized target electrons can be achieved by applying an external magnetic field towards the ferromagnetic samples. In a ferromagnetic sample the interaction between the primary electrons and the ordered net spin density of the sample electrons gives rise to a spin-dependent exchange interaction.

By using a primary beam of polarized electrons together with a polarized ferromagnetic target, it is possible to determine directly the effects of the exchange interaction by studying the spin dependence of the backscattered intensity when the initial polarization of the primary beam is flipped.

4.3. Polarization produced by backscattering electrons

The experimental setup where the magnetized Fe-target is used to produce polarized electrons is schematically shown in Figure 4-1 [Ber-05].

An unpolarized electron beam is produced by a commercial available electron tube. The energy of the electron beam can be changed between 2-14 keV. The beam current may be varied between 1 and 50 μA and is stabilized at the desired value. The energy and the focus of the beam are adjusted manually. The position of the beam is controlled by two pairs of

magnetic coils behind the gun. The residual gas pressure in the device is typically $5 \cdot 10^{-7}$ mbar.

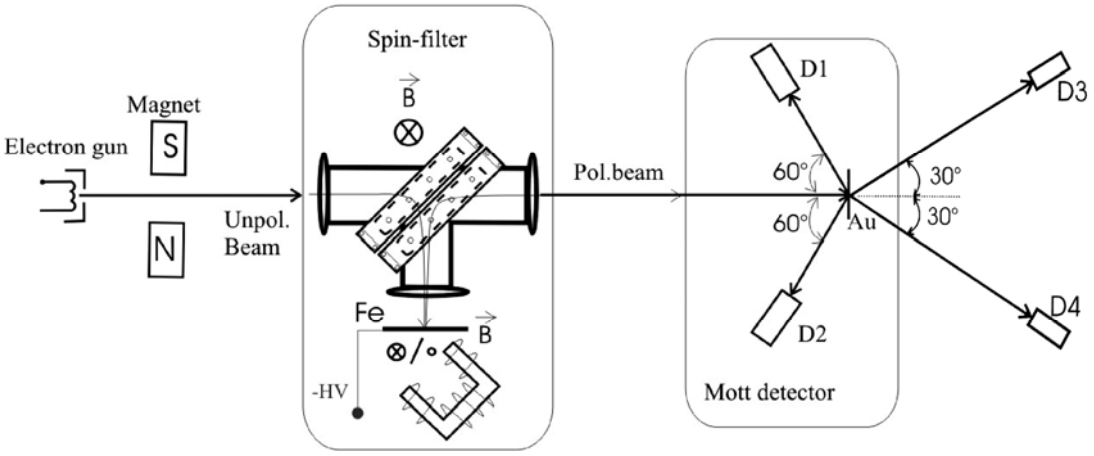

Figure 4-1: Schematic set up of the "spin filter" for the production and detection of polarized electrons. An unpolarized electron beam is deflected from the magnetized Fe-target. The polarization of backscattered electrons from the Fe-target is analyzed in the Mott polarimeter.

The Mott analyzer described in paragraph 3.4.2 has been used for presented experiment. Due to the lower spin asymmetry of the Mott chamber at low energy, the gold target and the inner sphere in the Mott polarimeter have been putt on high voltage (+24 keV) to accelerate the electrons and to reduce also innelastically scattered electrons. The outer sphere of the Mott chamber is on ground potential.

In order to check whether the changes of the beam polarization made to eliminate instrumental asymmetries affect by position and angle of the beam, and also the influence of the magnetic field on the beam trajectory the two additional detectors at forward direction have been installed in the Mott analyzer (Figure 4-1). Making use of the fact that for the scattering angle $\Theta = \pm 30°$ the Sherman function is almost zero and a measurement here determines therefore an instrumental asymmetry.

The unpolarized beam is entering the spin filter and is deflected by a magnetic coil in direction to the ferromagnetic target (Figure 4-2).

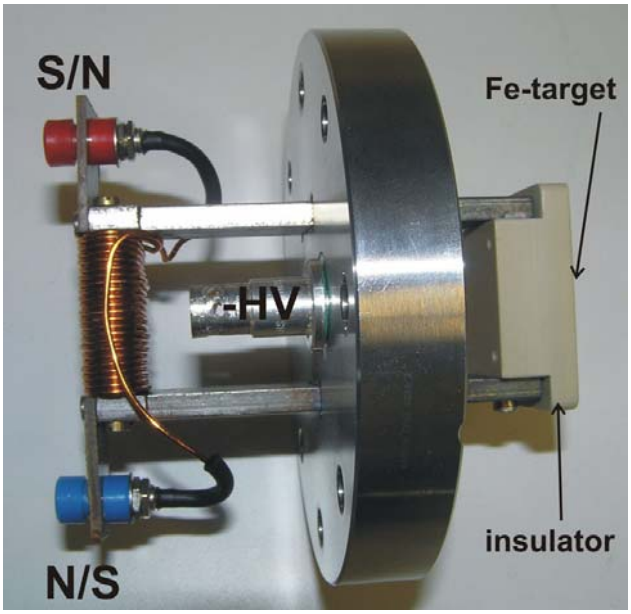

Figure 4-2: Picture of the holder for Fe-target. The different polarity is applied from south to north and opposite. Additional high voltage of several kV is applied on the Fe-target.

The Fe-target is magnetized by an external magnetic field of several mT parallel or anti-parallel to the scattering plane of the Mott chamber. A negative voltage of several kV is applied to the Fe-target to decelerate the electrons before they enter the target and to accelerate them after leaving the target again. After leaving the target, the electrons are directed by a second coil towards the Mott detector. To obtain a spin asymmetry for the Mott scattering the magnetization of the Fe-target is periodically turned from north to south and back.

4.4. Spin asymmetry of backscattered polarized electrons from Fe-target

This paragraph is devoted to the experimental result of measuring left-right asymmetry by the Mott analyzer (experimental setup is presented in Figure 4-1). The Fe-target is magnetized by an external magnetic field of several Millitesla parallel or anti-parallel to the scattering plane of the Mott chamber. To obtain a spin asymmetry for the Mott scattering the magnetization of the Fe-target is periodically turned from north to south and back. The scattering left-right asymmetry with depends from current in the

second coils for turning polarized beam to the direction of the Mott analyzer is shown in the Figure 4-3.

The blue line shows current in the Faraday cup, which is mounted behind Mott analyzer. The maximum current in the faraday cup is achieved at 0,39 A, where the secondary polarized beam is transported directly to the center of the gold target. The red line is shown instrumental asymmetry which is measured by two additional detectors at forward direction, making use of the fact that for Θ=±30° the Sherman function is almost zero and the measurement here shows therefore an instrumental asymmetry.

The green line shows the results of scattering left-right Mott asymmetry by the two detectors which are mounted at the angle of 120° where the Sherman function has its maximum. The real asymmetry (green line) has two maxima: one maximum is in agreement with the current in the faraday cup when the beam comes to the centre of target. The second maximum appears mainly due to misalignment of the electron beam, when the beam touches f.g. a support for the target. In this case the instrumental asymmetry (red curve) measured by two additional detectors has also maximum.

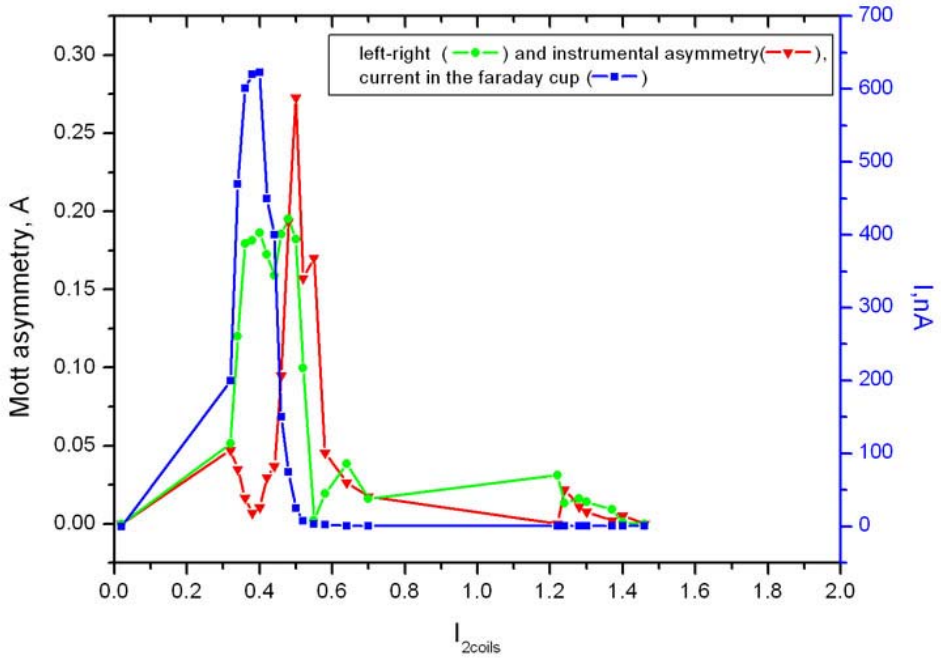

Figure 4-3: The scattering left-right asymmetry, instrumental asymmetry and current in the faraday cup in dependence from the current in the second turning coils.

The experimental results (Figure 4-3.) show that a scattering asymmetry of approximately 15-17% is obtained. Since the analyzing power of the instrument was calibrated to Seff=0.2 (see section 3.4.2) during the experiment at U-Mainz, this demonstrates a high polarization $P = A / S_{eff}$ of almost 70% of the backscattered electrons. The thickness of the target was the same 100 µg/cm² but energy was 10 keV smaller compare calibration at U-Mainz.

4.5. Monte Carlo simulation of electrons in a ferromagnetic target

The backscattering efficiency from a ferromagnetic target has been estimated with the Monte Carlo simulation of electrons in solids "CASINO", which is available at the web page for the SRIM- and TRIM-code for the stopping of heavy ions (http://www.srim.org/SREM.htm) (Figure 4-4).

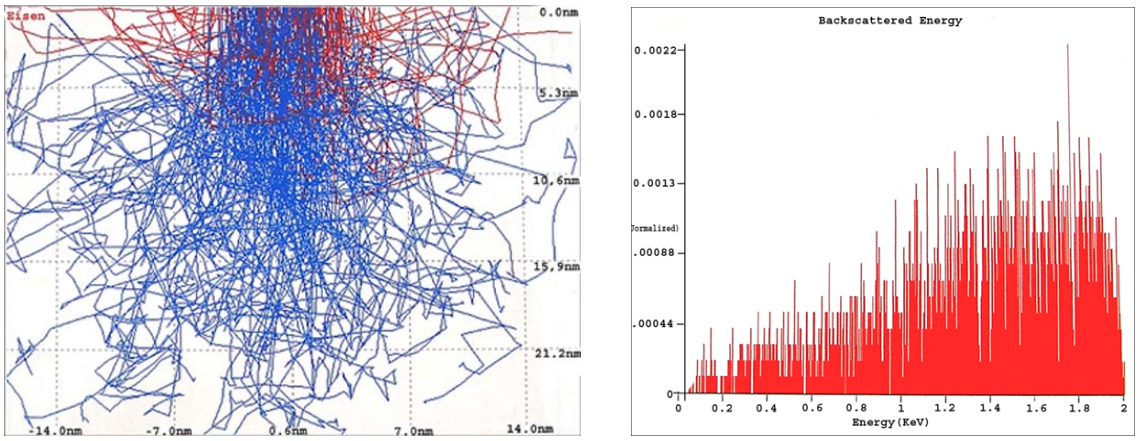

Figure 4-4: Left: Monte Carlo simulation of 2 keV electrons in a ferromagnetic target. Backscattered electrons (marked in red) have a 30 % probability for backscattering. Right: The energy spectrum of the backscattered electrons covers the full energy range with a maximum intensity between 1.4 – 2 keV at higher energy.

In a broad energy range between 1 – 10 keV the electron backscattering efficiency is nearly constant. About 30% of the particles are leaving the target again at the surface, where of course at a higher energy the particles penetrate deeper into target. Figure 4-4 shows an example for the simulation with a beam energy of 2 keV.

The backscattered electrons penetrate in a maximum depth of about 5 nm into the target. After backscattering the electrons have a broad energy

distribution, where however the energy maximum is still above 50 % of the initial energy, i.e. above 1 keV. We propose to apply an additional high voltage to adapt the electron beam (e.g. –5 kV) on the Fe target; this voltage would reduce the initial electron energy (e.g. –7 kV) to the reference energy (2 kV) and in turn enhance the minimum electron energy after backscattering.

4.6. Efficiency of backscattered electrons from a ferromagnetic target

This paragraph is devoted to the experimental measurement of the efficiency of the "spin-filter". Which is calculated by the results of the measurement I/I_0 (detected electron current I referred to the incident current I_0). The Monte Carlo simulation that is described in the previous paragraph is compared here with our experimental data. The experimental dependence of the current in the ferromagnetic target by applying voltage on it for different incoming energy is presented in the Figure 4-5. The dependence has been made with incoming current of 1.1µA for the different initial electron beam energies (4, 6, 7, 9 keV).

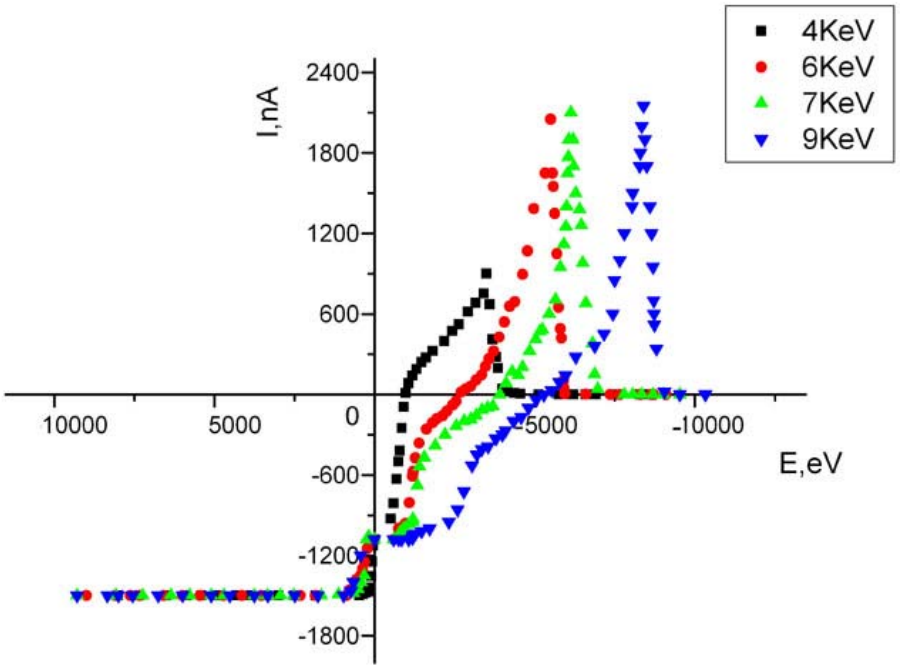

Figure 4-5: Dependence current in the Fe target from the voltage on it for different incoming energy (4,6,7,9keV).

According to Monte Carlo simulation the electron backscattering efficiency is nearly constant in a broad energy range between 1 – 10 keV and about 30% of the particles are leaving the target again at the surface. That was compared experimentally (Figure 4-5 (left side)) by measuring absorbed current in the Fe-target plus backscattered electrons with applying positive voltage at this target. As example, with putting positive voltage at the Fe-target to attract secondary electrons back to the target the negative current (which corresponds to electrons) is increasing from -1100nA to - 1450nA (in the picture left side) that correspond to approximately 30% according to the estimations of the Monte Carlo simulations.

By applying negative voltage on the target (in the picture right side) the current is increasing from the negative value and changes sign to positive values which corresponds to increasing the value of electrons that leaving Fe-target. By increasing negative voltage further in the Fe-target the current after achieving maximum value is decreasing from positive value to zero when the Fe-target has a higher voltage compared to the initial electrons, which of course, depends on the incoming energy. The error of this measurement is approximately 5-7% (not included in the graphic).

The overall efficiency of the whole device is calculated by the ratio of detected electron current in the faraday cup of Mott analyzer after leaving T-piece (see Figure 4-1) referred to the incident current that coming to the Fe-target. Of course, not all backscattering electrons from the Fe-target are coming to the faraday cup. In the Figure 4-6 presented efficiency for the initial beam energy 7keV with incoming current 1300 nA with variable voltage on the Fe-target.

In the maximum value for 6,5 keV in the Fe-target the highest calculated value of the efficiency (sensitivity I/I_0) is $7.7 \cdot 10^{-1}$. The efficiency is one of the important parameter in the anticoincidence experiment. Due to a high efficiency of the backscattering process a “spin filter” polarimeter has the potential to achieve a figure of merit for keV electrons which is 2-3 orders of magnitude higher than the values for a Mott polarimeter. But, of course, the asymmetry of the spin filter polarimeter has to be known. Even if this asymmetry would be small the high efficiency of the backscattering spin filter enables a new type of a spin polarimeter which would be of high importance for spin resolved coincidence measurements. The main difficulty with

measurement of asymmetry and analyzing power is described in paragraph below.

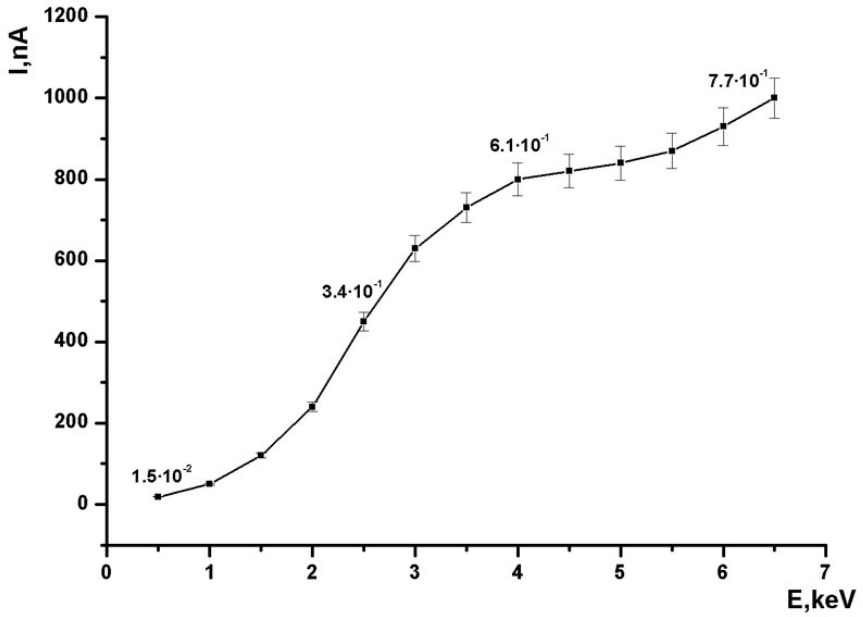

Figure 4-6: The measurement of the efficiency with dependence from the applying voltage on the Fe-target (Initial current 1300nA, and energy of the electron beam 7keV).

4.7. Determination of the Sherman function

For investigation of performance of the "spin filter" it should be tested to observe the Sherman function and asymmetry with known polarized beam. The Sherman function S_{eff} of the spin detector can be directly measured with well known polarized beam where the polarized electron beam interacts at the spin filter with partially polarized target electrons. Because the stopping of electrons (i.e. the inelastic mean free path) of electrons is spin dependent the backscattered intensity I/I_0 depends on the polarization of beam and target electrons which is observed at the final detector. From the asymmetry of the count rate for different beam polarization the analyzing power of the spin filter polarimeter is determined.

This measurement has been performed in collaboration with IKP Mainz. However, the experimental result in this step was not successful and future improvement would be necessary to perform of using the presented device as

a "spin-filter"for the coincidence double scattering experiment. First of all, the main reason was due to the high initial energy by the polarized source the measurement of asymmetry by backscattering electrons seems quite difficult mainly because of poor possibility to detect backscattering electrons to the detector compare to the initial electrons which has a higher energy. The observed result has shown the asymmetry close to 1%. This value is difficult to analyze due to the error of the asymmetry measurement that mainly results from the instability of intensity due to the application of magnetic field reversal and the absence of normalizing detectors and also necessary eliminating of the instrumental asymmetry. The lower energy close to 10 keV would be a prerequisite for the presented "spin-filter" in order to achieve higher value of asymmetry.

A known difficulty is also related to surface conditions of the magnetic film and the better preparing is necessary, as cleaning sample with cycles of $Ar^{+\text{-ion}}$ sputtering and heating of the target [Ham-92]. Over the course of many hours or days, the absorption of contamination from rest gas present in UHV considerably reduces both the reflectivity and the spin asymmetry. [Gra-05] have performed a detailed time and annealing temperature dependence of the reflectivity. The value of reflectivity and asymmetry was measured every 24h for 3 days and already after 24 hours reflectivity is substantially suppressed. The spin asymmetry was reduced by 50% and the maximum figure of merit was diminished by almost 90%. This aging effect can be easily reversed with a thermal treatment. The careful annealing leads to substantial recovery of the film's original exchange scattering characteristics but not to the 100%.

4.8. Conclusions

To increase low efficiency for the anticoincidence experiment a new design for a high efficient electron spin detector that could lead to the construction of a novel spin detector for electron has been investigated. The high value of efficiency near to 1 has been observed. Polarization that produced from the Fe-target has been estimated to the value narrow to 70% that gives a possibility for creating a polarized source with lower energy.

The performance of this device as a "spin-filter" has been tested with known polarized beam in collaboration with the IKP Mainz. However,

additional improvements, as a special cleaning target and better resolution between incoming beam and backscattered electron are necessary to determine the analyzing power of the device, and to determine the conditions where an optimum FOM is achieved in order to use this “spin filter” for spin resolved coincidence measurements.

5. Experimental setup and results

This chapter describes the optimized experimental setup, the procedure of the measurements and the main results of the asymmetry produced from elastic scattering of unpolarized electrons. Firstly an overview of the energy selection between high and low energy components is given. Some of the detectors that are used for the experiment are also discussed.

The data analysis that has been programmed in Labview is presented here together with the scheme of the acquisition setup. A high ratio of coincidences normalized to random coincidences is demonstrated here. The experimental results of the experimental efficiency are also showed here.

5.1. Cross section for Mott and Moeller scattering

By the scattering of an electron beam on a C-target two energy components could be observed by having energy selection: one belongs to the low-energy Moeller scattering (electrons with electrons), and the other to the high energy Mott scattering (electrons with an atomic nucleus). Energy selection is therefore important to reduce background electrons, resulting from the high energy Mott scattering.

As example, estimations of the scattering cross section for Moeller scattering and Mott scattering by using the Rutherford formula in the center of mass system are presented here:

$$\frac{d\sigma}{d\Omega} = \left(\frac{z_1 z_2 e^2}{16\pi \varepsilon_0 E} \right)^2 \cdot \frac{1}{\sin^4\left(\frac{\Theta}{2}\right)} \tag{5.1}$$

where z - atomic number of particles, e-elementary charge of an electron, Θ-scattering angle, ε_0-electric constant and E - energy of the beam.

The difference of the cross section between these two components appears from three parameters E, z, Θ. The energy in the center of mass system for Moeller components is two times smaller compared to the Mott component $E^{Moeller} = 1/2 E^{Mott}$. For electron-electron scattering the atomic number is $z_1 = z_2 = 1$ where for electron scattering of an atomic nuclei by using a carbon target is $z_1 = 1$ and $z_2 = 6$. And the scattering angle for Moeller scattering $\Theta^{Moller} = 90°$ and for Mott $\Theta^{Mott} = 45°$.

A comparison of the calculated value for Mott and Moeller components in dependence from the initial energy are presented in the Table 5.1.

Table 5.1: The scattering cross section for the Mott and Moeller components.

E(keV)	$\frac{d\sigma}{d\Omega}^{Mott}$ (m^2/sr)	$\frac{d\sigma}{d\Omega}^{Moller}$ (m^2/sr)
10	$2{,}17 \cdot 10^{-24}$	$2{,}07 \cdot 10^{-26}$
20	$5{,}44 \cdot 10^{-25}$	$5{,}18 \cdot 10^{-27}$
35	$1{,}77 \cdot 10^{-25}$	$1{,}69 \cdot 10^{-27}$

The calculated value of the cross sections gives a theoretical factor of the difference between high and low energy components:

$$\frac{d\sigma}{d\Omega}^{Mott} = 104 \frac{d\sigma}{d\Omega}^{Moeller} \qquad (5.2)$$

It shows that with one Moeller electron we will detect about 100 electrons of the Mott components if no energy selection is performed.

5.1.1. Mott and Moeller scattering

As already mentioned, Moeller scattering (electron-electron scattering) can be separated from Mott scattering (electrons with an atomic nucleus) by performing an energy selection of the scattered electrons. As example, it could be managed by electrostatic lens (Figure 5-1(left)), that focuses the beam to the detector. The electrostatic lens consists of a centre cylinder which is putting to higher or lower potential and two additional plates placed at each end of the device. The plates are at a ground potential.

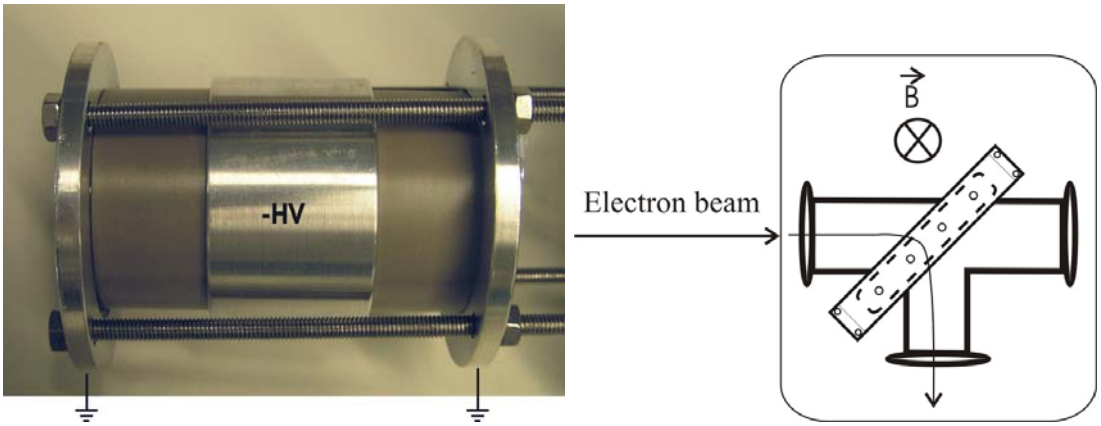

Figure 5-1: Picture of the electrostatic lens (left), the centre cylinder at high voltage and two plates at each end of the device which are at ground potential. The magnetic coils in a T-piece branch (right).

Another possibility, to have energy selection could be done by using magnetic coils in a T-piece branch (Figure 5-1(right)). Due to the different moment of both components, the bending radius in the magnetic field (R~p) changes accordingly, so that only one Moeller component reaches the detector.

However, the complication of magnetic coils is that with applying magnetic field the influence to the spin can disturb the final results of the expected spin resolved measurements. And also by using this construction we increased the distance from the scattering chamber to the Mott analyzer what in our experiment lead to a loss of two orders of intensity. This, in turn, reduces possibility to achieve a higher ratio of measured coincidence compared to background signal.

Figure 5-2 shows the experimental results (with initial beam energy 7keV) of Moeller and Mott components depending from the applied voltage on the electrostatic lens. With a slit or smaller hole between Mott analyzer and lens it is possible to distinguish low-energy from the high-energy components.

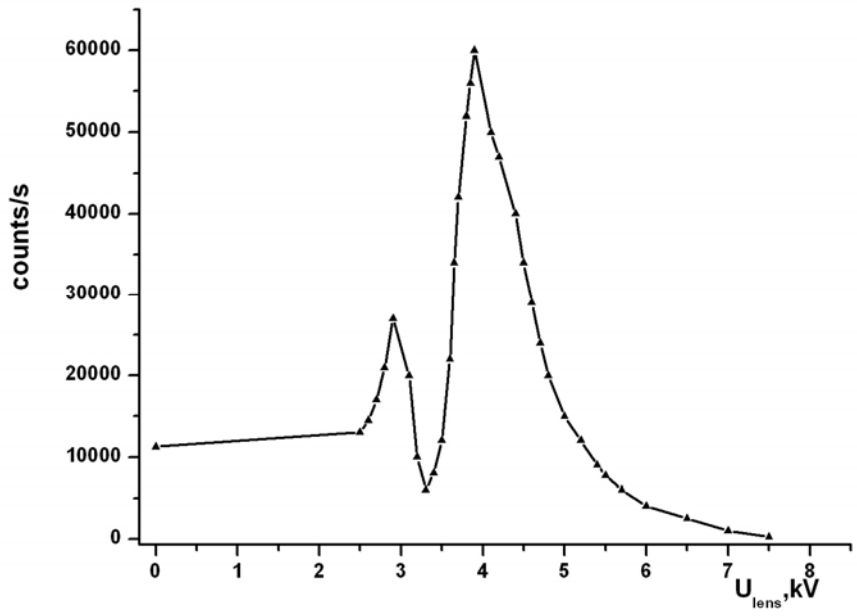

Figure 5-2: Experimental results of low-energy-(Moeller) and high-energy (Mott) components with dependence from the applied voltage to the lens.

The first peak corresponds to the Moeller component that have a lower energy of the beam $E^{Moeller} = 1/2E^{Mott}$. The second peek belongs to the high energy - Mott component. By focusing to the first peek it is possible to reduce the possibility to detect high energy components in the detector. However, with the lens it is difficult to achieve a good energy selection. By focusing to the first peek Mott components can still penetrate through the lens and can reach the detectors. This in turn produce additional background for the performed coincidence resolved measurement.

Another way to perform energy selection and also increase experimental efficiency by reducing distance between scattering chamber and Mott analyzer have been done by using electrostatic deflectors. Figure 5-3 shows a photo of the scattering chamber together with the electrostatic deflectors. The carbon target is mounted inside of the cylinder. The electrostatic deflectors consist of two condensator plates connected to the cylinder immediately behind the C-target. To the inner deflector a positive voltage is applied and to the outer a negative voltage.

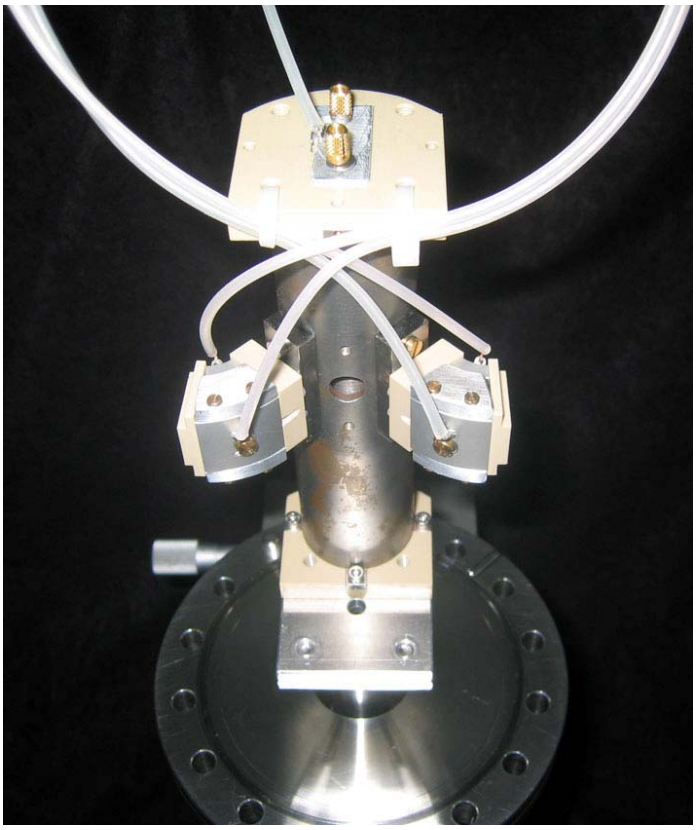

Figure 5-3: The picture of the electrostatic deflectors that mounted at once after scattering C- target.

To increase the scattering energy and to reduce the straggling in the target an additional voltage could be applied on the carbon target that is mounted inside the cylinder.

5.2. Detectors

5.2.1. Electron multiplier

Several kinds of detectors have been tested during the presented work. The first kind of detectors is Channeltrons (electron multiplier) that are common used for the detection of electrons and ions. The signal amplification is high, which enables the detection even of single particles.

Figure 5-4 illustrates the basic structure and operation of a Channeltron. A glass tube having an inner diameter of approximately 1mm and an outer diameter of 2, 3, or 6mm is constructed from a specially formulated lead

silicate glass. When appropriately processed, this glass exhibits the properties of electrical conductivity and secondary emission.

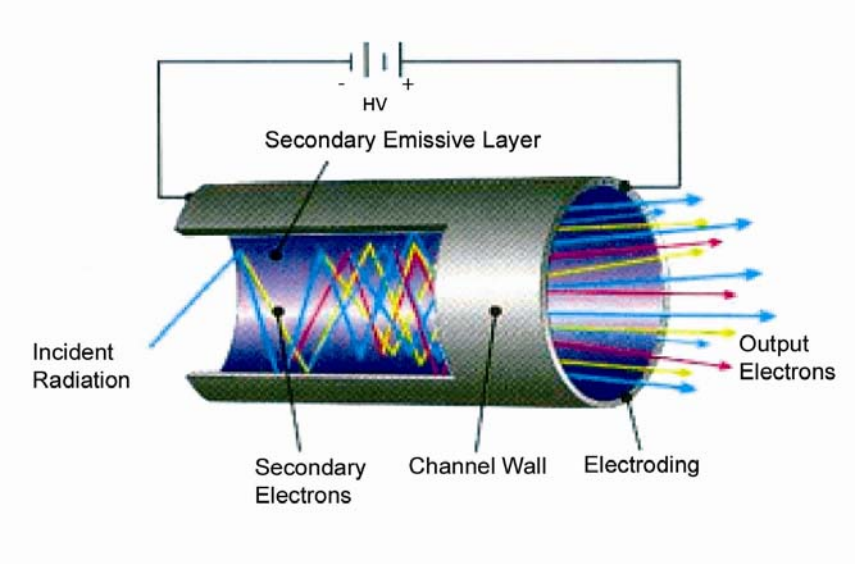

Figure 5-4: The basic operation of the Channeltron.

Typically 2-3 secondary electrons will be produced when an electron strikes the input of the device. These electrons are accelerated down the channel by a positive bias. The electrons strike the channel walls, an by continuous multiplication create finally an avalanche of 10^7 to 10^8 electrons. For positive ions, the input is generally at a negative potential of 1200 to 3000 volts and the output is at ground. For detection of electrons, the input is generally at ground or some positive potential and the output is at a high positive voltage.

The amplification due to electron multiplication requires however the application of a high voltage inside the vacuum system where high rates of background events are obtained from low energy electrons and ions produced from the residual gas.

5.2.2. Optical detection of keV-electrons

To solve the background problem resulting from low energy electrons and ions produced from the residual gas; two types of optical detectors have been designed and tested. They allow a high detection rate together with a low background count rate [Ber-04]. Possible applications of these detectors are the diagnostics of secondary ions emerging from ion beam heated target as well as particle detection in low energy scattering experiments [Jac-01].

The first detector is shown schematically in Figure 5-5. It consists of a YAP- Yttrium Aluminum Perovskite doped with Cerium [chemical formula YAIO3(Ce)] single crystal scintillator disc which is covered with a 50 nm Al entrance window, connected to a quartz view port and a photon counting system.

The YAP (Ce) is a non hygroscopic, glasslike, inorganic scintillator with a high density – 5.55 g/cm3. The diameter of the YAP (Ce) discs is 8.73 mm and with a 2mm metal ring, one side is polished. The wavelength of the maximum light emission is 350 nm, with a fast decay time in the order of – 27 ns, what allows high count rates up to several MHz. The non-hygroscopic nature of YAP (Ce) enables a long detector life time. The light output of YAP (Ce) crystals is 18 photons per KeV. Another beneficial property of YAP (Ce) is, that the rate of change of light output is almost not depending on the temperature – 0.01%/°C.

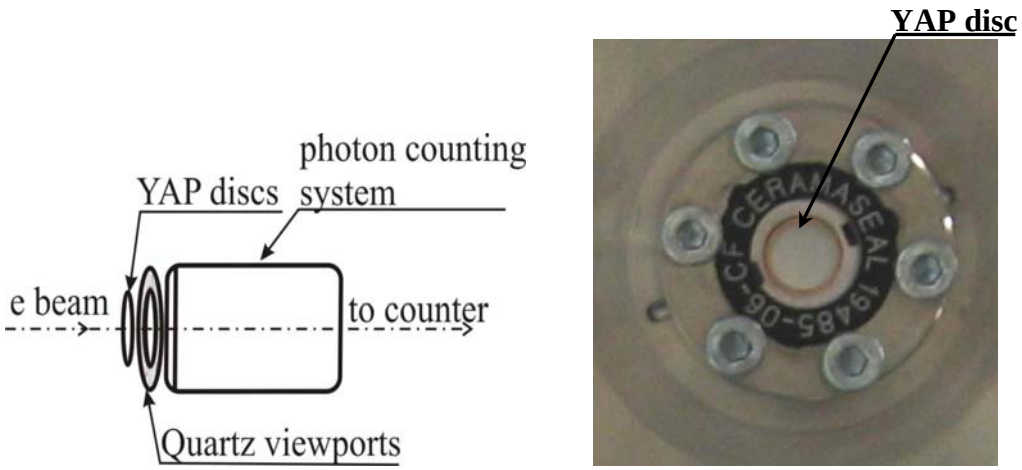

Figure 5-5: The optical detector with a YAP scintillator.

The quartz viewport behind the YAP(Ce) allows a transmission higher than 90% in a wavelength range between 250 – 2500 nm.

YAP(Ce) crystals are coated with 50nm of aluminium layer. It shields the photomultiplier from background photons and also low energy ions can not penetrate through this coating. The 50 nm of Al layer can schield low energy background electrons from the detector.

Figure 5-6 shows an example for the simulation of a beam energy of 1.8 keV penetrating through YAP(Ce) crystal covered with a 50 nm aluminium layer.

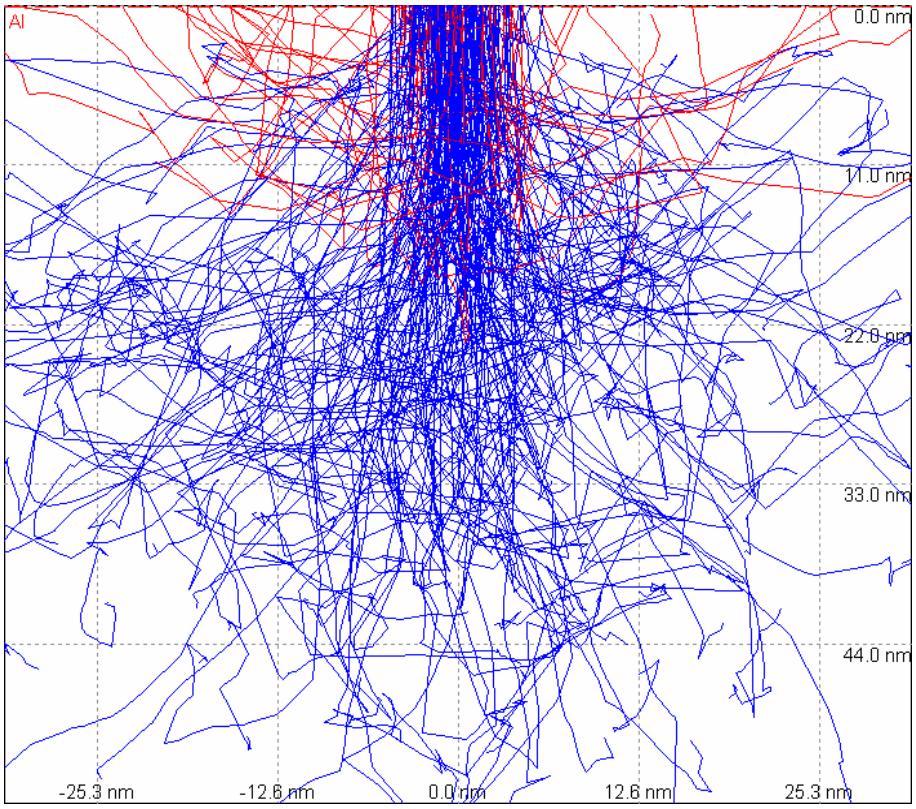

Figure 5-6: Monte Carlo simulation of 1.8 keV electrons through Al layer of 50 nm.

The red trajectory shows backscattering electrons and blue trajectory the electrons that penetrate in to 50 nm of Al layer. As can been seen, by covering detector with additional layer it is possible to reduce the background signal that is mainly coming form the walls or rest gas in the energy interval around 2keV.

For the detection of photons after the quartz view ports a photon counting head was used which consists of a 25 mm head-on photomultiplier tube, a voltage divider, an amplifier, a discriminator and a high voltage power supply circuit. All included in a compact metallic case. The sensitive spectral range reaches from 300 to 650 nm, a counting linearity up to 6×10^{6} s^{-1} and a dark count rate as low as 15 s^{-1} was achieved. Since the photomultiplier tube supply voltage and discriminator voltage are preset at the optimal levels, there is no need of adjustment before use. The main advantage of this series is the

low noise and the high detection efficiency. This photon counting method is also superior in comparison to analog signal measurement in terms of stability, detection efficiency and signal to noise ratio.

For the second type of detectors the YAP crystal has been replaced by a P47 phosphor scintillator (Figure 5-7) mounted at the same photon counting system.

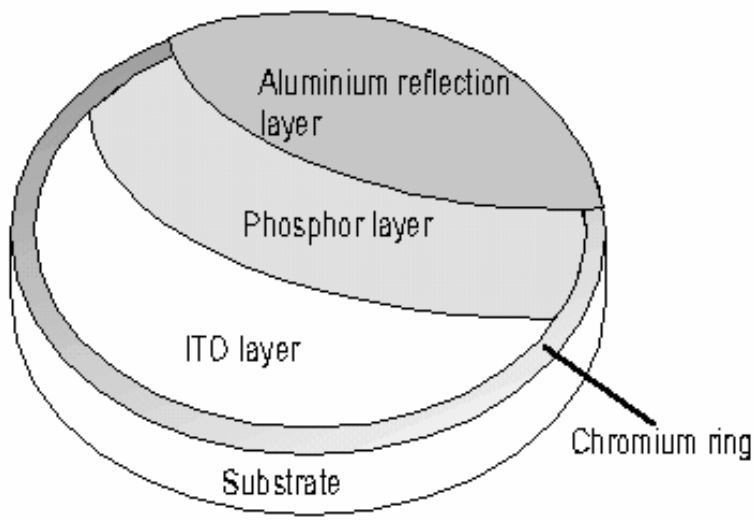

Figure 5-7: The construction of phosphor scintillator.

This P47 powder scintillator consists of a glass substrate, the P47 phosphor together with a proprietary polymeric binder for bonding the phosphor powder was covered onto a glass surface. For the glass surface we have used BK7 lens with a 40 mm in diameter. One side is coated with the P47 phosphor. The entrance of the phosphor was covered with a 40 nm Al layer. The diameter of the phosphor is here 30 mm with a thickness of 4 μm, with a maximum peak emission wavelength of 400 nm and a decay time of about 100 ns.

The third kind of detectors which has been tested is a high quality plastic scintillator ZA212 with an excellent light output and transmission. The Table 5.2 shows a comparison of some of the main parameters for these three detectors.

Table5.2: Specification of the different used optical detection system.

	YAP crystal	P47 phosphor	Plastic scintillator
Decay time (ns)	27	100	1,6
Life time	longer life time		
Sensitive area (mm)	8,73	30	30

The main advantages of the YAP single crystal in comparison to the P47 phosphor are the three times faster decay time together with the long life time, due to its high resistance to radiation damage. Its sensitive area is about ten times smaller than for the phosphor. The main advantage of the plastic scintillator compared to other two is the short decay time. The sensitive area is the same like for the phosphor or even bigger depending on the space solid angle in the Mott analyzer.

The time resolution of the detectors is one of the important parameters for coincidence resolved experiment. Since the random coincidence (background) is linearly depended on time resolution, the last should be made a small as possible to achieve difference between measured coincidences compared to the background signal. The most suitable detectors for our experiment are plastic scintillator and the so-called Magnum (electron multiplier) that provides a time resolution in the order of 3-5 ns.

5.3. Experimental setup

5.3.1. Vacuum system

As a vacuum system a combination of a dry, hermetic scroll prepump and a turbomolecular pump has been used. The single-stage prepump[1] produces a pumping speed of 110 L/m (on 60 Hz power) and achieves a pressure of $7 \cdot 10^{-2}$ mbarr. The turbomolecular pump[2] has a pumping speed of 210 liters per

[1] Varian SH-110

[2] TMU-260 (Pfeiffer Vacuum)

second. The vacuum inside the chamber was measured with an ionization vacuum gauge [3] and during the experiment a pressure of $5 \cdot 10^{-7}$ mbar was reached.

5.3.2. Alignment proceeding

The alignment is necessary to have a target in the middle of electron beam to reduce a part of scattering electrons from the holder (Figure 5-8). And mainly for having a scattering angle for the electrons $\Theta = 45°(\Theta_{cm} = 90°)$ because for identical fermions the scattering in this angle is not allowed.

Two He-Ne laser were located in the place of Mott analyzer and one additional laser in the place of the faraday cup (Figure 5-8 left). The apartures are used for both sides in every branch to bring the laser beam exactly to the axis. Figure 5-8 (right) shows the support of the target adjustment which is movable in three axes to bring the carbon target to the centre of the laser beam.

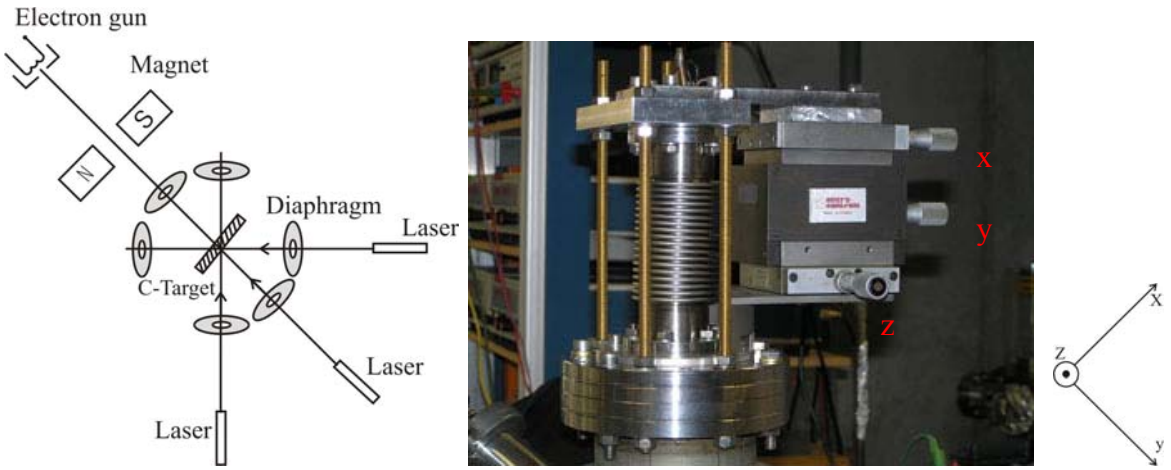

Figure 5-8: Alignment with laser (left) and adjustment support for target holder (right).

[3] EYASIS Mini-B/A (Varian)

5.3.3. Electron gun

An electron beam is produced by a commercially available electron gun presented in Figure 5-9.

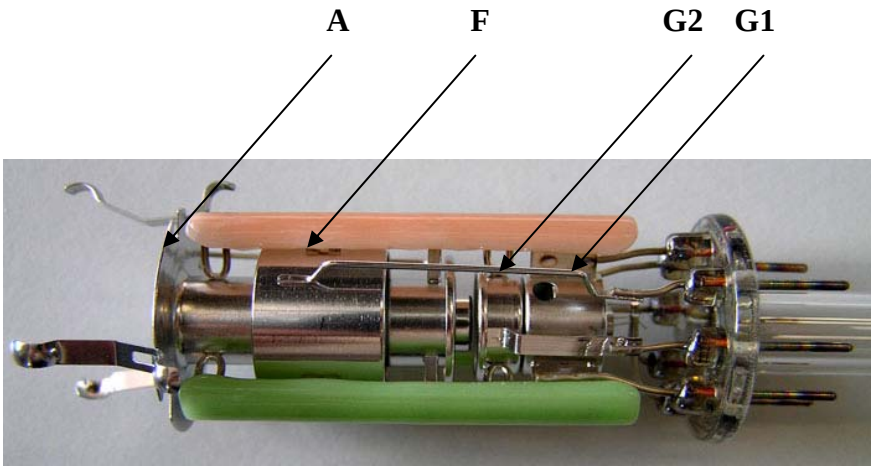

Figure 5-9: The picture of an electron tube.

At the cathode high voltage from -100V to -15000 was applied with a maximum current up to 200μA. The control grid 1 (G1) sets a negative potential from 0 to 200V against the cathode to suppress emission. The extraction grid 2 (G2) is connected to positive voltage of 600V. The focus electrode (F) has a varied voltage from +600V till -900V and the anode (A) is grounded.

5.3.4. Schematically experimental setup

The principal setup for the Moeller scattering experiment is presented in Figure 5-10. The pressure in the chamber is $5 \cdot 10^{-7}$ mbar. As already mentioned a several ten keV electron beam is produced by the electron tube. The beam current can be varied between 1 and 200μA and dynamically stabilized at the desired value. The energy and the focus of the beam are adjusted manually. The position of the beam is controlled by two pairs of coils. A free standing carbon target with some $\mu g/cm^2$ is used for the electron scattering. The beam current behind the target is measured with a faraday cup or an electron multiplier (Channeltron).

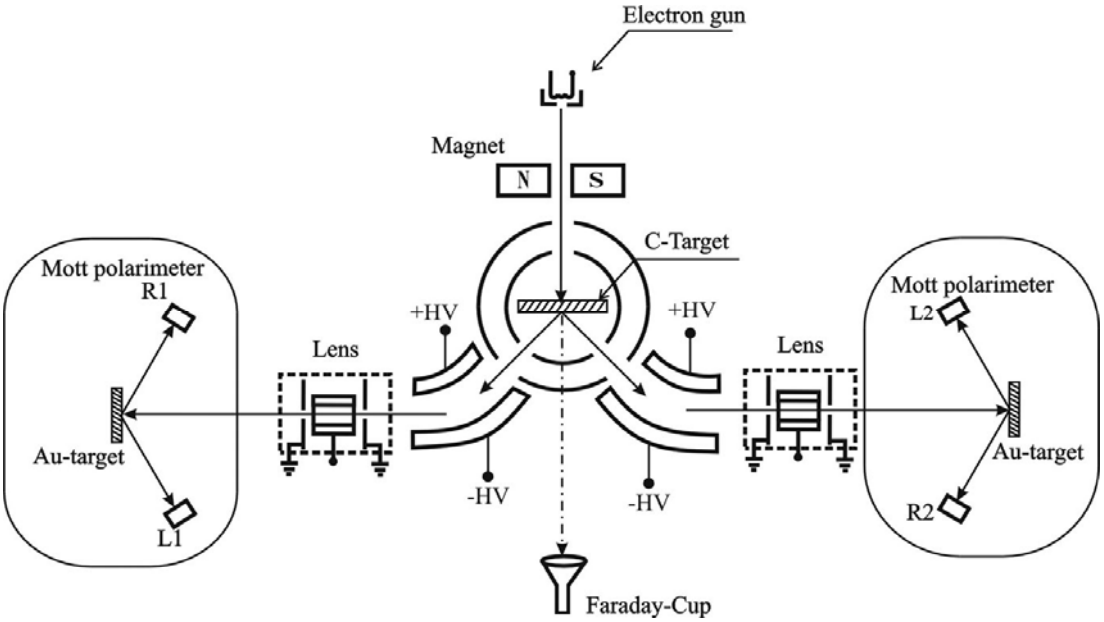

Figure 5-10: Schematic set up for a symmetric electron-electron scattering experiment.

An additional voltage could be applied on the C-target to reduce the straggling and further to increase the difference between the Mott and Moeller components. To perform an energy selection of these Mott and Moeller components electrostatic deflectors are used and applied immediately behind the C-target. A positive voltage is applied to the inner- and a negative voltage to the outer-cylinder.

After scattering at the C-target at $\Theta_{lab} = 45°(\Theta_{c.m.} = 90°)$ the two electrons may be directed into the Mott analyzer by the focusing with Einzel-lenses. Within the analyzer the electrons are scattered by a gold foil with an aerial density of 70µg/cm² (thikness-36nm). The coincidences between the detectors of one analyzer with detectors of the other are counted. The detectors of one analyzer are in reaction plane, and the detectors of the other are rotated by an angle Θ around the axis defined by the electrons entering in the analyzer. The electron multiplier (Magnum) or photomultiplier that are connected to a scintillator are used for the detection of the signal. The data acquisition of the device is connected to NIM-Modules, which are in turn connected to time resolved recorded in a four channel digital oscilloscope using LabVIEW.

Figure 5-11 presents a photo of the electron beam spot in the scintillator (in the place of C-target) that has been recorded by a fast shutter camera[4].

[4] Princeton Instruments (PI-Max2: 1003 Camera)

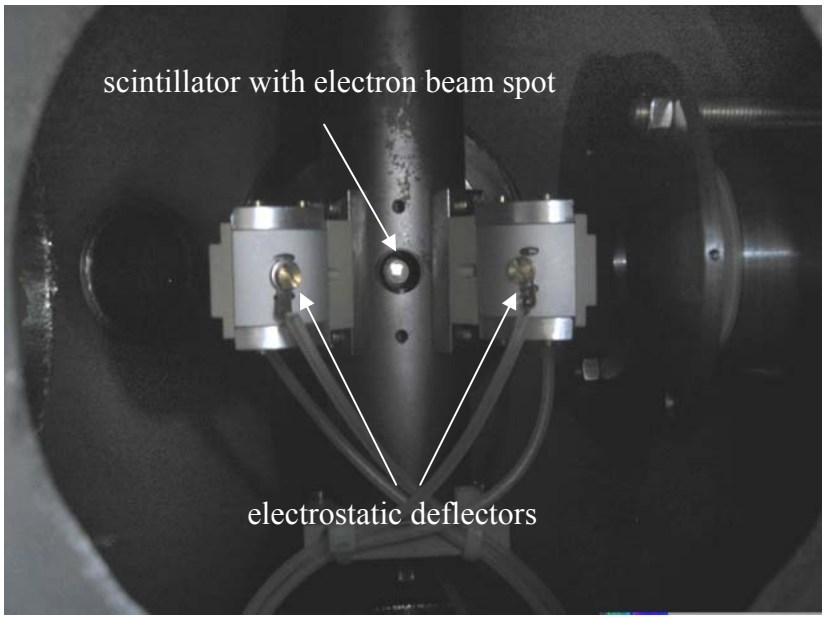

Figure 5-11: The electron beam spot is recorded by the Camera in scintillator. The electrostatic deflectors are also showed here that mounted at once after scattering target.

The electron beam spot is focused to the middle of the scintillator with 1 cm diameter. And a beam is approximately 4mm in diameter. Additional voltage (-23keV) has been applied to the electron gun to increase the initial energy of the electron beam mainly for the purpose to reduce straggling at the C-target and to further increase the experimental efficiency. For the protection of the electron gun and of the power supply NGR-15kV from the high voltage a transformer was used (Figure 5-12).

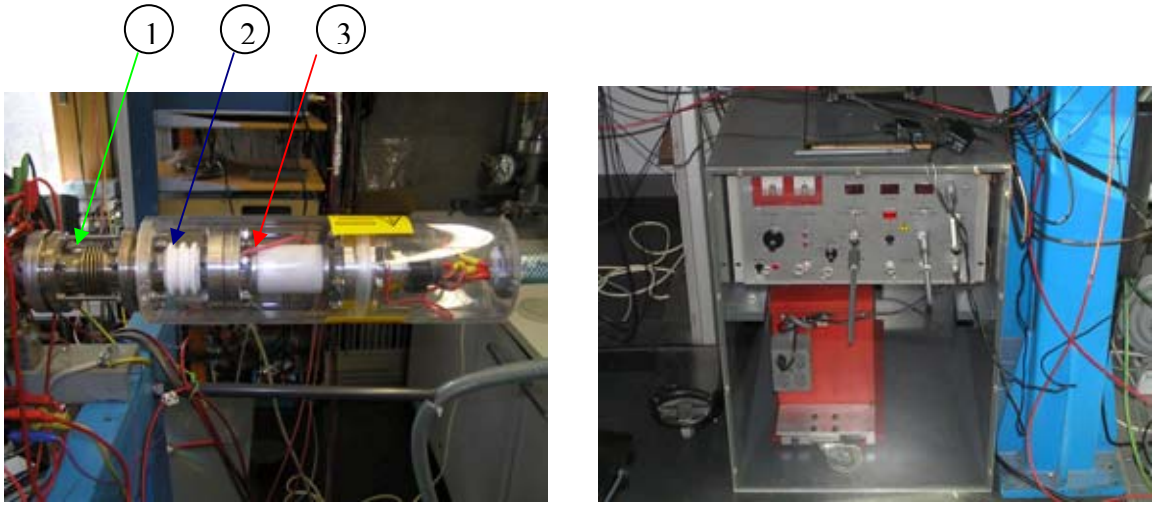

Figure 5-12: The electron tube (left)(1-allignment tube), (2-insolator), (3-electron gun) and power supply (right).

5.4. Real and Random coincidence

One of the main problems in our double scattering experiment is to achieve a high rate of real coincidences in comparison to random coincidences which are caused by the low detection efficiency of the correlated electron pairs.

Since the intensity of the electrons after a double scattering at the detector is small, the fractional background of unwanted electrons could be very high. This background appears because neither the electrons of the primary beam nor scattered electrons that hit the walls of the scattering chamber or of the polarization analyzer are completely absorbed there. They are instead reflected at the walls, and an appreciable portion of them, if not sufficiently suppressed, arrive at the counters and affect the measurement. Electrons that are reflected into the direction of observation by plural and multiple scattering must also be suppressed.

A scheme of the electronic circuits by which coincidences can be detected are shown functionally in the Figure 5-13. A circuit consists of two separate channels, each carrying pulses from one of the counters.

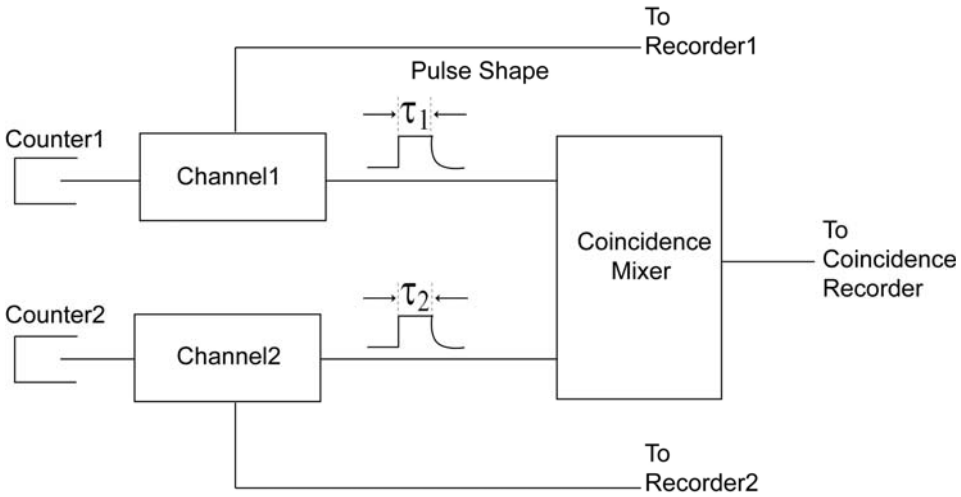

Figure 5-13: Schematically drawing of the coincidence circuit of the data analysis.

If R_1 and R_2 are the detection rates of electrons in detector 1 and 2 respectively, than the true coincidence rate is estimated from the probability i.e. the efficiency ε that an electron in one detector can be recorded simultaneous with the correlated electron in the second detector:

$$C_{real} = R_1\varepsilon_1 + R_2\varepsilon_2 \qquad (5.3)$$

The pulses are fed into a mixer, which delivers an output pulse when pulses arrive simultaneously in both channels.

In practice, these efficiencies ε are smaller than one and therefore also a probability exists that false coincidences can be arbitrary detected. These random coincidences can be calculated straightforwardly by mathematical statistics. This random coincidence rate increases with the detection rate in each detector multiplied with the time resolution of both channels, which may be denoted as τ_1 for channel 1 and τ_2 for channel 2. Thus, the random coincidence rate is given by [Sie-55]:

$$C_{random} = R_1 R_2 (\tau_1 + \tau_2) \qquad (5.4)$$

where $(\tau_1 + \tau_2)$ is called the total resolution time of both detectors together.

The random coincidence rate must be subtracted from the measured rate in order to obtain the true coincidence rate of equation 5.3. The resolution times τ_1 and τ_2 should be made as small as possible in order to reduce the random coincidence rate. But in another hand they must be long enough to accommodate the jitter in the separate detectors, or some true coincidence is lost.

5.5. Efficiency measurement

A preferable condition for the detection of coincidences is to achieve a high ratio of measured coincidences compared to random coincidences to reduce the error for the measurement. To estimate this ratio the efficiency ε of the experiment has to be determined. For the following efficiency measurements in order to reduce straggling in the carbon target the thickness of the target was reduced to 4 μg/cm^2 and the beam energy has been increased to 35 keV. Additional lenses and a set of magnetic coils have been mounted to distinguish electrons from Moeller-scattering (electron with electrons) from Mott-scattering electrons (electrons with an atomic nucleus). These efficiency measurements were performed with two scintillator detectors at the position of the Mott polarimeter in Figure 5-10.

The measured coincidence rate is a superposition of real and random coincidences. If we assume a symmetric set up of the experiment, we calculate the average efficiency with $\varepsilon=\varepsilon_1=\varepsilon_2$ from equation (5.3) and (5.4) with:

$$\varepsilon = \left(\frac{C_{measured}}{C_{random}} - 1 \right) \frac{R_1 R_2 (\tau_1 + \tau_2)}{(R_1 + R_2)} = \frac{(C_{measured} - C_{random})}{(R_1 + R_2)} \qquad (5.5)$$

In Figure 5-14 (black line) the ratio of measured coincidences to calculated random coincidence is shown for different detection rates. The ratio decreases with increasing intensity due to the increasing number of random coincidences. For small beam intensity with several kHz counting rate in the detectors the rate for real coincidences is several thousand times bigger than the rate for random coincidences.

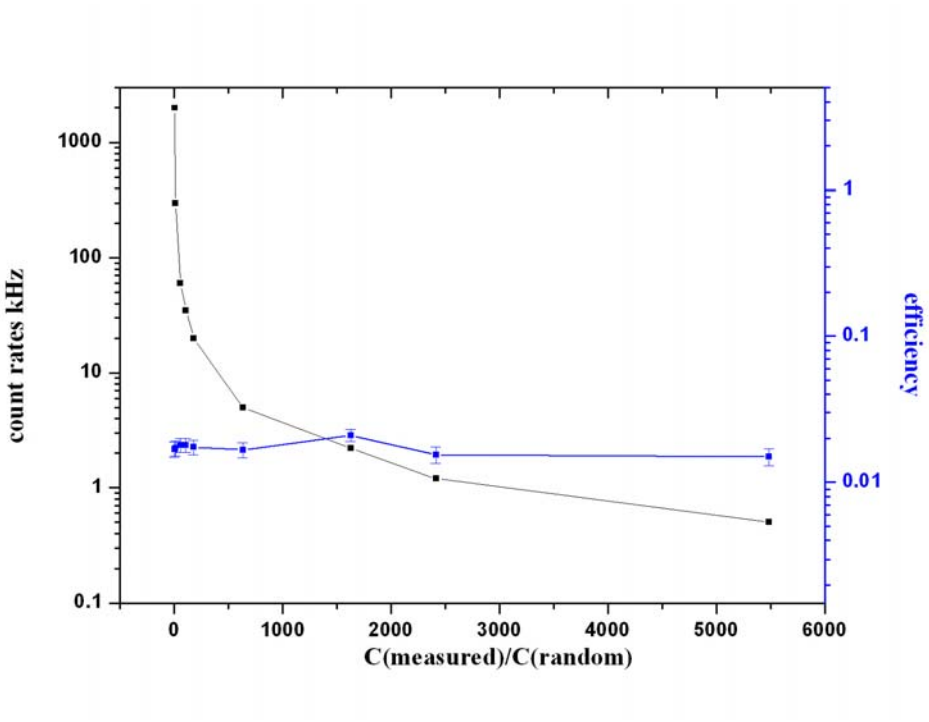

Figure 5-14: The experimental ratio of measured coincidences to random coincidences in dependence from the intensity of the electron beam (black line, left units), and the corresponding derived average efficiency (blue line, right units).

The efficiency ε however does not much depend from $C_{measured}/C_{random}$, which is demonstrated in the Figure 5-14 (blue line) [Ber-09a]. A high ratio of coincidences normalized to random coincidences is demonstrated here only without performing a spin measurement. It is shown, that this ratio is related

to an experiment depended nearly constant efficiency for the coincidence detection.

The maximum experimental efficiency that have been observed in this measurement was $\varepsilon \approx 2 \cdot 10^{-2}$. This efficiency could be increased further by increasing initial energy as presented in the Figure 5-15. By applying ground potential on the C-target (green curve) the efficiency is increasing linearly. As example, the experimental result is showing that by increasing energy from 32 to 40 keV the efficiency was increased almost by factor 2. The higher energy would be prerequisite to increase the experimental efficiency further.

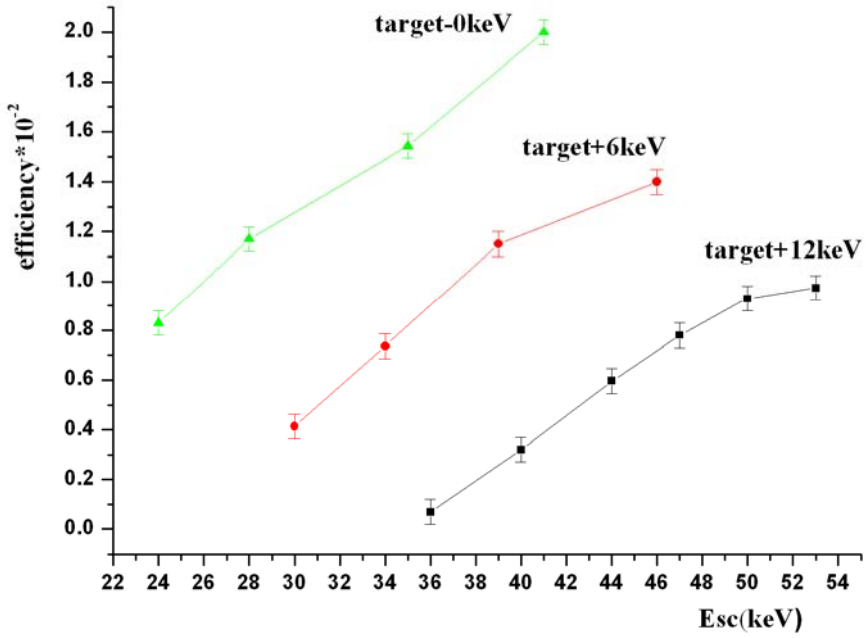

Figure 5-15: Experimental results of the efficiency with variable scattering energy in the C-target.

The increasing experimental efficiency by increasing initial energy is mainly explained due to the straggling in the carbon target. The straggling could be also reduced by decreasing thickness of the target. As experimentally has been observed by decreasing thickness of the target from 7 to 4 $\mu g / cm^2$ the efficiency was increased also almost by factor 2.

The scattered energy can be increased also by applying a positive voltage on the target. However, the experimental result shows here a decreasing

efficiency (rot curve with +6 keV applied on the target and black curve with +12 keV). It could be explained, that with applying positive voltage the electron beam after the scattering becomes more divergent and not all Moeller electrons coming to the detectors.

The presented experimental efficiency of the whole experiment would be further reduced approximately by three orders due to the efficiency of the Mott analyzer.

This experimental efficiency that depends from straggling and electronic optics is the one of the main parameter to observe spin entanglement from elastic scattering of unpolarized electrons.

5.6. Scheme of the acquisition setup

The electronics scheme between detectors and oscilloscope is presented in Figure 5-16. The signal from the Magnum (electron multiplier) comes to the octal fast amplifier [5] which consists of eight independent DC-coupled amplifiers packaged in a single-width NIM. Each section has a fixed voltage gain of 10, a high bandwidth and a wide dynamic range (<2ns rise and fall times to±0.6V).

After the amplifier signal comes to the Octal discriminator[6] which helps to reduce background signal from the multiplier by increasing threshold level. The minimum threshold is -30mV, variable up to -1V. A monitor point is provided to permit measurement of the threshold level with a voltmeter rather than the more difficult and less precise analog measurement via oscilloscope. The discriminator operates at maximum rates of 100MHz, output rise time are typically 2.1ns. The output signal from every channel comes to the Octal timer [7] to perform single count rate measurement and also to the digital phosphor oscilloscope[8] to capture all for channels. In order to send a trigger signal to the oscilloscope the signals from discriminator come to the coincidence unit[9] as example in the form:

[5] FA8000-octal fast amplifier

[6] OD 623B – octal discriminator

[7] SC 8000 – octal timer

[8] TDS 5000 – digital phosphor oscilloscope

[9] CO 4001 – coincidence unit

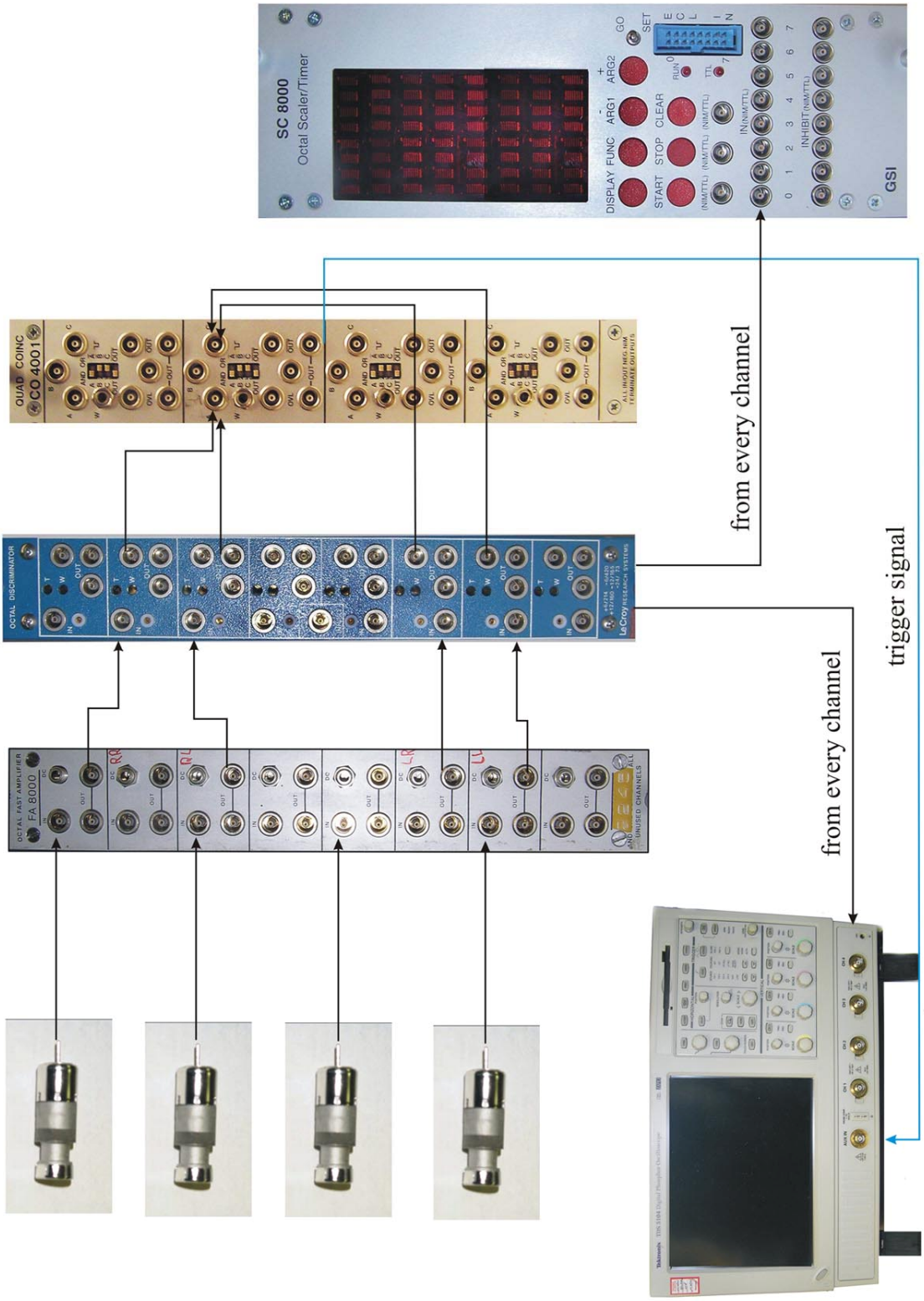

Figure 5-16: Scheme of the acquisition setup

$$(\mathrm{CH1} \vee \mathrm{CH2}) \wedge (\mathrm{CH3} \vee \mathrm{CH4})$$

where CH1 – count rates in detector 1 and so on.

So, the coincidences between channels CH1-CH3 and CH1-CH4 have to be compared with CH2-CH3 and CH2-CH4. After the coincidence unit the trigger signal send to the oscilloscope. The oscilloscope is working in the Fast Frame mode. Fast Frame is an acquisition mode that lets us capture many records in a larger record, and then view and measure each record individually. The data analysis that is using LABVIEW is described in detail in paragraph 5.7.

5.7. Data analysis

As already mentioned, one goal of our experiment is to reduce the total resolution time to a minimum, where still all true coincidences are captured and the random coincidence rate is respectively low to achieve a high $C_{measured}/C_{random}$ ratio. Of course the resolution time is given by the used equipment and may vary from channel to channel. For this reason we use a fast oscilloscope to capture all four channels and make a time coincidence analysis with a dedicated analysis program. The analogue logic NIM-module provides us with a resolution time of about 5 ns. On every observed coincidence this NIM-module sends a trigger signal to the oscilloscope, which acquires the original pulses from the detectors. The schematically view of the transferring data is shown in Figure 5-17.

Without this pre-selection the amount of data to acquire would be around a thousand times higher. The digitized data we obtain are analysed using different time windows as coincidence interval.

By shortening the time windows we can reduce the time resolution to values of around 1ns, identical for each channel. The analysis tool is programmed in LabVIEW and separated into two modules [Sch-09]. One is running on the oscilloscope itself and the other running on a PC connected via LAN. The first one manages the signal acquisition and writes data in packages to the local hard disc. Therefore it is kept as small and fast as possible to save the limited resources of the oscilloscope's system.

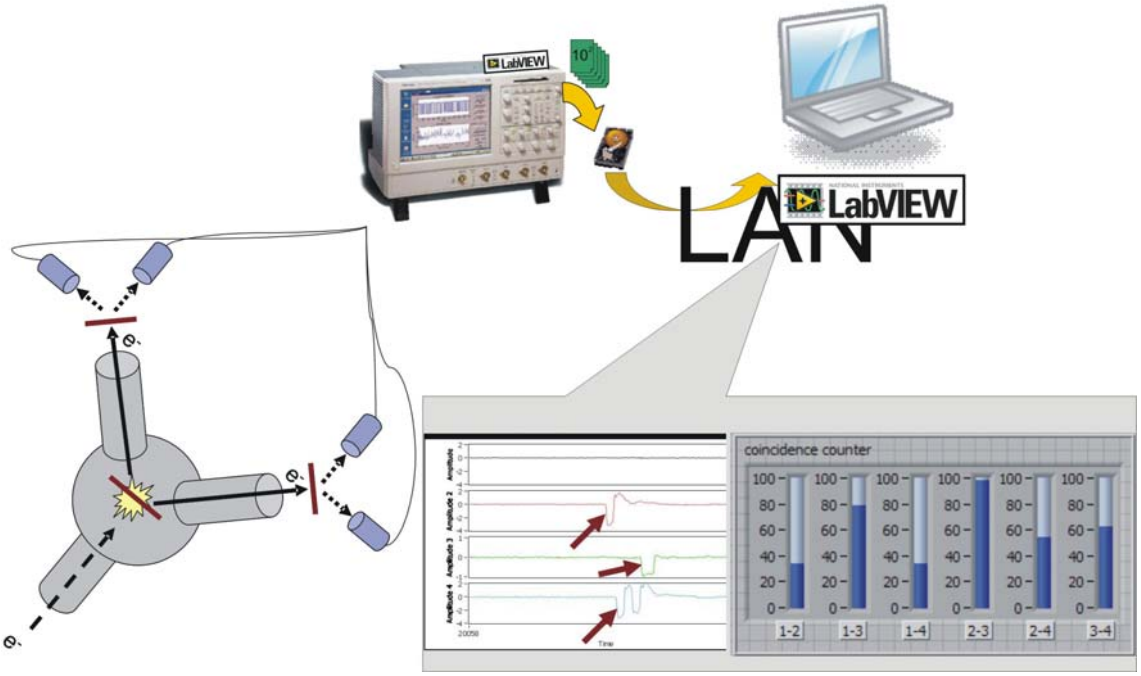

Figure 5-17: Schematically drawing of the transferring data analyses.

The oscilloscope's dead time during read-out is minimized using a 'fast frame' acquisition mode, where up to several thousand events (signals) are stored in one waveform and can be transferred to the hard drive at once. In addition to this the start and end time of a measurement is logged automatically. The second program module running on the remote system makes a slope detection in every channel for each event. Thereby linear interpolation between digital data-points on the linear domain of a pulse is used to increase accuracy.

By comparing the differences of slope versus time values with the user-specified coincidence time window we find the desired coincidences which we add up and visualize. To calculate random coincidences we need count rates from each single detector and the resolution time. Subtracting random coincidences from measured we find the wanted real coincidences.

Figure 5-18 presents the operating module of the described program. When the pulses come simultaneously to the detectors coincidence are detected. The programme shows us the measured coincidence between four detectors in the Mott analyzers. Subtracting random coincidences from measured we find the wanted real coincidences. This program allows us also to know the ratio of measured/random coincidence in the detectors of Mott analyzers at once after measurement.

The primary energy of the electron beam E=35keV, primary current I≈1μA, count rates reaching the second target ≈500kHz, scattered count rates that reaching detectors ≈ 3kHz.

As can been seen, for the full experiment we are observing a total coincidence rate approximately of a factor 4 above statistical coincidences (ratio (measured/random in the Figure 5-18). However, as picture illustrated by 6611s we observe approximately 100-150 real coincidences rate in the detectors. The bigger time is necessary in order to reduce the error of the measurement (described in detail in paragraph 5.8).

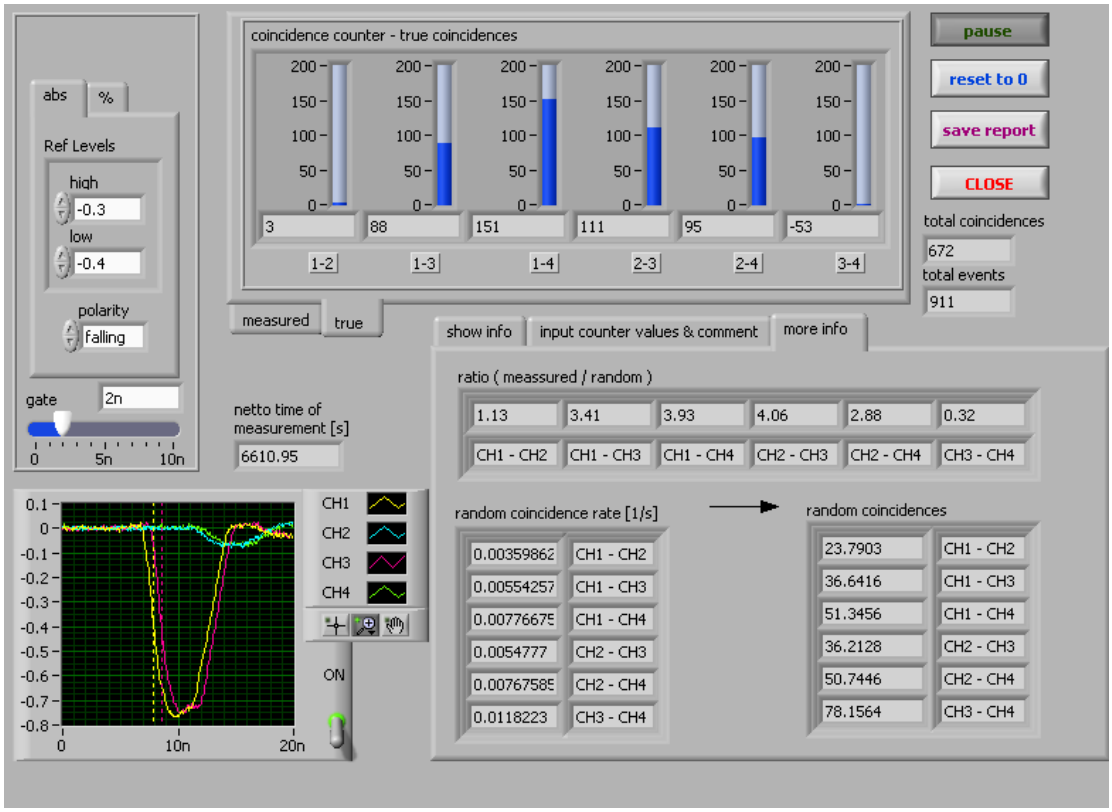

Figure 5-18: The operating module of the Labview program: 1-3 coincidence between right detectors of both Mott analyzers, 1-4 right and left, 2-3 left and right, 2-4 left and left.

5.8. Asymmetry measurement

One of the main important goals was to observe a high ratio of measured/random coincidence after a double scattering in the detectors of Mott analyzers. This task has been accomplished and we can demonstrate here for the full experiment a total coincidence rate approximately of a factor 4

above statistical coincidences, while a rate of about 1 – 2 kHz was applied in the magnum detectors [Ber-09a, Ber-09c].

It allows us to perform asymmetry measurement in the detectors of Mott analyzers in order to prove entanglement of the electrons. For this purpose one Mott analyzer has to be turned to 90° where expected anti-coincidence of the spin direction should disappear. The reduction of asymmetry by turning one Mott analyzer is a good test of quantum mechanical prediction.

In order to normalize to different intensities in the detectors it is convenient to introduce the factor Q [Jac-08]:

$$Q = \frac{Coin(R_1 L_2) \cdot Coin(L_1 R_2)}{Coin(R_1 R_2) \cdot Coin(L_1 L_2)} \tag{5.6}$$

where $Coin(R_1 L_2)$-coincidence between right detector of one Mott analyzer with left detector of second Mott analyzer and so on.

In this case the calculated asymmetry:

$$A = \frac{\sqrt{Q} - 1}{\sqrt{Q} + 1} \tag{5.7}$$

Figure 5-19 presents the experimental result of asymmetry (blue points) with dependence from the angle where one Mott analyzer is rotated around the axis.

The red point presents result of the instrumental asymmetry where gold has been replaced by aluminum target in one Mott analyzer. The instrumental asymmetry is smaller than the real one, however further investigation would be necessary in order to perform more precise measurement of the instrumental asymmetry.

The black line shows the estimated theoretical curve for coincidence double scattering experiment including the error of the instrumental asymmetry. From the calibration at U-Mainz with known polarized beam we have estimated the value of asymmetry ≈ 3.3% (paragraph 3.4.3). The offset which is estimated by the value of instrumental asymmetry in the double scattering experiment equal 5% (red point in the Figure 5-19) with the error of ± 2%.

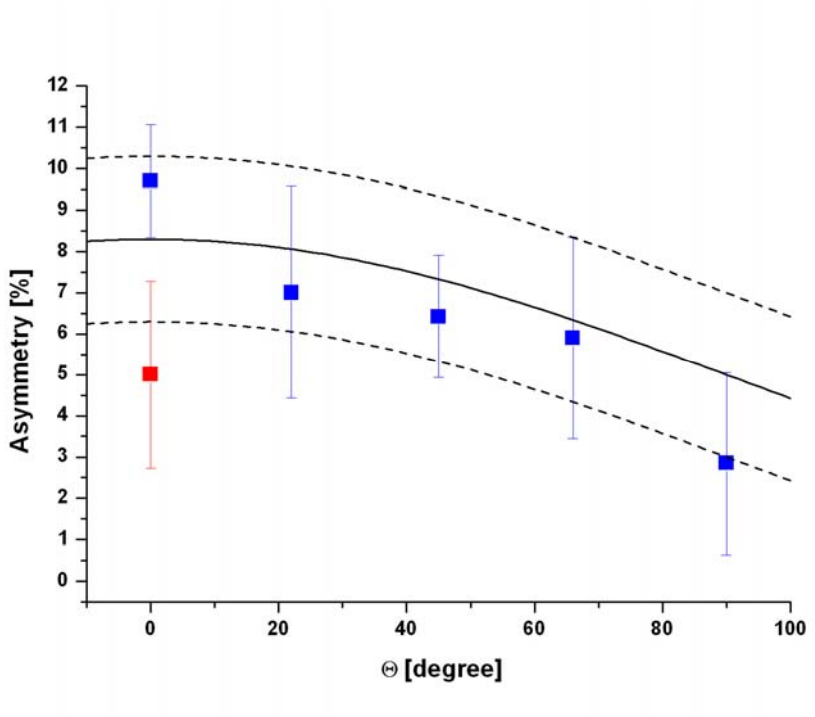

Figure 5-19: Experimental result of the asymmetry with dependence from the angle Θ where one Mott analyzer is rotated around the axis (blue points) and result of instrumental asymmetry (rot point). The expected theoretical curve (black line) and the error of this curve including error of the offset ±2% (dotted line).

In this case the expected theoretical curve for the coincidence double scattering experiment with including quantum mechanical prediction (cosinus behaviour) is presented in Figure 5-19 and calculated by:

$$Y = Amp \cdot \cos(x) + Offset$$

where Amp – is the value of asymmetry with known polarized beam,

$Offset$ – the value of instrumental asymmetry in double scattering experiment,

x – the angle where one Mott analyzers are rotated around the axis.

The observed reduction of asymmetry in dependence of the rotation angle is in agreement with a prediction of quantum mechanic. However, the high errors of the measurement have been estimated. And due to these errors we can presently not distinguish between prediction of quantum mechanic (where cosinus behavior is predicted) and prediction of Bell's inequality (prediction of linear behavior).

The high error of the experimental results is explained due to the low statistic of the measurement. As example, in order to minimize error in the order of 1% we need a higher static with the number of real coincidence close to $N = 10000$. The time necessary to perform this measurement with in dependence of efficiency could be estimated as following:

Since the measured coincidence rate is a superposition of real and random coincidences than according to (5.3) and (5.4):

$$\frac{C_{MEASURED}}{C_{RANDOM}} = \frac{C_{REAL} + C_{RANDOM}}{C_{RANDOM}} = \frac{(R_1\varepsilon_1 + R_2\varepsilon_2) + R_1R_2(\tau_1 + \tau_2)}{R_1R_2(\tau_1 + \tau_2)} \qquad (5.8)$$

where R_1, R_2 -detection rates of electrons in detector 1 and 2;

$\varepsilon_1, \varepsilon_2$ - the efficiency that an electron in one detector can be recorded simultaneous with the correlated electron in the second detector;

$(\tau_1 + \tau_2)$ - total resolution time.

If we assume a symmetric set up of the experiment than with $R_1 = R_2$, $\varepsilon_1 = \varepsilon_2$ and $\tau_1 = \tau_2$ we receive:

$$\frac{\varepsilon}{R\tau} = \frac{C_{MEASURED}}{C_{RANDOM}} - 1 \qquad (5.9)$$

In this case the estimated time of the measurement to have number of real coincidence in the order of $N = 10000$ with a total resolution time of (4-5)ns for different efficiency is:

1. $\varepsilon = 10^{-4} \Rightarrow$ Time of the measurement $T = 6000\,\text{sec}.$
2. $\varepsilon = 10^{-5} \Rightarrow T = 625000\,\text{sec}. \approx 174 hours$
3. $\varepsilon = 10^{-6} \Rightarrow T = 10 \cdot 10^6\,\text{sec}. \approx 723 days$

Now in the presented experiment we are in the order of 10^{-5} for the overall efficiency. In order to minimize error of the measurements and distinguish prediction of quantum mechanics with Bell's inequality it is necessary to increase the overall efficiency further. This could be accomplished by increasing initial energy in order to reduce straggling in the target further.

Another way to increase our statistic of the measurement could be performed by applying new detector as Microchannel plates which would allow us to reduce total resolution time by almost a factor of ten. In this case with the overall efficiency in the order of 10^{-5} we would be need approximately 17 hours in order to perform measurement with a better statistic.

6. Conclusions and outlook

In this chapter the conclusions from the presented work and the main experimental results are summarized. Also, some suggestions for the next steps to the future experiment are given.

6.1. Conclusions of the present work

The presented work has been devoted to determine the experimental parameters necessary to produce a source of entangle electrons. In order to perform this result several tasks have been accomplished.

Six kinds of detectors have been tested for presented experiment. The main important parameter for the detectors is resolution time. It should be made as small as possible to reduce detection of random coincidence in the detectors. But in another hand it must be long enough to accommodate the jitter in the separate detectors, or some true coincidences are lost. The Magnum (electron multiplier) and scintillator with photomultiplier have been found to be most appropriate for our experiment and allows us to have a total resolution time in the order of 2-4ns.

The two kinds of Mott analyzer have been tested and calibrated with known polarized beam during presented work in order to observe asymmetry and estimated efficiency of the analyzers. The first version of Mott analyzer has smaller efficiency that can prevent electron spin resolved coincidence measurements because of the necessarily induced random coincidences in low efficiency spin detectors.

The new design of a compact mini-Mott spin analyzer has been performed to increase this efficiency, which is a prerequisite to the electron spin resolved coincidence measurement. Due to the compact small size the

cylindrical-electrode Mott polarimeter achieves high detection sensitivity almost by two orders higher if compared to the previous design.

A preferable condition for the detection of coincidences is to achieve a high ratio of measured coincidences compared to random coincidences to reduce the error for the measurement. To estimate this ratio the efficiency of the experiment has been determined. For the purpose the thickness of the target was reduced to 4 $\mu g/cm^2$ and the beam energy has been increased to 35 keV in order to reduce straggling in the carbon target. Additional lenses and a set of the electrostatic deflectors have been mounted to distinguish Moeller-scattering (electron with electrons) from Mott-scattering electrons (electrons with an atomic nucleus). The energy selection is important to reduce background electrons, resulting from the high energy Mott scattering. The electrostatic deflectors allow us also to reduce distance between scattering chamber and analyzer in order to prevent reducing of intensity that comes to the detectors of Mott analyzers.

For small beam intensity with several kHz counting rate in the detectors the rate for real coincidences have been achieved to several thousand times bigger than the rate for random coincidences. It is shown, that this ratio is related to an experiment depended nearly constant experimental efficiency for the coincidence detection. This efficiency and higher ratio of measured/random coincidence are the main important parameters for observing entanglement. A maximum efficiency of $2 \cdot 10^{-2}$ have been achieved after scattering in carbon target.

The overall efficiency of the whole experiment would be further reduced approximately by three orders due to the efficiency of the Mott analyzer. However, with this target efficiency in the order of 10^{-2} we could demonstrate here for the full experiment a total coincidence rate approximately of a factor 4 above statistical coincidences, while a rate of about 1 – 2 kHz was applied in the Magnum detectors.

The asymmetry measurement in the detectors have been performed where one Mott analyzer rotated by an angle around the axis. The reducing asymmetry is in agreement with a prediction of quantum mechanic. However, the large systematic errors of the measurement have been estimated and are presently too large to distinguish between the predictions of quantum

mechanic and Bell's inequality. Further investigation would be necessary to minimize error of the measurement, especially for more detail illumination of instrumental asymmetry.

The next step would be to increase the overall efficiency of the experiment. This could be performed by having higher initial energy. As example, by increasing energy from 32 to 38 keV the efficiency has been increased almost by factor 2. The higher energy would be prerequisite to increase the experimental efficiency further.

In order to minimize error of the measurement new detectors as (Microchannel plates) would be applied. They would allow us to reduce total resolution time in the order of 10 that would lead to the higher ratio of measured/random coincidence.

The two years of presented PhD thesis have been also devoted to investigation of the spin asymmetry of backscattered electrons from magnetized targets as additional option for spin detection with high efficiency. A high value of efficiency near to 1 has been observed. Polarization that produced from the Fe-target has been estimated to the value narrow to 70% that gives a possibility for creating a polarized source with lower energy. However, additional improvement, as a special cleaning procedure for the target and better resolution between incoming beam and backscattered electrons is necessary to perform the using this "spin filter" for spin resolved coincidence measurement.

6.2. Suggestions and outlook for future experiments

In order to produce the source of the entangled electrons it is necessary to increase the overall efficiency and minimize error of the measurement.

The next step in order to increase statistic of the measurement could be done by applying Microchannel plates which gives a time response Full Width at Half Maximum < 1ns and a rise time of < 300ps.

Microchannel (MCP) plates are widely used in many types of analytical equipment such as for mass spectroscopy, semiconductor inspection and surface analysis. MCP consists on a two dimensional sensor for detection of electrons, ions, X-rays and so on, and multiplies the detected signals with

high efficiency, high speed and thus resulting high temporal resolution [TECT].

Figure 6-1 presents the structure and operating principle of MCP.

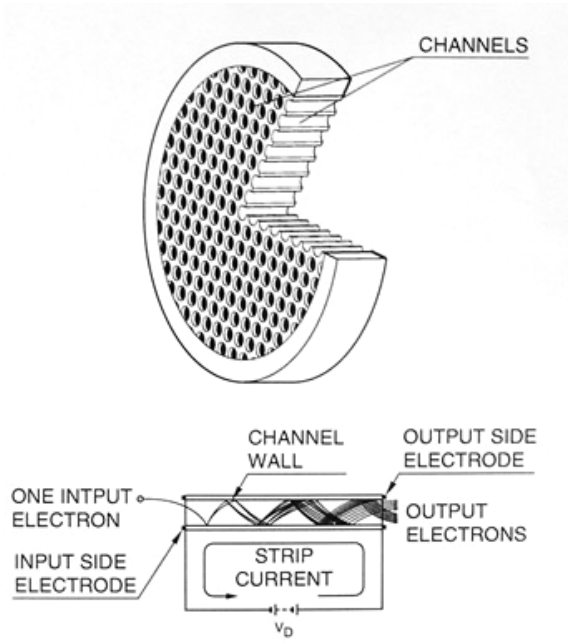

Figure 6-1: The basic operation of Microchannel plate.

A potential gradient is established along the channel when the voltage V_D is applied between the input and output sides of the MCP. Multiple secondary electrons are emitted when an electron enters a channel from the input side and strikes its inner wall. These secondary electrons are accelerated by the potential gradient to draw parabolic trajectories that are determined by their initial velocities. They then strike the opposite wall n the channel causing further secondary electrons to be emitted. The electrons in this way travel towards the output end while striking the inner wall of the channel repeatedly. As a result, a large number of exponentially increased electrons are extracted from the output side.

This detector would help us to reduce random coincidence that is linearly dependent from the resolution time. And in turn the higher ratio of measured/random coincidence is expected.

The further possibility to increase the experimental efficiency could be done by applying higher initial energy. As example, the experimental result has been shown that by increasing energy from 32 to 40 keV the efficiency

was increased almost by factor 2. The higher energy would be prerequisite to increase the experimental efficiency further. For this reason new electron gun would be necessary to increase energy further. One of the proposed guns is shown in the Figure 6-2 [KIMB].

Figure 6-2: The photo of the proposed electron gun (EGH-8102).

The gun can deliver electrons over a very broad range of energies from 1 keV to 100 keV and currents from picoamps to tens of milliamps can be achieved.

By increasing efficiency further would allow us to minimize the error of the measurement and would give us a possibility for detail comparison of prediction of quantum mechanics with Bell's inequality. In turn, the increasing efficiency would open a path for a new class of experiments, where fundamental quantum properties of free charged particles at large distances can be measured.

Bibliography

[Asp-81] - A. Aspect, P. Grangier, and G. Roger, Phys. Rev. Lett. Vol.47, 460 (1981); Phys. Rev. Lett. Vol.49, (1982); Vol.49, 1804, (1982).

[Asp-99] - A. Aspect, Nature (London), Vol.398, 189, (1999).

[Aul-97] - K. Aulenbacher et. al. Nucl. Instr. and Method A, 391, p.498-506, (1997).

[AXUV] - AXUV Photodiodes Operating Principle, IRD-Inc. website, URL: http://www.ird-inc.com.

[Bar-01] - I.V. Bargatin, B.A. Grishanin, V.N. Zadkov: *Entangled quantum states of atomic system*, Physics-Uspekhi 44,(6) 597-616, (2001).

[Bau-09] - S. Baunack et. al. Phys. Rev. Lett. PRL 102, 151803, (2009).

[Bell-64] - J.S. Bell: *On the Einstein Podolsky Rosen Paradox*, Physics 1, 195, (1964).

[Ben-92] - Ch. Bennet and S.J. Wiener, Phys. Rev. Lett. Vol.69, 2881, (1992).

[Ber-04] - R. Berezov, J. Jacoby, V. Arsov: *Optical detection of keV-electrons*, GSI Annual Report, (2004).

[Ber-05] - R. Berezov, J. Jacoby, S. Böttger: *Investigation of backscattered electrons for spin detection with high efficiency*, GSI Annual Report, (2005).

[Ber-09a] - R. Berezov, J. Jacoby, T. Rienecker, J. Schunk: *Investigation of spin entanglement produced from elastic scattering of unpolarized electrons*, Nucl. Instr. and Method A, 606, p.120-123, (2009).

[Ber-09b] - R. Berezov, J. Jacoby, J. Schunk: *Efficiency measurement for investigation of entanglement produced from unpolarized electrons*, GSI Annual Report, (2009).

[Ber-09c] - R. Berezov, J. Jacoby, J. Schunk: to be published, (2009).

[Bie-82] - J.B. Biersack and J. F. Ziegler, *The Calculation of Ion Ranges in Solids with Analytic Solutions*, 157-176, in Ion Implantation Techniques, H. Ryssel and H. Glawischnig, Springer Verlag, Berlin, (1982).

[Bou-97] - D. Boumeester et. al., Nature (London), Vol.390, 575, (1997).

[Bru-77] - M. Bruno, M. d'Agostino and C. Maroni, Nuobo Cim., Vol.40, B142-52, (1977).

[Cam-85] - D.M. Campbell, C. Hermann, G. Lampel and R. Owen, J. Phys. E, Vol.18, 664, (1985).

[Cla-69] - J.F. Clauser, M.A. Horne, A. Shimony, and R.A. Holt, Phys. Rev. Lett. Vol.23, 880, (1969).

[Cla-74] - J. Clauser and M. Horne, Phys. Rev. D, Vol 10, 526, (1974).

[Cla-78] - J. Clauser and A. Shimony, Rep. Prog. Phys 41, 1881, (1978).

[Daw-92] - A.S. Dawydow, *Quantenmechanik*, ISBN 3-335-00326-8, (Heidelberg, 1992).

[Dei-65] - H. Deichsel and E. Reichert, Z. Phys. Vol.185, 169, (1965).

[Deu-98] - D. Deutsch, A. Ekert: Phys. World, Vol. 11 (3) 41, (1998).

[Edw-01] - Edward S. Fry and Thomas Walther: *Atom based tests of the Bell inequalities-the Legacy of John Bell continues...*, Department of Physics, Texas A&M University, (2001).

[Ein-35] - Einstein, B. Podolsky and N.Rosen: *Can Quantum-Mechanical Description of Physical Reality Be Considered Complete?* Physical Review, 47, 777-780, (1935).

[Eke-92] - A.K. Ekert, J.G. Rarity, P.R. Tapster, and M. Palma, ibid., Vol.69, 1293, (1992).

[Eng-96] - B.-G. Englert, Phys. Rev. Lett. Vol.77, 2154, (1996).

[Far-74] - C. Faraci, D. Gutkowski, S. Notarrigo and A. R. Pennisi, Lett. Nuovo Cimente Vol.9, 607, (1974).

[Fas-92] - G. Fashold, M.S. Hammond and J. Kirschner, Solid State Commun. Vol.84, 541, (1992).

[Fey-65] - R. Feynmann, R. Leighton, M. Sands, The Feynmann Lectures on Physics, Vol. 3, Addison Wesley, Reading, (1965).

[Fil-98] - Filipe, H.J. Drouhin et. al.: *Spin-dependent transmission of electrons through the Ferromagnetic metal base of a hot-electron transistorlike system,* Phys. Rev. Lett., Vol.80, 2425, (1998).

[Fra-57] - H. Frauenfelder, R. Bobone, E. von Goeler, N. Levine, H.R. Lewis, R.N. Peacock, A. Rossi, and G. DePasquali, Phys. Rev. vol. 106, 386, (1957).

[Fre-72] - S.J. Freedman and J.F. Clauser, Phys. Rev. Lett. Vol.28, 938, (1972).

[Fry-76] - E.S. Fry and R.C. Thompson, Phys. Rev. Lett. Vol.61, 2921, (1976).

[Gay-92] - T.J. Gay, F.B. Dunning: *Mott electron polarimetry*, Rev. Sci. Instrum. 63(2), (1992).

[Gel-91] - A. Gellrich and J. Kessler, Phys. Rev. A, Vol.43, 204 (1991).

[Gra-05] - J. Graf, C. Jozwiak, A.K. Schmid, Z. Hussain and A. Lanzara, Phys. Rev. B, Vol.71, 144429, (2005).

[Gre-60] - J.S. Greenberg, D.P. Malone, R.L. Gluckstern and V.W. Hughes, Phys. Rev. Vol.120, 1393, (1960).

[Ham-92] - M.S. Hammond, G. Fahsold, and J. Kirschner, *Absorption and elastic and inelastic reflection of spin-polarized low-energy electrons from Fe(110)* Phys. Rev. B, Vol.45, 6131, (1992).

[Har-96] - P. Hartmann, J. Bermuth, K. Aulenbacher et. al., *Picosecond polarized electron bunches from a strained layer GaAsP photocathode*, Nucl. Inst. And Method in Ph. Res. A 379 15-20, (1996)

[Hil-02] - F.U. Hillebrecht, R.M. Jungblut, L. Wiebusch et al., Rev. Sci. Instrum. Vol.73, 1229, (2002).

[Hod-79] - L.A. Hodge, T.J. Moravec, F.B. Dunning, and G.K. Walters, Rev. Sci. Instrum. Vol. 50, 5, (1979).

[Hol-64] - G. Holzwarth and H.J. Meister, *Tables of Asymmetry, Cross section and related functions for Mott scattering of electrons by screened Au and Hg nuclei,* University of Munich, (1964).

[Jac-01] - J. Jacoby: *Which-path Information and coherence of elastic scattering*, Physica scripta, Vol. 64, 220-225, (2001).

[Jac-07] - J. Jacoby, private communication (2007).

[Jac-08] - J. Jacoby, private communication (2008).

[Joo-85] - E. Joos, H.D. Zeh, Z. Phys. B, Vol. 59, 223, (1985).

[Jos-66] - K. Jost and J. Kessler, Z. Phys. Vol.195,1, (1966).

[Jos-81] - K. Jost, F. Kaussen and J. Kessler, J. Phys. E, Vol.14, 735, (1981).

[Kas-71] - L.R. Kasday: *Foundations of Quantum Mechanics*, ed B d'Espagnat (New York: Academic), 195-210, (1971).

[Kas-75] - L.R. Kasday, J.D. Ulman and C.S. Wu, Bull. Am. Phys. Soc. Vol. 15, 586, (1975).

[Kes-85] - J. Kessler: *Polarized electrons*, Springer-Verlag, Berlin, New-York, (1985).

[Kie-93] - T.E. Kiess et al., Phys. Rev. Lett. Vol.71, 3893, (1993).

[Kil-99] - S. Ya. Kilin, Usp. Fiz. Nauk, Vol.169 507, (1999).

[KIMB] - Electron gun, Kimball physics inc, website, URL: http://www.kimballphysics.com.

[Kit-93] - M. Kitagawa, M. Ueda: Phys. Rev. A, Vol.47,5138, (1993).

[Klu-87] - D.N. Kluschko, A.I. Penin: Physics-Uspekhi 152, 653, (1987).

[Koi-86] - K. Koike, H. Matsuyama, K. Mitsuoka and K. Hayakawa, Jpn. J. Appl. Phys. Vol.25, L758, (1986).

[Kwi-95] - P.G. Kwiat et al., Phys. Rev. Lett. Vol.75, 4337, (1995).

[Lam-76] - M. Lamehi-Rachti and W. Mittig: *Quantum mechanics and hidden variables: A test of Bell's inequality by the measurement of the spin correlation in low-energy proton-proton scattering*, Physical Review D, 14, 10, (1976).

[Lan-85] - M. Landolt, R. Allenspach, and D. Mauri, J. Appl. Phys. Vol.57, 3626, (1985).

[Magn] - Electron multiplier (Magnum), Operating Principle, website, URL: http://www.burle.com.

[May-79] - Mayer-Kuckuk, T., "Kernphysik", ISBN 3-519-23021-6, Stuttgart, (1979)

[Men-00] - M.B. Menskij, Physics-Uspekhi 170, 631, (2000).

[Moe-04] - D.L. Moehring et al., Phys. Rev. Lett. Vol.93 090410, (2004).

[Mot-29] - N.F. Mott, Proc. R. Soc. A, Vol.124, 425, (1929).

[Mot-64] - Motz et.al.: Rev. Nod. Physics, 36,4 p.881, (1964).

[Par-64] - D. Park, Introduction to the quantum theory, (1964).

[Pol-04] - C. Polachic et al., Phys. Lett. A, Vol.323, 176, (2004).

[Pre-78] - C.Y. Prescott et al., Phys. Lett. B Vol.77, 347, (1978).

[Ran-90] - C. Ranganathaiah, et al., J. Electron Spectros. Rel. Phenom. Vol.51, 331, (1990).

[Rau-84] - R. Raue, H. Hopster, E. Kisker: Rev. Sci. Instrum. Vol.55, 383, (1984).

[Rei-95] - E. Reicherz, Proc. Int. Workshop on Polarized Gas Targets. Cologne, Germany, (1995).

[Rob-88] - J.L. Robins, R.J. Celotta, J. Unguris, D.T. Pierce, B.T. Jonker and G.A. Prinz, Appl. Phys. Lett. Vol.52, 1918, (1988).

[Row-01]- M.A. Rowe et al., Nature(London), Vol.409, 791, (2001).

[Sak-06] - H. Sakai, T. Saito, T. Ikeda, K. Itoh et. al.: *Spin correlation of strongly interacting massive Fermion pairs as a test of Bell's inequality,* Phys. Rev. Lett. Vol.97, 150405, (2006).

[San-96] - E. Santos, Phys. Lett. A, Vol.212, 10, (1996).

[Sch-89] - M.R. Scheinfein et al, Rev. Sci. Instrum. Vol.60, 1 (1989); Rev. Sci. Instrum. Vol.61, 2501, (1990).

[Sch-98] - D.De Schepper, L.H. Kramer et.al. Nucl. Instrum. and Method A, Vol.419, 16-44(29), (1998).

[Sch-09] - J. Schunk, Diploma thesis, in work, (2009).

[Shi-88] - Y.H. Shih and C.O. Alley, Phys. Rev. Lett. Vol.61, 2921, (1988).

[Shu-43] - C.G. Shull, C.T. Chase and F.E. Myers, Phys. Rev. Vol.63, 29, (1943).

[Sie-55] - Kai Siegbahn, Beta- and gamma-ray spectroscopy, North-Holland publishing company Amsterdam, (1955).

[Sie-81] - H.C. Siegmann, D.T. Pierce, and R.J. Celotta: *Spin-dependent absorption of electrons in a ferromagnetic metal*, Phys. Rev. Lett. Vol.46, 452, (1981).

[Ste-93] - K.-H. Steffens, Dissertation. Johannes Gutenberg-Universität, Mainz, (1993).

[TECT] - Microchannel plate, Operating principle, website, URL: http://www.tectra.com.

[Tho-26] - L.H. Thomas, Nature, Vol.117, 514, (1926).

[Uhl-25] - G.E. Uhlenbeck and S.A. Goudsmit, Naturwiss. 13, 953, (1925).

[Uhr-89] - M. Uhrig, A. Beck, J. Goeke, F. Eschen, M. Sohn, G.F. Hanne, K. Jost, and J. Kessler, Rev. Sci. Instrum. 60, 872, (1989).

[Ung-86] - J. Unguris, D.T. Pierce and R.J. Cellota, Rev. Sci. Instrum. Vol.57, 1314, (1986).

[Wai-78] - P.F. Wainwright, M.J. Alguard, G. Baum, and M.S. Lubell, Rev. Sci. Instr. Vol.49, 571, (1978).

[Wei-98] - G. Weihs et al., Phys. Rev. Lett. Vol.81, 5039, (1998).

[Wil-76] - A.R. Wilson, J. Lowe and D.K. Butt, Phys. G: Nucl. Phys. Vol. 2, 613-24, (1976).

[You-08] - Young-Dae Jung, Daiji Kato: Physics of Plasma, Vol.15, 104503, (2008).

[Zdy-02] - R. Zdyb and E. Bauer, Surf. Rev. Lett. Vol.9, 1485, (2002).

[Zei-86] - A. Zeilinger, Phys. Lett. A, Vol.118(1), 1, (1986).

Acknowledgements

At the end of my work I would like to thank everyone who in one way or another contributed to this work and whose help and support was so necessary for its successful performing.

First of all, I wish to express my gratitude to my supervisor Prof. Dr. Joachim Jacoby from the Insitute of Applied Physics (IAP) at Frankfurt University (JWG-Uni Frankfurt-am-Main) for his scientific support, comments, discussions and useful remarks on the subject of my work as well as for his care during my stay in Germany. I have learned a lot of during this time. I thank also to him for correction of my PhD thesis and for giving me chance to visit several interesting conferences. Without his help this experiment would have not be accomplished.

My very special thanks are addressed to my second supervisor Priv. Doz. Dr. Kurt Aulenbacher from the Institute of Nuclear Physics at Johannes Gutenberg University in Mainz. During my PhD thesis I have worked several times in his group. It was a very nice time with a good and friendly atmosphere. I thank him a lot for possibility to perform calibration of the Mott analyzers and for his help and advices during experiments in Mainz. I am also very grateful to him for providing corrections and detailed comments on the thesis, which has significantly improved its quality.

A lot of thanks I would like to say to my colleagues of the IAP at University of Frankfurt for the great time I had in our group. I enjoyed the atmosphere, their friendship and their support. My special thanks are addressed to my very good friend Dr. Marcus Iberler for his helps with German translation and English correction of my PhD thesis. He was always glad to help me and have never refused in a lot of things during my live in Germany. My special thanks related also to Astrid Hergt for help in many administrative questions.

I would like also to express my gratitude:

To Dr. Vladimir Arsov for his support and care during the first year of working together. His knowledge and advice has helped me a lot in the

beginning of my PhD thesis. I thank him also a lot for a nice time spent together.

To my colleague Julian Schunk for his very important help with writing program in Labview for data analysis. This work was helping me a lot to accomplish faster and better the experimental results. I thank him also for the help in the mounting of experimental set up.

To Dr. Valerij Tioukine from the Instutute of Nuclear Physics in Mainz for his help with mounting and perform experiments during our collaboration. It was a pleasant time spent together.

To Ilja Müller my special thanks for his help with repair and preparation of electronic equipments which was so necessary to accomplish my PhD thesis.

To Tim Rienecker for primary program in Origin that has been used for the first data analysis of the experimental results.

To Mr. Hausen, Sven Reploeg and the other member of the workshop for a lot of produced materials with good quality which was so necessary to accomplish this experiment.

Finally, a special thought is devoted to my parents, my sister and parents of my wife for a never-ending support during several years away from home. I am forever indebted to my parents for their love, understanding, endless patience and encouragement when it was most required. I would like to say also a Great Thanks to my beloved wife Tetyana and to my love son Florian for their warm encouragement and support. Without their help this thesis would not have been possible. I dedicate this thesis to my son, my wife, my parents, and my father-in-law (who died in 14.05.2009, may his memory live forever).

Curriculum Vitae

Name:	Rustam Berezov
Birth date:	14. October 1980
Birth place:	Kharkov, Ukraine
Citizenship:	Ukraine
Parents:	farther: Berezov Dimitriy Valentinovich
	mother: Berezova Raziia Mixajlovna
Marital status:	married

Educational Profile:

1986 – 1989:	Primary school, Kharkov, Ukraine
1989 – 1997:	Secondary and high-school, Kharkov, Ukraine
June 1997:	School leaving certificate
1997 – 2003:	Kharkov National University, Ukraine
February 2003:	Certificate of degree “Engineer-Physicist”
since October 2003:	PhD student at Johann Wolfgang Goethe-University,
	Frankfurt am Main, Germany.